Functionalization of Alumina Nanofibers with Metal Oxides

MARINA AGHAYAN

TUT
PRESS

TALLINN UNIVERSITY OF TECHNOLOGY
FACULTY OF MECHANICAL ENGINEERING
DEPARTMENT OF MATERIALS ENGINEERING

Dissertation was accepted for the defense of the Degree of Doctor of Philosophy in Engineering on 17.03.2016

Supervisor: Professor, Dr. Irina Hussainova, Department of Materials Engineering, Tallinn University of Technology, Estonia

Opponents: Kaupo Kukli, Professor, Institute of Physics, University of Tartu, Tartu, Estonia

Maarit Karppinen, Professor, Department of Chemistry, Aalto University, Espoo, Finland

Defense of the thesis: 18.04.2016, room U06-220, Tallinn University of Technology, Ehitajate tee 5, Tallinn

Declaration:

Hereby I declare that this doctoral thesis, my original investigation and achievement, submitted for the doctoral degree at Tallinn University of Technology has not been submitted for any academic degree elsewhere.

Alumiiniumoksiidnanokiudude funktsionaliseerimine metalloksiididega

MARINA AGHAYAN

TTÜ
KIRJASTUS

Contents

LIST OF PUBLICATIONS

The present dissertation is based on the following publications, which are referred in the text by the Roman numerals I–V.

Paper I.   Aghayan, M.; Hussainova, I.; Gasik, M.; Kutuzov, M.; Friman, M. Coupled thermal analysis of novel alumina nanofibers with ultrahigh aspect ratio. *Thermochimica Acta*. 2013, 574, 140−144. DOI: 10.1016/j.tca.2013.10.010.

Paper II.   Aghayan, M.; Voltsihhin, N.; Rodríguez, M.A.; Marcos, F.R.; Dong, M.; Hussainova, I. Functionalization of gamma-alumina nanofibers by alpha-alumina via solution combustion synthesis. *Ceramics International. 2014,* 40 (8), 12603−12607. DOI: 10.1016/j.ceramint.2014.04.087.

Paper III.   Aghayan, M.; Gasik, M.; Hussainova, I.; Rubio-Marcos, F.; Kollo, L.; Kubarsepp, J. Thermal and microstructural analysis of doped alumina nanofibers. *Thermochimica Acta.* 2015, 602, 43−48. DOI: 10.1016/j.tca.2015.01.009.

Paper IV.   Aghayan, M.; Hussainova, I., Fabrication of $NiO/NiAl_2O_4$ nanofibers by combustion method. *Key Engineering Materials.* 2016, 674, 31-34. DOI: 10.4028/www.scientific.net/KEM.674.31.

Paper V.   Kirakosyan, K.; Aghayan, M.; Taleb, M.; Hussainova, I.; Rodríguez, M. A., Homogeneous deposition of copper oxide on mesoporous 1D alumina nanofibers by combustion approach. *Proceedings of the Estonian Academy of Sciences*. 2016, 65 (2) 1−4. DOI: 10.3176/proc.2016.2.06

Author's contribution:

I.   Design of the experiments; Testing; Data analysis

II.   Design of the experiments; XRD and DTA analysis; Discussion of the results; Writing

III. Design of the experiments; FESEM examination; chemical analysis; Data analysis, Writing

IV.   Design and optimization of the processes, Analysis of thermal stability; Writing

V.   FESEM and XRD analysis; Discussion of the results

ABBREVIATIONS

ANF – alumina nanofiber

EDXS – energy dispersive X-ray spectrometer

1D – one dimensional

DTA – differential thermal analysis

DSC – diffraction scanning calorimetry

SEM – Scanning electron microscope

TEM – transmission electron microscope

TG – thermogravimetric

TM – transition metal

RE – rare earth

XRD – X-ray diffraction

wt.% – weight percentage

vol.% – volume percentage

1 REVIEW OF THE LITERATURE

Introduction

Reasonable estimates indicate that the world population will be around 10 billion in the middle of the 21st century. The growing needs of humankind require new materials. In this context, the ready availability of "tailored-to-use" materials appears to be the main issue that determines the speed of progress. The development of innovative systems requires extensive research to design, develop and produce materials with increasing functionalities and lifetime expectancy as it is declared in "A Vision of Materials Science in the Year 2020" [5].

One dimensional (1D) structures such as nanofibers and nanotubes exhibit unique properties that make them potential building blocks for the next generation nano-devices and emerging applications. Recent advances in research on 1D objects indicate that nanofibers with a range of predefined properties (such as size and shape, chemical composition and crystalline structure) can offer an excellent paradigm to develop novel functional device prototypes: catalyst support, chemical and bio-sensors, membranes, and nanofillers for advanced composites. The key step is a proper functionalization of the raw network of the fibers to meet requirements for their further application in novel nano-devices being beyond state-of-the-art.

Among other ceramic nanostructures, fibers have unique= geometrical parameters such as a high aspect ratio combined with a large surface area, which ensure wide usage of the fibers in different industrial applications. These nanostructures are the ideal candidates for filtration, catalysis and adsorption. Moreover, their large length to diameter and small mass to volume ratios make them promising candidates for reinforcing additives to composite materials.

Amongst the 1D nanomaterials, alumina nanofibers have drawn a noteworthy attention due to alumina specific properties such as high strength and stability at high temperatures (up to 1200 ºC), low density and thermal conductivity, good corrosion resistance and electrical insulation. Studies utilizing γ-alumina nanofibers instead of traditional

particulate γ-alumina are of tremendous interest for both fundamental research and technological application.

However, to improve the targeted properties and/or to add new functionalities to alumina nanofibers (ANF) network, the well-developed process of functionalization is needed. Moreover, composite fibers may display a higher complexity and a wider range of properties as compared to non-functionalized materials. These characteristics are not only derived from the simple addition of properties of parent constituents but also result from their morphology and interfacial states.

To further develop 1D functional nanofibers, the γ-alumina nanofibers network recently developed and produced in Estonia was functionalized by aluminium, zirconium, nickel, copper oxides. Metal oxides were homogeneously deposited onto high self-aligned network of alumina nanofibers in a single step by a novel strategy, where the network of nanofibers serve as a mesoporous reactive-template. This strategy involves combination of sol-gel, deep coating and combustion synthesis methods. Urea and glycine as basic fuels and metal nitrate as precursor of metals and oxidant were used. In the present study, a template assisted sol-gel method was suggested as an alternative method to fabricate composite nanofibers.

Alumina and alumina fibers

Aluminum oxide (Al_2O_3) exists in several polymorphs, such as metastable γ-, δ-, η-, θ-, κ- phases as well as thermodynamically stable α-Al_2O_3 (Fig. 1.1). Boehmite or γ-alumina forms through dehydration of aluminum hydroxide when heated at elevated temperatures (~500 ºC). High temperature heating may lead to decrease of surface area of the alumina because of phase transformations from γ- to another forms (δ-alumina then θ-alumina) which have much lower surface areas. Finally, over 1100 ºC the structure changes drastically resulting in formation of a highly stable alpha phase [6].
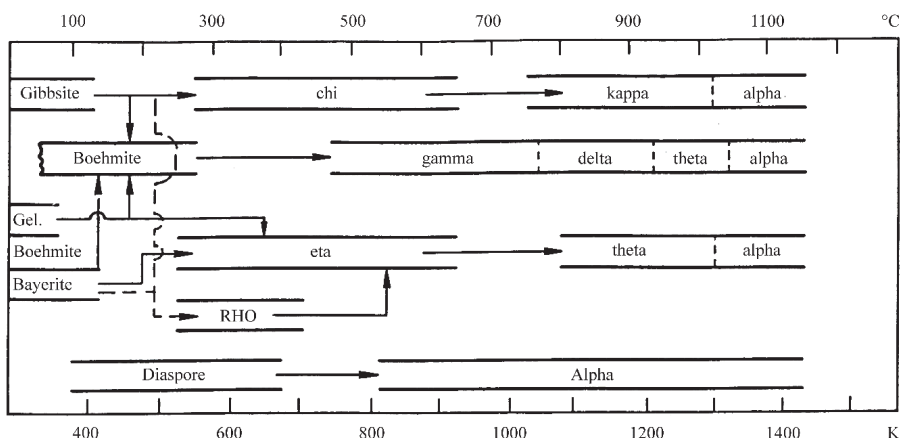
Figure 1.1 Thermal transformation sequence of the aluminum hydroxides (adapted from Ref. [7]).

Among other transition aluminas, γ-alumina is one of the most important. The applicability of γ-Al_2O_3 is traced to a unique combination of its structural properties (e.g. pore size and distribution, high surface area, specific acid/base features). However, the structural and chemical instability is a critical point of γ-alumin for even wider applications of γ-Al_2O_3 [8].

To understand the instability of γ-Al_2O_3 phase, it is important to understand the principal features of the γ-Al_2O_3 microstructure that represents a face centred cubic packing of oxygen atoms with Al^{3+} cations which fill the octahedral and tetrahedral interstitial sites among the oxygen atoms. γ-Al_2O_3 has a defective spinel type structure. The defected structure is caused by the presence of only trivalent Al cations existing in spinel structure. In the case of ideal spinel magnesium atoms exist instead of aluminum atoms, which have smaller atomic radius (Fig. 1.2 (a)) [9]. Thus, to satisfy the γ-Al_2O_3 stoichiometry, some of the lattice positions remain empty creating vacancies, although their precise location is still controversial. Due to the formed vacancies the γ-alumina containing Al^{3+} vacancy defect sites possess unique structural and phase [10].

The heat treatment of γ-alumina leads to the formation of other transition aluminas, which possess lower porosity and surface areas compared with γ- phase. However, transition aluminas are applied widely in different areas. They can be used as membranes, catalyst

supports and filters, fillers in composite materials with enhanced mechanical properties, etc. The conventional alumina is usually powder of particulates [9]. Recently, interest in preparation of 1D structures by different method spurred a fury investigation (Fig.1.2 (b-e)). Mostly because it is believed that such kind of structures possess new set of properties, such as enhanced sinterability, strength, catalytic activity, absorption ability, etc.
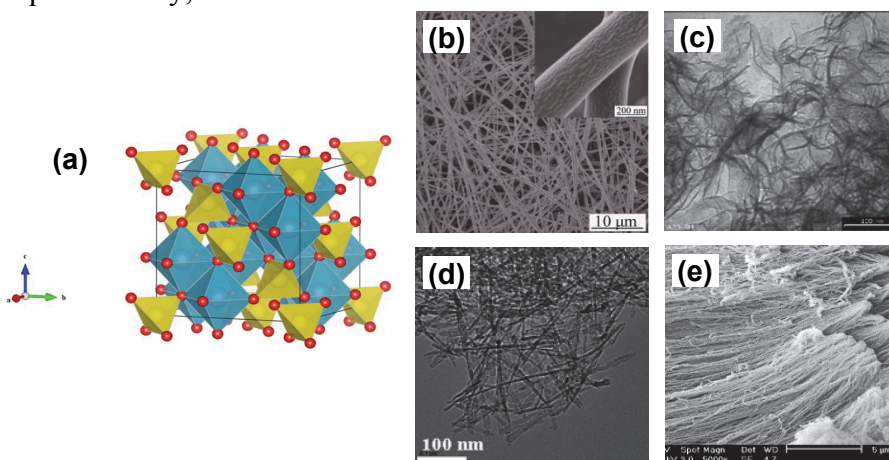
Figure 1.2 (a) The crystal structure of MgAl₂O₄. The Mg atoms sit within the yellow tetrahedral and the Al atoms sit within the blue octahedra. (Generated by VESTA (Visualisation for Electronic and Structural analysis) software); SEM images of alumina nanofibers obtained by different methods; (b) electrospinning [1], (c) sol-gel [2], (d) hydrothermal [3], (e) mercury-mediated method [4].

There are a lot of reports that demonstrate the textural properties of alumina nanofibers are different to that of conventional alumina [9, 11]. For instance, the alumina nanofibers have higher thermal stability caused by lower contact area of primary fibers [12, 13]. Another important parameter of nanomaterials is surface area, which is much larger compared to larger particles due to the small diameter of fibers and the increased number of fibers per unit volume. Thus, nanofibers possess different unique properties compared to the microscale fibers made of the same material [14]. Nanodimentianality has a potential to the efficiency of catalysts. In this sector super high aspect ratio nanofibres are also very favorable since it is possible to easily form entangled structures of such fibers by using techniques similar to conventional fiber processing [11].

Alumina nanofibers

Recently γ-alumina nanofibers with enormous specific surface area combined with nanoscale fiber diameter, highly aligned and high purity in crystal structure were developed in Estonia. Combination of such unique propertied of γ-alumina makes the nanofibers excellent candidates for different applications (Fig. 1.3).

Compared to microscale reinforcement fibers, the weight fraction of nanofibers is considerably lower. This is especially important in transportation applications (e.g. ceramic brakes, bearings and other components).
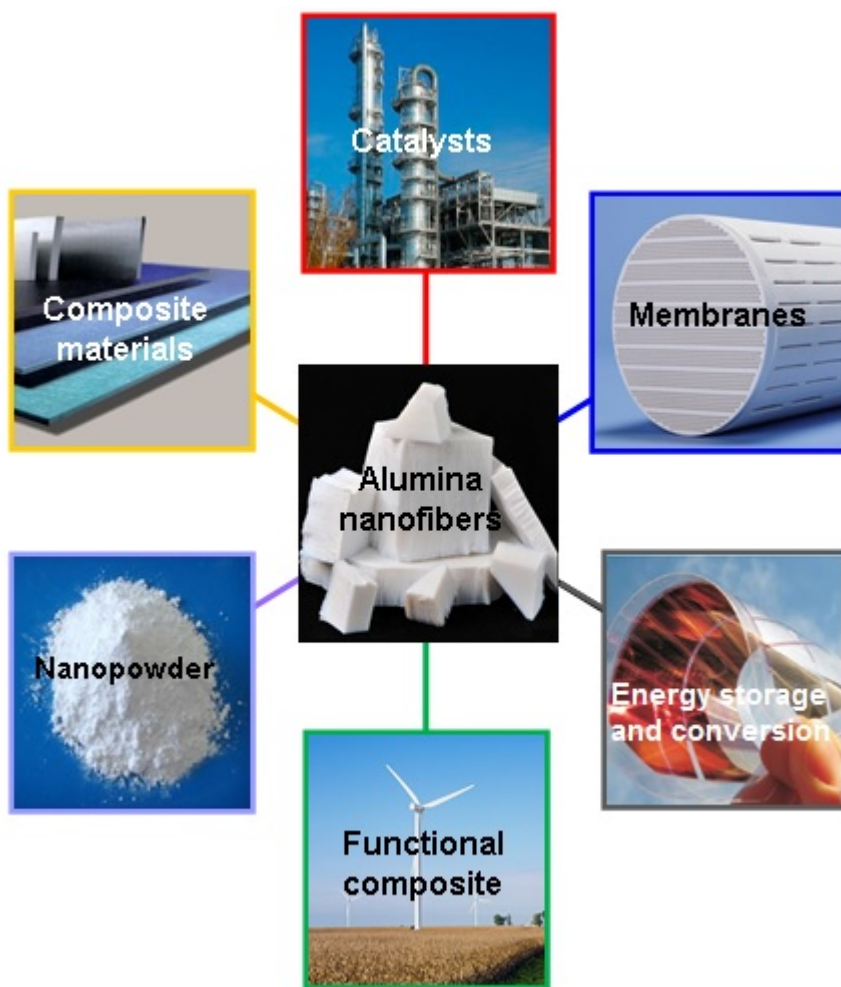
Figure 1.3 Areas of application of alumina nanofibers and functionalized alumina.

Super high aspect ratio nanofibres are favourable also if considering health and safety risks. Compared to typical nanotubes and other nanoparticles high aspect ratio nanofibres form larger agglomerates so that the danger of inhalation or skin penetration, for example, is considerably smaller than in the case of conventional nanosize particles.

Due to the purity in crystal structure, the developed alumina nanofibers possess superior tensilte strength close to the theoretical value of inter-atomic bond strength [15]. Such properties make the fibers very attractive reinforcement material in all sorts of composite materials, but especially in ceramic and metal matrix composites where polymer fibres cannot be used due to high processing temperatures that polymers cannot withstand.

Incorporation of alumina nanofibers in ceramic matrices as the reinforcement is a relatively new field. It was reported [16] that reinforcing alumina toughened zirconia by alumina nanofibers noticeably improved the hardness of the composite. The composite of Al_2O_3 containing ZrO_2 nanofibers had toughness values 3 times higher and strength values 2 times higher than conventional alumina [17, 18]. Reinforcing alumina matrix with alumina nanofibers enhanced strength and toughness of the composite via crack deflection, crack bridging and stress induced toughening [19].

As it has been already proven, the nanofibers enable to enhance mechanical properties of ceramic composites better than traditional nanoparticles, as well as they can serve as templates to produce functional nanofibers (nanofillers).

However, amongst the mentioned advantages, nanofibers have a drawback: low dispersiblity, which is a challenge to be overcome to facilitate the application of nanofibers as fillers. The low dispersibility of one dimensional nanostructures in substrate may limit the enhancement of the mechanical properties. Moreover, at high loading , the fibers tend to agglomerate and even lower the mechanical properties [9]. Many methods are adopted to facilitate good dispersion in the substrate [20]. One of the attempts to improve the miscibility of the fibers in the host matrix and improve interphase interaction between them is their functionalization. In future development of alumina nanocomposites, it is of great interest to promote dispersion or/and bonding alumina nanofibers and the matrix by adding dopants.

Moreover, to enhance performance to a great extent nanofibers must possess to generally required, high physicochemical (stability at high temperatures, wear resistance, etc.) properties. For many applications, the alumina nanofibers should be further functionalized in order to improve their mechanical properties and chemical stability for processing of specific functional material.

The effect of dopants and/or nano-layer coatings on the properties of nanostructured aluminas was studied by many research groups, for example, the thermal stability of nanomaterials can be dramatically increased by doping metal ions or metal oxides in to the structure [6, 10, 21, 22]. It was reported that the higher thermal stability was achieved by addition of silica, which sidelines the phase conversion from γ to θ and α-alumina under the high temperature calcination [23]. The significant improvements in mechanical and electrical properties adding small amount of graphene coated alumina nanofibers in alumina matrix have been reported in [24, 25]. An increase in electro-conductivity of 13 orders of magnitude as compared to the monolithic alumina is achieved at as low load of the nanofillers as 3 wt.%. Moreover, an increase in hardness of the composites with ≤10 wt.% nanofillers was approximately 20% while an improvement in an indentation fracture toughness was 40% for the composites containing 5 wt.% graphene covered nanofibers.

Alumina is one of the most widely used catalyst supports for commercial catalytic applications. In fact, in many cases alumina is shown to have catalytic activity of its own and will, therefore, often enhance the activity of the catalyst [26]. Fibrous, highly aligned structure of alumina enhances the efficiency of catalyst. Alumina nanofibers are also important precursors for building structures catalysts. It was reported that coating microsilica fibers by alumina nanofibers improves the soot-capturing capacity of diesel catalytic converters [27].

Apart with the advantages of γ-alumina as catalyst support, there is an important drawback: the fibers are not structurally stable at a high temperature. Many researchers suggested to use alumina based spinel as a catalyst support due to its high thermal stability [28]. For instance, $NiAl_2O_4$ possesses various advanced properties, such as resistance to high temperatures and acidic or basic environments, providing chemical and physical stability for the catalyst [29]. In addition, the reforming activity of these reduced $NiAl_2O_4$ catalysts is typically superior in

comparison with other structurally similar phases such as $CuAl_2O_4$, $NiFe_2O_4$ or $NiMn_2O_4$ [30, 31].

Besides the application in catalyst and advanced composites, the ANF can also be used to fabricate ceramic membranes. Ke et al. [32] coated alumina and titanate nanofibers onto a porous ceramic substrate in order to fabricate a new kind of high-performance ceramic membrane. In this arrangement, the layer of randomly oriented alumina nanofibers acts as the separation layer. When compared with traditional ceramic membranes fabricated using the aggregated nanoparticles as the separation layer, the new membrane supported a high flux while still maintaining good selectivity. The performance of the membrane was tested by filtering 60 nm latex spheres with the proposed application being to separate the pathogens, such as the common cold virus, from the human blood. Following this work Ke et al. proposed membrane for separation of bio-species in an industrial scale.

Recently, a new filter composed by coating a layer of alumina nanofiber on a microglass fiber backbone was developed to remove microbioilogical agents in aqueous environments. It is claimed that the novel alumina nanofibers filter exhibited potential for removal and retention of viral aerosols [11].

In this study, the functionalization of alumina nanofibers (ANF) are considered in three main application areas, i.e. additives in functional composites, catalysts and membranes; however, their performance in these specific areas remains beyond a scope of the work.

Methods and procedures for functionalization

Numerous recent efforts have been directed toward the fabrication of alumina and functionalized alumina 1D nanostructures to enhance their performance in currently existing applications and to open new prospective areas of applications. Many reports are devoted to the preparation of alumina nanostructures possessing well-defind dimensionalities such as nanoparticles, nanorods, nanowires, nanotubes, nanorings, nanobelts, etc., by variety of methods, such as sol-gel [2, 33, 34], electrospinning [35, 36], hydrothermal [37-39], flame aerosol method [40, 41], laser spinning [42], mercury mediated method [4], etc. The most typical methods like hydrothermal and sol-gel process include a hydrolysis of the starting aluminium compound and an aging of the sol over 24 h. Then the calcination process follows at elevated temperatures

typically ranging from 500 ºC to 1200 ºC for several hours. Thermal treating is not just time and energy consuming, but also risky of sintering nanostructures reshaping and decreasing the surface area. However, the shape and size of the components may strongly influence the properties of composite materials. In some cases, the shape–dependent effect of the components can be versatility used to perform a superior properties [43, 44]. Essentially, the shape can determine the specific crystal faces exposed on the surface of nanocrystals, and the number of atoms located at the corners and edges, as well as defects that are intrinsically more active for a structure-sensitive reaction.

Moreover, the properties of the composite nanostructures are crucially dependent on the interaction, i.e. wettability, between the components. Dispersion of the components in composites can be controlled by controlling their wettability. Thus, improving the wettability may result in homogeneous dispersion of the components. Usually the wettability of the components can be improved adding different metal oxides. For instance, it was shown [45] that addition of small amount of CeO_2 can improve the wettability of alumina-iron oxide surface. Moreover, cerium oxide is known to improve active sites dispersion and decrease the phase transition from active γ-Al_2O_3 to low surface α-Al_2O_3 [46].

Thus, functionalization of nanofibers by highly dispersed particles uniformly distributed over the fibrous supports is of high scientific and technological interest and plays a crucial role in many industrially important applications.

Recently, the well-defined nanostructures of alumina based composites with different dimensionalities have been obtained by a variety of solution chemistry routes [47, 48] and chemical vapor deposition techniques [24]. For example, Ivanov et al. covered alumina nanofibers by graphene layers by catalyst-free one-step chemical vapour deposition (CVD) process. The carbon nanotube/alumina nanocomposite with enhanced hardness and fracture toughness was successfully fabricated as well as by sol-gel process [49].

The solution chemistry routes allows to obtain materials with different morphologies by simply changing the initial parameters, such as composition of solution, temperature, heating way, etc. For instance, preparation of silica-modified-alumina with high surface area using

different sol-gel method was reported in [48]. Shutilov et al. [47] used an impregnation method to make a stable silica-doped alumina. Frost et al. [50] synthesized chromium doped boehmite nanofibers by modifying the so-called steam assisted wet-conversion process. However, the wet-chemical methods usually include long-lasting calcination step that may result in undesired sintering of the nanostructures.

Feng et al. [51, 52] recently developed a novel sol-flame method to synthesize hybrid structure of nanoparticle-decorated nanofibers. The sol-flame method combines the merits of sol-gel, dip coating and flame spray pyrolysis. Due to the short duration (few seconds) of high treatment flame treatment, the deposited nanoparticles were small and less aggregated.

Another possibility to escape from long-lasting calcination step, is combustion synthesis which provides high flash temperature at short time. The high temperature provides the decomposition of the precursors. However, the short duration of the process prevents surface diffusion of metal species and, therefore, their agglomeration and sintering.

Combustion synthesis is a suitable method for fabrication of different materials, such as oxides, carbides, nitrides, etc. Due to its short duration, simplicity and cost-effectiveness, combustion synthesis is widely used for the preparation of various nanostructured composites [53-55].

1.1.1 Wet-combustion deposition synthesis

Solution combustion is an attractive method for the synthesis of ceramics, intermetallics, composites, and functionally graded materials, which requires precise phase composition and high specific surface area [56]. Recently, different modes of combustion synthesis were developed to deposit/impregnate various compounds in nanostructural matrix. Varma and Mukasyan suggested to combine solution combustion synthesis with impregnation techniques to synthesize oxide based supported catalysts with a very high surface area (>200 m^2/g) [55, 57].

Aruna et al. incorporated SCS nanosized powders such as zirconia, alumina, ceria, yttria doped ceria, alumina–zirconia etc., into the metal (e.g. Ni) matrix during electrodeposition for the first time[58]. Colussi et al. prepared Pd- and Pt-based catalysts supported on CeO_2 and Al_2O_3 by traditional incipient wetness impregnation and solution combustion

synthesis. They found out that combustion synthesized Pd-based materials are much more active than the corresponding impregnated ones for propane and DME combustion [59].
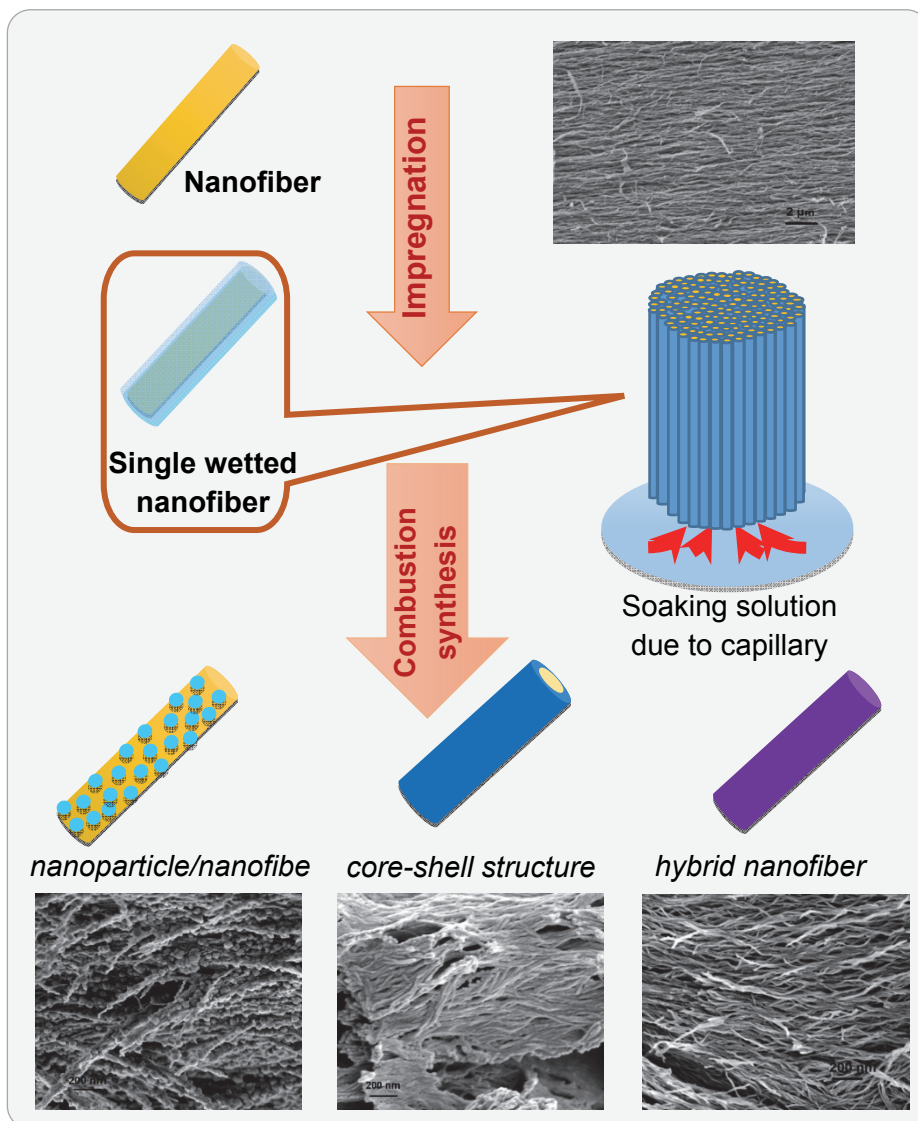
Figure 1.5 Schematic steps of the wet-combustion synthesis-deposition method to synthesize different composite nanofibers with corresponding SEM images.

In this work, a novel method was developed to fabricate various composite nanofibers in a controllable combustion mode in one step.

This method is a combination of sol-gel, dip coating and combustion synthesis and is schematically illustrated together with corresponding SEM images in Fig. 1.5.

Reactive solution containing metal nitrates as a precursor of desired metal and oxidizer, and an organic fuel were dropped to the bundle of nanofibers. Due to the nanoscale distance between the fibers, and therefore, high capillary forces, the reactive solution uniformly covers the entire surface of the nanofibers by dip coating in few minutes. After heating (400 ºC) in air, the wetted bundle self-ignites and burns. The combustion process itself last few seconds. Huge amount of gazes eliminating during the combustion process facilitates the fast cooling of the sample. Thus, the high temperature generated during the combustion process, short annealing time, and high cooling rate lead to a high nucleation rate and suppress grain growth; therefore, nanosized particles deposition is provided. Depending on the condition of combustion process and choices of materials (fuel type, salt of metal, nanofiber composition), different composite nanofibers can be obtained (Fig. 1.5).

1.1.2 Template assisted sol-gel deposition

Wet chemical deposition has been widely used for development of different nanostructures. In general, the sol-gel process is associated with a gel composed of sol particles. At first, colloidal suspension of desired particles (colloidal powders, alkoxide precursors, or nitrate precursors) is prepared from a solution of precursor molecules. Later, a template is immersed into the sol suspension, so that the sol aggregates on the template surface. In the case of mesoporous template, the sol is self-injected into the pores due to capillary forces. With an appropriate deposition time, the sol particles can fill the channels and form structures with a high aspect ratio. The schematic steps of this method is illustrated in Fig. 1.6. This technique offers some advantages of controlling the composition and nanostructure of the particles, an asset for eventual technological applications [60-63].
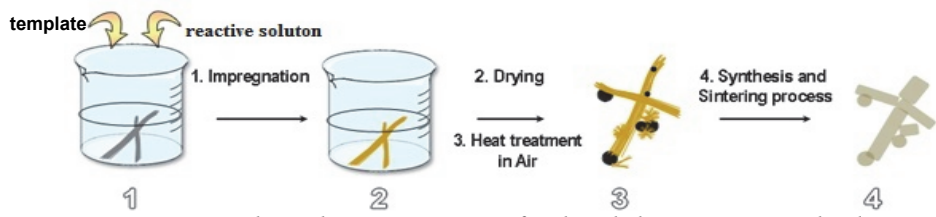
Figure 1.6 The schematic steps of sol-gel deposition method.

Objectives of the study

This research is motivated by the fact that in many cases the development of top-end products has limits set by the limited capabilities of currently existing materials. New horizons of products performance are directly connected with an intense need for innovative materials and processing routes to perform multiple functions. The overall objective for the research work is functionalization, optimization and production of nanofibers of alumina-based composites being beyond reach with conventional incremental materials development.

The main objective of this work is to produce one-dimensional fibrous structures for their further application as nanofillers in functional composites, catalysts support substrates and membranes via functionalization of the recently developed γ-alumina nanofibers by wet – combustion synthesis and sol-gel methods. It should be particularly emphasized that the material solution relays on designed Estonian unique product (inorganic nanofibers with ultra-high aspect ratio), which is complemented by functionalization of these materials. Therefore, the main activities of the work are:

1. Structural and thermal characterization of as-recieved alumina nanofibers.

2. Development of the novel method for functionalization of mesoporous nanostructures.

3. Functionalization of the alumina nanofibers of specified composition.

4. Optimization of the process parameters for controlling the morphology and composition of the final materials.

The sequence of the technological problems that should be solved during this work realization can be described as following:

— to investigate the thermal behavior of the precursor γ-alumina and its possible phase transformation during the heat treatment;

— to develop a strategy for homogeneous deposition of metal oxide onto alumina nanofibers keeping highly aligned structure of the network;

— to study the influence of process parameters (deposition method, fuel type, fuel-to oxidizer ratio, etc.) on the process pathway;

— to study the influence of the condition of the process on the chemical composition and morphology of the final product;

— to achieve a precise control over chemical composition, size and morphology of the doped material and its morphology.

The main part of this research is devoted to (i) development of the procedure for nanofibers network functionalization, and (ii) comprehensive characterization of the functionalized composite nanofibers.

Two main strategies, i.e. wet – combustion synthesis and sol-gel deposition, have been chosen for consideration because of their relative simplicity and possibility of scale-up for practical application.

2   EXPERIMENTAL AND MATERIALS

Precursor materials and designed systems

Recently developed self-aligned gamma-alumina nanofibers network (Fig. 2.1) with single-fiber diameter of 7±2 nm and high aspect ratio was functionalized by four different metals oxides: zirconium, aluminium, nickel and copper by the wet-combustion synthesis and the template assisted sol-gel deposition techniques.
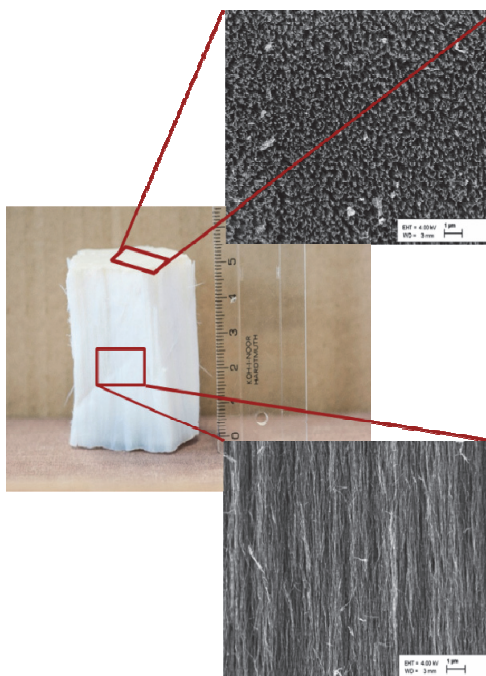
Figure 2.1 γ-alumina nanofibers network recently developed and produced in Estonia.

Nitrates of the abovementioned metals were used as oxidizers while two different organic compounds, i.e. glycine and urea, as fuels. The raw materials used are listed in Table 2.1 along with the description.

Table 2.1 Components for composites fibers processing

Compound	Purity, %	Supplier
Al(NO3)3*9H2O	>95	Merck
ZrO(NO3)2*xH2O	>99	Sigma-Aldrich
Ni(NO3)2*6H2O	≥98.5	Sigma-Aldrich
Cu(NO3)2*3H2O	≥98	Sigma-Aldrich
Glycine	≥99	Sigma
Urea	>99	Merck
Citric acid	≥99.5	Sigma-Aldrich

Four basic systems were designed in this work:

System of zirconia - alumina nanofibers

Zirconia is an important ceramic material, which exhibits enhanced corrosion, oxidation and abrasion resistance combined with relatively high fracture toughness and hardness[11]. ZrO_2 is also attractive as a catalyst and catalyst support [64]. Thus, fabrication of a novel ZrO_2-Al_2O_3 fibrous systems with controllable morphology and enhanced structural stability can exhibit a great potential for their commercial applications.

System of alumina - alumina nanofibers

Different polymorphs of alumina has different properties: γ-alumina has a high surface area, while losses its surface when heated. α-alumina is the only polymorph, which is stable above 1200 ºC. Cooperation of different polymorphs of alumina may results in exceptional properties. For instance, α-alumina/γ-alumina nanocomposite is believed to have a high specific surface and a high thermal structural stability.

Systems of nickel oxide – alumina nanofibers

Nickel aluminate spinel has received attention as a catalyst solid support due to its stability, strong resistance to acids and alkalis, and high melting point [30, 31]. Several authors pointed out that the $NiAl_2O_4$ spinel can be a promising precursor to develop suitable catalysts for hydrocarbons reforming [42, 65, 66].

System of copper oxide - alumina nanofibers

Copper oxide is a material of primary importance for heterogeneous catalysis and, therefore, attracts considerable research attention [67, 68]. Copper oxide and supported copper oxides are known

to be highly active for CO oxidation [69], catalytic incineration of organic compounds [70], etc. Preparation of the highly dispersed metal nanoparticles that uniformly cover oxide supports plays a crucial role in many industrially important catalytic applications. For instance, Acharyya et al. [71] demonstrated that Cu(II) oxide nanoparticles supported on $CuCr_2O_4$ spinel displayed excellent catalytic performance in the sustainable hydroxylation of benzene due to the morphology controlled ultra-small Cu(II)−spinel interaction, which has a great influence on the benzene hydroxylation reaction. Mo et al. reported that due to the high proportion of defect sites and highly dispersed Cu particles, Cu/SiO_2 exhibited good activities for water–gas shift reaction [49].

Functionalization of alumina nanofibers

Process of functionalization of alumina nanofiber network was carried out by two methods: combustion deposition and chemical vapor deposition as sketched in Fig. 2.2.

In both cases, an aqueous reactive solution was prepared to contain a metal precursor. To study an influence of the fuels on product composition and morphology, different fuels were added into the reactive solution. The prepared solutions were dropped onto the bundles of ANFs. After aging at an appropriate temperature and the specimens were placed into a furnace preheated to 400 ºC for 30 minutes.

Characterization of raw materials and final products

2.1.1 Phase analysis and microstructure examination

In this study, scanning electron microscopy (SEM Zeiss EVO MA 15, Germany) equipped with EDS with voltage of up to 20 kV and magnifications up to 50 kX was used for examination of the precursor materials and the functionalized final product. The samples were studied under different regimes, including secondary and backscattered electrons modes. The samples were coated with gold before examination.

Additionally, field emission scanning electron microscopy (FESEM S-4700, Hitachi, Japan) was used to characterize the microstructure of the product, which was beforehead coated with silver.
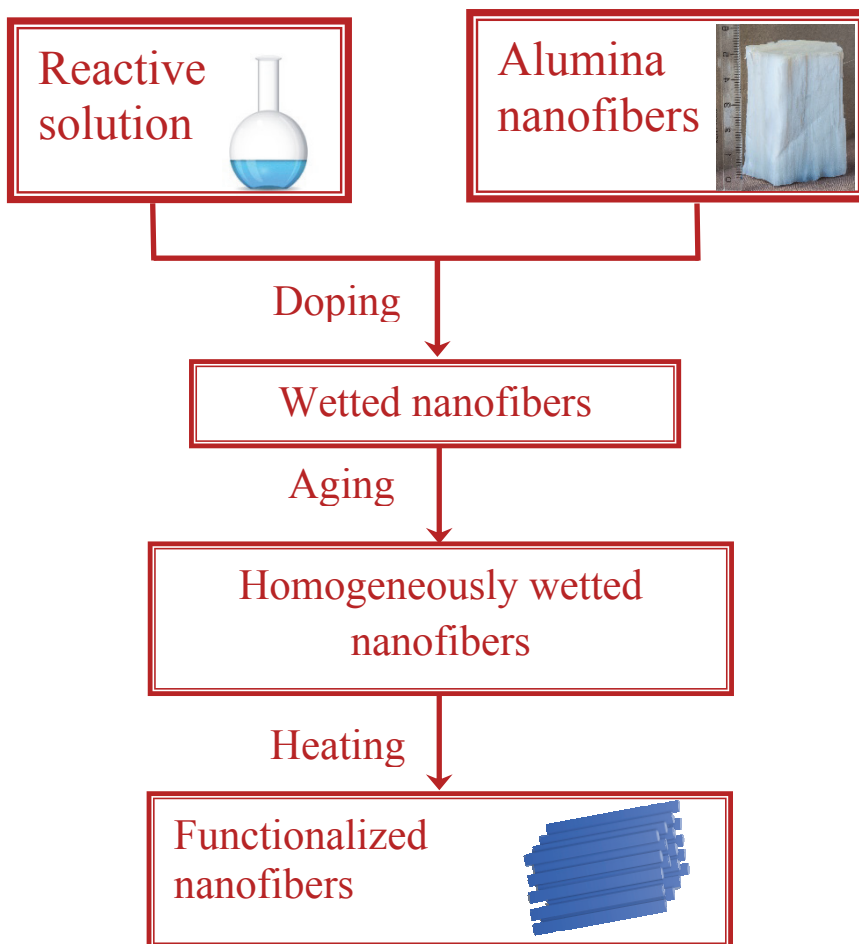
Figure 2.2 Schematic diagram of typical process of functionalization of alumina nanofibers

The morphology of the materials under investigation were evaluated using a JEOL 2100F transmission electron microscope (HRTEM) operating at 200KV and equipped with a field emission electron gun providing a point resolution of 0.19 nm. The microscope was coupled with an EDXS energy dispersive X-ray spectrometer (INCA x-sight, Oxford Instruments) for chemical elemental analysis.

The phase compositions of the powders mixtures and bulk samples were analyzed with the help of two X-ray diffractometers (XRDs): Philips PW3830 X-ray Generator, 4 kW, Cu-Anode and Siemens Bruker D5005 analyzer with CuKα –radiation. Samples were irradiated with CuKα radiation at 40 kV and 30 mA, in a θ – 2θ scan with a step size of 0.02° and a count time of 0.4 s.

2.1.2 In situ thermal and pyrometric analyses

The temperature-time history of the synthesis process is recorded by highly accurate MPAC IGAR 12-LO Digital 2-color pyrometers with fibre optic and a response time of 2ms. The pyrometer measures in the 2-color principle (ratio principle) in which two adjacent wavelength are used to calculate the temperature in the range from 300 up to 2200 ºC.

Differential scanning calorimetry (DSC) monitors heat effects associated with phase transitions and chemical reactions as a function of temperature. The kinetics of the processes were studied with simultaneous coupled thermal analysis (TG-DSC-FTIR) with STA449C "Jupiter" (Netzsch Gerätebau GmbH) and "Tensor-27" Fourier transform infrared spectroscopy FTIR spectrometer (Bruker Optics). Experiments were performed in synthetic dry air (21% O_2, balance nitrogen; Linde AGA) flow of 20 ml/min with heating and cooling rates of 10 ºC/min and maximal temperature of 1480 ºC. Alumina crucibles were used without a lid and an empty crucible was used as a DSC reference. Evolved gas analysis was performed by FTIR with automatic CO_2 bands compensation in transmission mode on a gas flow taken off the furnace via heated (300 ºC) and shielded capillary. Data collection and analysis were made using Proteus 6.1 (Netzsch Gerätebau GmbH) and OPUS 5.5 (Bruker Optics) software with a proprietary spectral database.

DSC analysis was used to study the thermal stability of the specimens. Meanwhile, to study the phase and microstructural changes occurred during the thermal treatment, the samples were heated and then quenched.

3 RESULTS AND DISCUSSION

Thermal analysis of the alumina nanofibers

Nanofibers possess unique properties as compared to the microscale fibers made of the same material. Properties of a product, even with a well-defined composition, are highly dependent on its crystalline structure, morphology, and microstructure of the polymorph. The investigations on the thermal treatment of alumina demonstrate that the thermal behavior strongly depends on phase composition and morphological parameters of the precursor material [Paper I]. In this work the thermal behavior of novel alumina was studied with simultaneous coupled thermal analysis (TG-DSC-FTIR). The investigation was carried out under synthetic dry air flow of 20 ml/min with heating rate of 10 ºC/min and maximal temperature of 1480 ºC.

The results of thermal analysis are displayed in Fig. 3.1. The total mass loss for the specimen during the whole scan is about 6 wt.% which has a clearly separated stage for mass loss over 1200 ºC. Eventually all mass losses are corresponding to water release, as no other gases were observed by FTIR (Fig.3.1(e)). There are endothermic effects at the beginning of heating which is explained by the evaporation of chemically and physically adsorbed water (Fig.3.1(c)). It might be assumed that unsaturated Al^{3+} linked to three oxygen atoms might lead to water dissociation. The cation Al^{3+} then binds to hydroxyl OH^-, and protons from hydrogen bonds localized on the neighboring Al-O-Al bridge. Both terminal OH^- groups and bridging groups forms (Fig.3.1(e)) can be suggested. An exothermal effect detected in the range 1200–1400 ◦C is slightly associated with release of additional water (∼0.61%). It is expected to be transformed into more stable α-Al_2O_3 over 1150 ◦C (Fig.3.1(d)). This transformation is accompanied with exothermic effect. The small release of water might be associated with this phase transformation, which release possible water traps inside the fibers and allows it to escape with gas [Paper I]. The terminal OH-groups are preferentially linked to tetrahedral Al and bridging groups are linking tetrahedral and octahedral Al^{3+} positions. This might explain thermal effects as the brutto-composition could be written in a form typical for γ-

based aluminas $Al_2O_3 \cdot xH_2O$ (x < 0.6) [Paper I]. Such hypothesis needs additional studies to be confirmed.

The XRD pattern did not reveal differences in spectra below 1200 ºC, expect some variations in intensities of α-Al_2O_3 (Fig.3.1(b)). At the highest temperature, however, most of the phase is already converted into alpha-alumina with sharp peaks, indicating good crystalline degree.
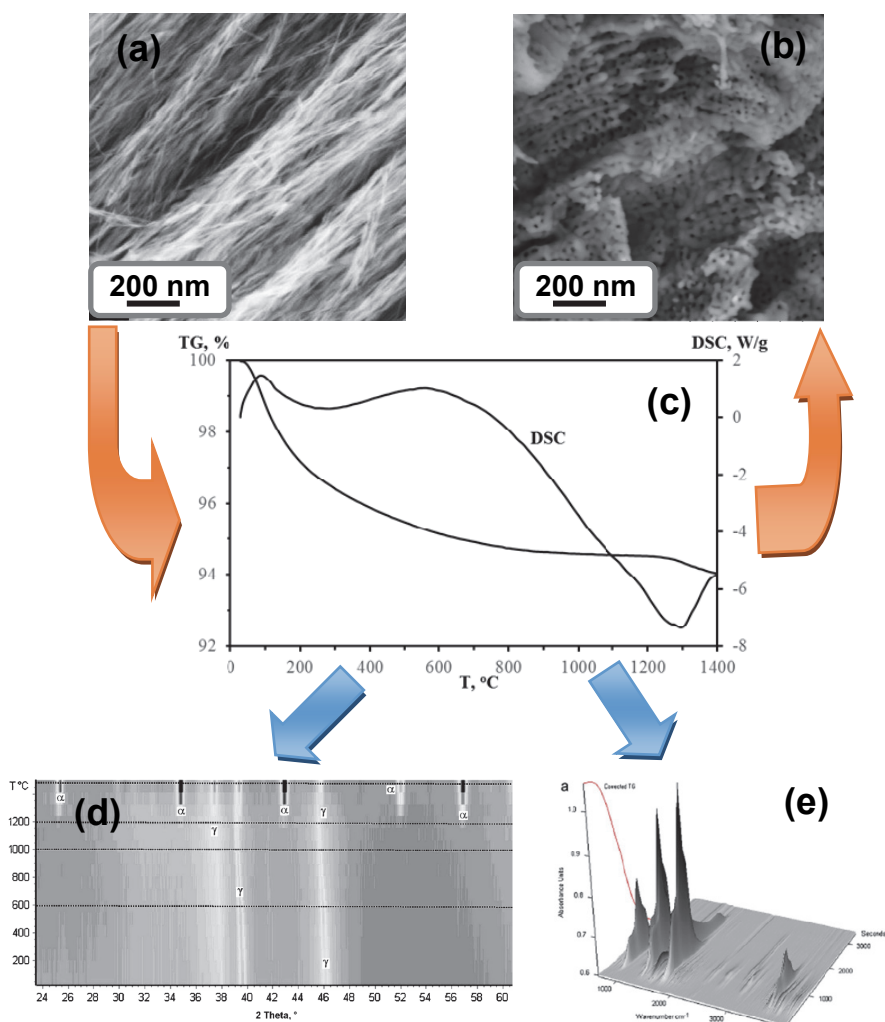

Figure 3.1 SEM images of (a) alumina nanofibers, (b) alumina nanofibers after heat treatment at 1480 ºC for 2 hours, (c) thermal analysis of alumina nanofibers, (b) FTIR spectra of the gases evolution, (c) XRD patterns made for different heat treatment temperatures.

The microstructural analyses showed that the fibers morphology changed drastically after heat treating them at 1200 ºC for 2 hours (Fig.3.1(a-b)).

System of zirconia-alumina nanofibers

In this work, a template assisted sol-gel deposition method has been used to fabricate ZrO_2-Al_2O_3 one-dimensional core-shell structured nanocomposite fibers. Alumina nanofibers have been dispersed in a distilled water by stick ultrasound, then zirconium (IV) oxynitrate has been added into the suspension. The obtained slurry has been dried at 95 ºC and heat treated at 600 ºC for decomposition of the nitrate. Figure 3.2 shows HRTEM images of ANF covered with 10 vol.% of zirconia.
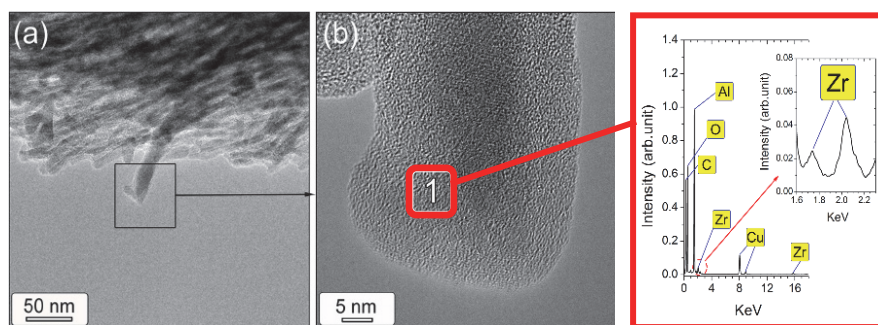
Figure 3.2 HRTEM and EDXS analysis of ANF-10 vol.% ZrO₂ nanocomposite with increased magnifications from (a) to (b) [Paper II].

XRD and EDXS analyses indicate that ANF substrate has a thin ZrO_2 coating with a low degree of crystallinity. Notably, no free exposed surface of alumina appears in the TEM visualization suggesting that there exists a strong interaction between the ZrO_2 coating and the core alumina.

Thus, the template assisted sol-gel deposition can be considered as a suitable method to fabricate 1D zirconia-alumina nanocomposite with core-shell structure using alumina nanofibers as templates. The decomposition mechanism of zirconium oxynitrate are proposed. An optimal heating way of preparation the mentioned nanocomposite by sol-gel method is described in [Paper II].

System of alumina - alumina nanofibers

In this chapter, deposition of a homogenous α- and γ-alumina thin film onto the surface of ANF is studied. For this purpose, the wet-combustion and template assisted sol-gel deposition techniques were used to deposit correspondingly α- and γ-alumina [Paper II, III].

3.1.1 Wet-combustion deposition method

Aluminum nitrate aqueous solution containing stoichiometric amount of urea was prepared and dropped onto ANFs followed by baking as it was described in 2.2 (Fig. 2.2).
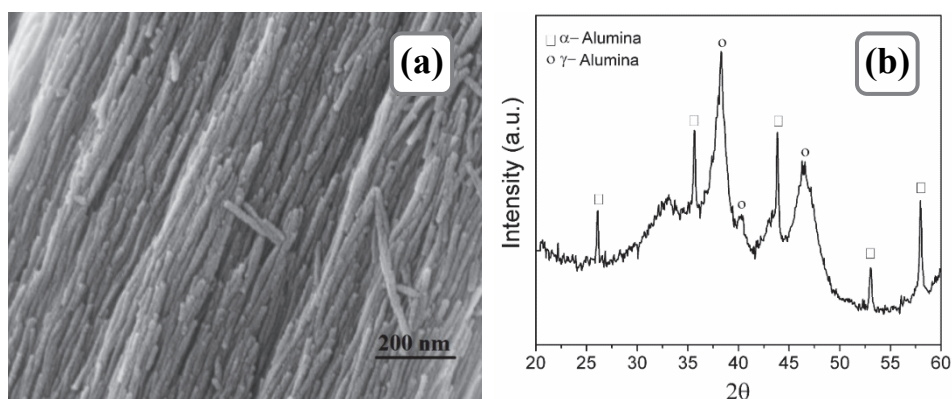

Figure 3.3 Characterization of combustion product: (a) FESEM micrograph, (b) X-ray diffraction pattern of as synthesized alumina/ANF sample.

XRD diffraction pattern of the obtained combustion product is depicted in Fig. 3.3(b). Two polymorphs of alumina, including α-Al_2O_3 and γ-Al_2O_3, are clearly recognized. To prove this hypothesis the original fibers have been tested under the similar combustion condition. The comparison of XRDs indicates a higher degree of crystallinity of the heat-treated sample, while no phase transformation of the γ-ANFs is detected [Paper III]. Therefore, no phase transformation of γ-Al_2O_3 takes place caused by solution combustion synthesis. Thus, the detected α-phase in the combustion product relates to the covering layer, leading to core-shell structure of γ-alumina – α-alumina composite nanofibers [59].

Microstructural analysis shows that α-alumina is deposited onto ANF homogeneously and continuously (Fig. 3.3(a)). It is remarkable that as obtained nanostructured composites has 1D structure. However, the

diameter of the fibers seems to be increased. For more details, see [Paper III].

3.1.2 Template assisted sol-gel method

Template assisted sol-gel deposition method have been used to fabricate alumina-alumina 1D nanocomposite with a core-shell structure. Alumina nanofibers have been dispersed in distilled water by stick ultrasound. Aluminium nitrate has been added into the obtained suspension. The obtained slurry has been dried at 95 ℃ and heat treated at 600 ℃ for decomposition of the nitrate.

The microstructure and chemical elemental analysis was studied by FESEM, HRTEM and EDXS correspondingly. According to HRTEM examination (Fig. 3.4(a)), ANF covered with Al2O3 consist two zones. FESEM examination proves that the fibers are covered homogeneously (Fig. 3.4(b)). The obtained nanostructured fibers have 1D structure, however, the length of the newly obtained nanocomposite nanofibers are shorter than the initial ANFs.
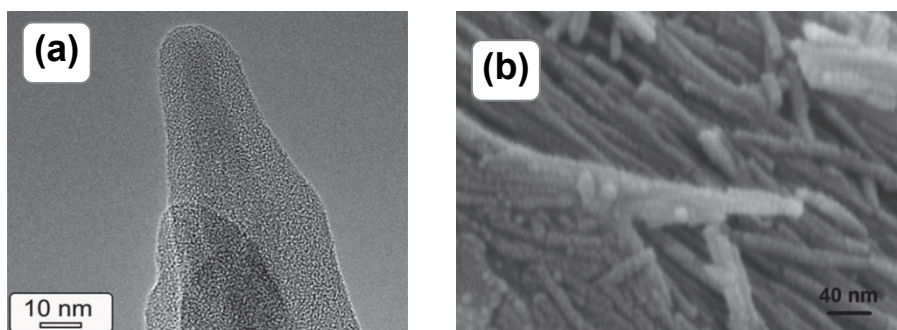
Figure 3.4 Fabricated Al$_2$O$_3$-ANF nanocomposite nanofibers: (a) HRTEM, (b) FESEM image.

Two preparation methods, namely wet-combustion synthesis and sol-gel deposition were used to synthesize alumina-alumina composite nanofiber. Comprehensive physicochemical characterization showed that α-alumina-γ-alumna composite with core-shell structure formed when wet-combustion synthesis was applied, while γ-alumina-γ-alumna composite nanofibers form when sol-gel synthesis method is applied.

System of nickel oxide-alumina nanofibers

Since the chemical and hydrothermal instability of γ-Al_2O_3 are still critical problem for catalytic applications in various chemical processes. Suitable support should be resistant to the high temperature, be able to maintain catalyst high dispersion, have good mechanical properties, high specific surface area, low reactivity, etc.

In this work 1D NiO-$NiAl_2O_4$ composite nanofibers were fabricated by combustion synthesis using network of the alumina nanofibers, described in chapter 3.1., nickel aluminate as precursors and different fuels (glycine, urea citric acid).

To prepare the reactive solution 5.7 g of nickel (II) nitrate hexahydrate [$Ni(NO_3)_2*6H_2O$] as a source of nickel and stoichiometric amount of fuels (1.6 g of glycine, 0.64 g of urea and 2.09 g of citric acid) were dissolved in 15 ml of deionized water. The further proceedings was described in 2.2 (Fig. 2.2).

To study influence of the fuels on the product composition and thus to better understand the combustion process mechanism to make it more controllable, the alumina nanofibers wetted by fuel-free solution of nickel nitrate, which was heated at the similar condition as others. The XRD pattern of the as synthesised product is presented in Fig.3.5 (e).

The peaks related to NiO along with traces of $NiAl_2O_4$ are detected. This composition is quite close to the composition of nickel nitrate – glycine – ANF system (Fig.3.5(d)) (see in Paper IV). It should be noted that due to large difference in the atomic scattering factors of Al and Ni, the lines of γ-Al_2O_3 are not identified. When urea is used as a fuel, only peak of NiO is detected in the XRD pattern (Fig.3.5(e-blue line)). While using citric acid, mainly nickel aluminate spinel with traces of nickel oxide is obtained (Fig.3.5(e-yellow line). This is supposed to be caused by more or less chelating character of the urea and citric acid correspondingly. However, more detailed investigation is needed to described the reason of such difference in product composition and describe the mechanism of the process.

The SEM images of the fabricated nanocomposites are demonstrates in Fig. 3.5(a-c). Homogenous composite nanofibers form when glycine is used (Fig. 3.5(a)). When citric acid is used, the as obtained nanocomposite consists of particles with less than 200 nm diameter along with nanofibers (Fig. 3.5(b)). The combustion product

obtained from nickel nitrate – citric acid – ANF system, consists of nanosheets with regular shape distributed on well aligned nanofibers (Fig. 3.5(c)). For the first time in the literature, $NiO/NiAl_2O_4/Al_2O_3$ nanofibers in diameter of <50 nm and high aspect ratio were produced using a novel single-step approach, while simultaneously avoiding additional calcination procedures. It was shown that utilizing different fuels it is possible to control product composition.

More details about the microstructures and thermal stability of the obtained production can be find in Paper IV.

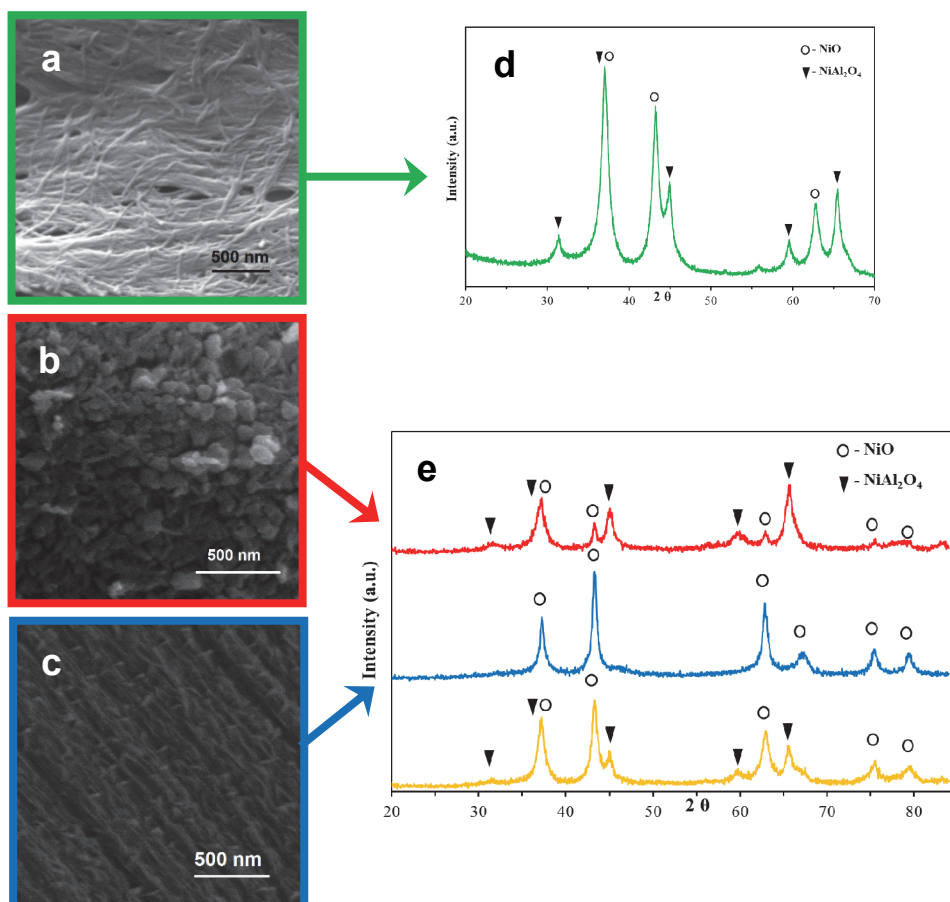*Figure 3.5 SEM images of the combustion products of (a) nickel nitrate – glycine –ANF, (b) nickel nitrate – citric acid –ANF, (c) nickel nitrate – urea –ANF systems, and XRD patterns of the combustion product of (d) nickel nitrate - glycine - ANF; (e) nickel nitrate –ANF (yellow line), nickel nitrate – urea –ANF (blue line) and nickel nitrate – citric acid – ANF (red line) systems.*

System of copper oxide - alumina nanofibers

Many research efforts are related to synthesize the copper oxide powder by the solution combustion method [72-74]. In the present study, the wet-combustion synthesis deposition technique was used to deposit copper oxide nanoparticles onto the support of self-aligned network of alumina nanofibers. To obtain continuously and uniformly deposited nanoparticles on the support with the shape of nanofibers, aqueous solutions of 7g of copper nitrate and different amount of urea or glycine as the fuels are dropped onto 2g of alumina nanofibers (ANF) block and heated in a muffle furnace preheated to 400 ºC for 30 min. Fig.3.6 specifies the composition of the initial solution prepared to drop onto ANF.
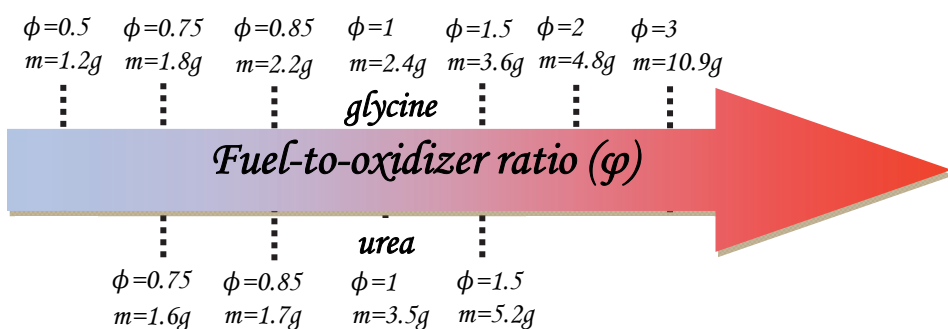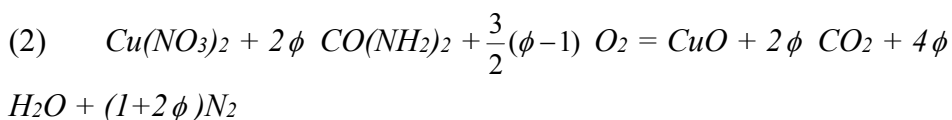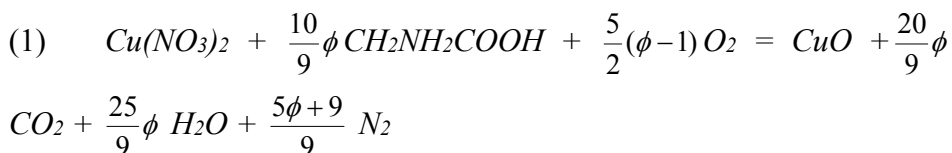

Figure 3.6 The amount of fuel added in reactive solution.

The mechanism of this combustion impregnation process as well as the influence of the fuel type and amount on the composition and morphology of the combustion product is thoroughly studied. More details can be found in [Paper V].

The DTA-TGA results of the copper nitrate –fuel stoichiometric mixture on ANF are shown in Fig.3.7. The stoichiometric ($\phi = 1$) combustion reaction of both glycine and urea systems are represented by the following equations ((1) and (2)):

$$(1) \quad Cu(NO_3)_2 \ + \ \frac{10}{9}\phi\, CH_2NH_2COOH \ + \ \frac{5}{2}(\phi-1)\, O_2 \ = \ CuO \ +\frac{20}{9}\phi$$

$$CO_2 + \frac{25}{9}\phi\, H_2O + \frac{5\phi+9}{9}\, N_2$$

$$(2) \quad Cu(NO_3)_2 + 2\phi\, CO(NH_2)_2 + \frac{3}{2}(\phi-1)\, O_2 = CuO + 2\phi\, CO_2 + 4\phi$$

$$H_2O + (1+2\phi)N_2$$

where ϕ is fuel-to-oxidizer ratio ($\phi = 1$ implies that all oxygen required for complete combustion of a fuel derives from the oxidizer; while $\phi > 1$ (<1) implies fuel-rich (or lean) conditions).
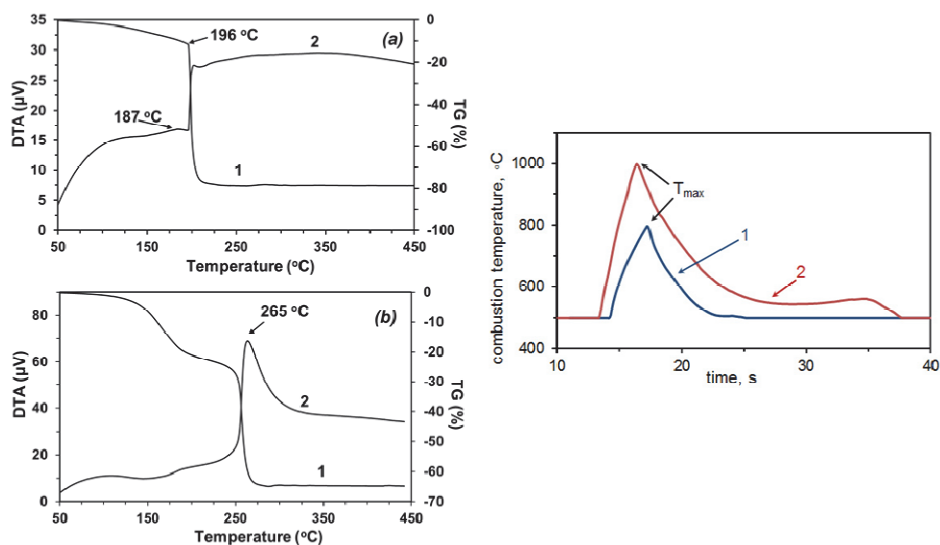

Figure 3.7 In-situ study of combustion process: TG-DTA results for (a) copper nitrate – glycine - ANF ($\phi_{gly}=1$) system, (b) copper nitrate – urea –ANF ($\phi_{ur}=1$) system, and (c) temperature-time history of the combustion in stoichiometric ($\phi=1$) iron nitrate - glycine - ANF system with (curve 1) and iron nitrate - urea - ANF (curve 2).

Figure 3.7(a) demonstrates the DTA-TGA response of a cupper nitrate–glycine stoichiometric ($\phi = 1$) precursor soaked in ANF. The glycine fuel batch shows low weight loss of 11 wt.% up to 180 ºC that is accompanied by a slight endothermic effect. This weight loss is very likely due to dehydration of copper nitrate hydrate. Subsequently, a slight exothermal peak at 187 ºC is due to the ignition of the combustion process. This stage is followed by a dramatic mass loss (77 wt.% of initial value) and a pronounced change in the base line at 196 ºC due to release of the gases. These temperature intervals are well corresponding to the region of precursor's decompositions and the mixtures self-ignition temperature (T_{ig}) as discussed by Kumar et al [72].

The DTA-TGA curves for the stoichiometric reactive mixture of copper nitrate-urea obtained under the same condition as for the previous

system are presented in Fig. 3.7b. The first stage of mass loss takes place at a temperature range from 80 ºC up to 170 ºC with the endothermic effect. In this stage the endothermic effect is associated with decomposition of copper nitrate hydrate, hydrate water emission [72] and decomposition of urea [75]. The second stage of mass loss is recorded at ~200 ºC accompanying a weak exothermic effect. A sharp exothermic peak in the temperature range of 250-280 ºC and corresponding weight loss (44 wt.%) relate to the combustion reactions among the decomposed products of urea and the nitrate.

X-ray diffraction analyses shows that in both systems copper (II) oxide is synthesized-deposited at fuel-lean and stoichiometric ($\phi \leq 1$) reactive mixtures. At fuel-reach reactive mixtures reduced copper (I) oxide along with copper (II) oxide is determined.
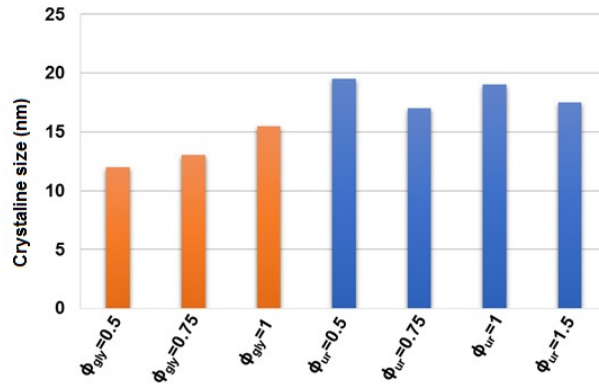

Figure 3.8 The size of the crystallites of the obtained copper oxide.

The size of the crystallites was measured by X-ray diffraction. It can be seen in Fig.3.8, that the crystal size of the obtained CuO depends on the fuel type. It is obvious that the crystal size of as-synthesized CuO is relatively small when glycine is used as a fuel. This is caused by lower maximum temperature developed during the combustion process (~800 ºC) in the glycine system ($\phi_{gly}= 1$) as compared to the urea system ($\phi_{ur}=1$) (1000 ºC) (Fig.3.7(c)). Moreover, the duration of the combustion process is longer when urea is used as a fuel, which provides the increase of the particle size during the process. In the glycine – copper nitrate system, the particle size increases with increasing the glycine-to-oxidizer ratio from 0.5 to 1.

Figures 3.9 and 3.10 represent the SEM micrographs of as-synthesized-deposited product on ANFs obtained from various fuel containing batches of urea and glycine, respectively. At the fuel-lean glycine system, copper oxide with a fine particle size (<50 nm) is deposited quite homogeneously on the surface of ANFs. However, with increase in the amount of glycine the particle size of the deposited copper oxide increases, which can be explained by the maximum combustion temperature increasing with φ growth.
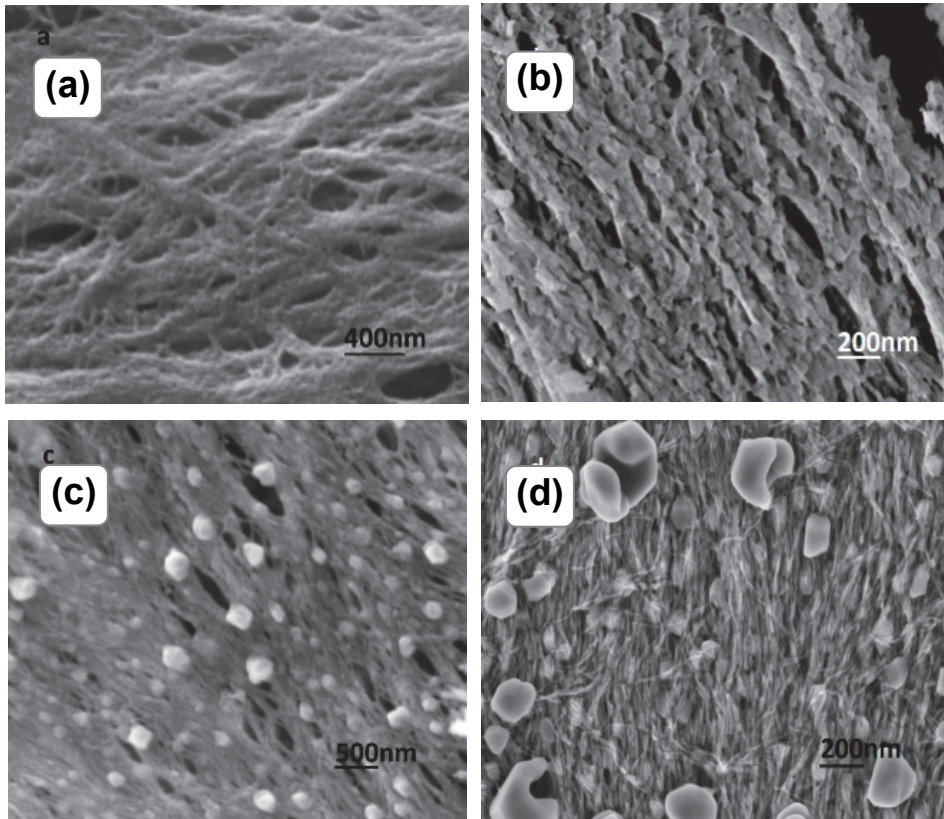
Figure 3.9 SEM micrographs of as fabricated combustion impregnation product using different amount of glycine (a) ϕ_{gly}=0.75, (b) 0.85, (c) 1, (d)2.

The deposited particles are quite inhomogeneous in size and morphology when urea is used as the fuel. Increasing the amount of urea leads to the formation of particles with two characteristic sizes: up to 30 nm ("hugging" the fibers) and 100-200 nm (disperse all over the bundle

of fibers) can be distinguished (Fig. 3.10). In the fuel-rich systems the size of particles increases.
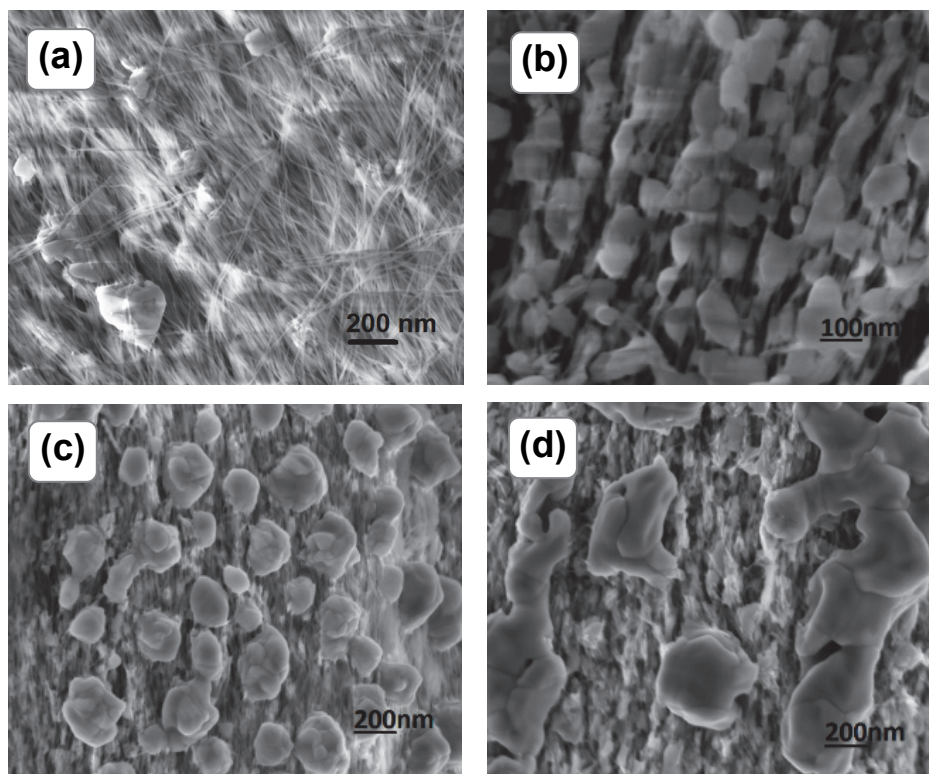
Figure 3.10 SEM micrographs of as fabricated combustion impregnation product using different amount of urea ϕ_{ur}= (a) 0.5, (b) 0.75, (c) 1, (d) 1.5.

Thus, the feasibility of the synthesis of copper (II) oxide by simple and cost-effective heterogeneous combustion deposition using precursors of copper nitrate, glycine and urea dissolved in aqueous, and furthermore introduced onto support of the alumina nanofibers network has been shown. The mechanisms of the combustion process of both systems containing glycine and urea as fuels are investigated. Effect of the fuel type and fuel-to-oxidizer ratio on the composition and structure of the combustion product is demonstrated. The finest crystallite size of CuO was obtained with glycine in the fuel-lean mixtures. The crystallite size of CuO is higher when urea-containing mixtures are used as compared to glycine containing mixture.

CONCLUSIONS

In this work, one-dimensional composite nanofibers are prepared by 2 methods without further calcination. The network of self-aligned alumina nanofibers of a huge aspect ratio is functionalized by different oxides (i.e, ZrO_2, Al_2O_3, NiO and CuO) with the help of a novel single-step template-assisted wet-combustion synthesis and sol-gel synthesis deposition methods. From these studies the following conclusions are obtained:

1. The defected structure of alumina nanofibers contains unsaturated Al^{3+} binded to hydroxyl groups and protons form hydrogen bonds localized on the neighboring Al-O-Al bridge. Transformation of γ-phase into α-phase takes place at 1200℃ following by substantial change in morphology of the nanofibers network.

2. A novel template-assisted wet-combustion method based on sol-gel, dip coating and combustion synthesis is developed. This never-available-before technique is flexible, one-step process for production of mesoporous nanocomposites with tailored phase composition and morphology. It is shown that template-assisted sol-gel method might be an alternative approach to functionalize alumina nanofibers.

3. Alumina nanofibers are functionalized with different oxides to produce highly-aligned one-dimensional nanostructures of less than 50 nm in diameter avoiding additional procedures of calcination.

> *ZrO_2-Al_2O_3 system*: the precursor (zirconium oxynitrate) is completely decomposed to oxide over 600 ℃. As a result a continuous, homogeneous nanolayer of zirconia is deposited onto ANF.

> *Al_2O_3-Al_2O_3 system*: alumina nanolayer is homogeneously deposited onto ANFs. Wet-combustion route allows deposition of α-Al_2O_3 on γ-Al_2O_3 with a core-shell structure using urea as a fuel. Urea catalyses the formation of α- phase formation in combustion mode.

> *NiO-Al_2O_3 system*: for the first time, NiO-$NiAl_2O_4$-Al_2O_3 composite nanofibers with less than 50 nm in diameter and high aspect ratio of 10^6 is produced in a single-step process. The ratio

of the component is controlled by changing the fuels (glycine, citric acid, urea).

> *CuO-ANF system*: the particle size of the deposited CuO is highly influenced by the fuel type and amount. The crystallite size of CuO is larger when the urea-containing mixtures are used as compared to the glycine containing mixture. The deposition of pure CuO and CuO with traces of mixed valence copper oxide phases and metallic copper was demonstrated by varying the fuel and fuel to oxidizer ratio.

4. The chemical composition and morphology of the final product can be controlled by changing the initial parameters, mainly the content of the reactive solution. Thus, considering the requirements for the final product, the optimum material can be obtained by choosing appropriate processing parameters.

The scientific novelty and practical importance

The thermal behavior of the newly developed alumina nanofibers network, which has been recently produced in Estonia, was thoroughly studied. Besides release of water, no other phase transformation was found below 1200–1250 ∘C. The surface morphology of the fibers changed substantially, because of the peculiarities of water release together with $\gamma \rightarrow \alpha$ transformation in a wide temperature range.

The novel controllable single-step wet-combustion synthesis-deposition method was suggested to functionalize nano-objects. The influence of the process conditions on the process mechanism and final product morphology and structure was studied.

The composite nanofibers with core-shell structure were produced by sol-gel and wet-combustion synthesis-deposition methods without additional calcination step for different application.

At the very first time, NiO-$NiAl_2O_4$, $NiAl_2O_4$-Al_2O_3 and NiO-Al_2O_3 nanofibers with the tailored structured were fabricated by wet-combustion method.

REFERENCES

1. Wang, Y.; Li, W.; Xia, Y.; Jiao, X.; Chen, D., Electrospun flexible self-standing [gamma]-alumina fibrous membranes and their potential as high-efficiency fine particulate filtration media, *Journal of Materials Chemistry A,* 2014, 2 (36), 15124-15131.
2. Teoh, G. L.; Liew, K. Y.; Mahmood, W. A. K., Synthesis and characterization of sol–gel alumina nanofibers, *Journal of Sol-Gel Science and Technology,* 2007, 44 (3), 177-186.
3. Shen, S.-C.; Ng, W. K.; Zhong, Z.-Y.; Dong, Y.-C.; Chia, L.; Tan, R. B. H., Solid-Based Hydrothermal Synthesis and Characterization of Alumina Nanofibers with Controllable Aspect Ratios, *Journal of the American Ceramic Society,* 2009, 92 (6), 1311-1316.
4. Yang, Q.; Deng, Y.; Hu, W., Synthesis of alumina nanofibers by a mercury-mediated method, *Ceramics International,* 2009, 35 (1), 531-535.
5. Planning and Research Office, N., A Vision of Materials Science in the Year 2020, Ed. Planning and Research Office, 2007.
6. Singleton, A. H.; Oukaci, R., Highly active fischer-tropsch catalyst having increased thermal stability. In Google Patents: 2003.
7. Wefers, K.; Misra, C., Oxides and hydroxides of aluminum, ALCOA: Pennsylvania, USA, 1987, vol. 19.
8. Zhang, Z. Model study of platinum nanoparticle interactions with γ-alumina single crystal supports, University of Pittsburgh, 2012.
9. Noordin, M. R.; Liew, K. Y., *Synthesis of Alumina Nanofibers and Composites, Nanofibers*. InTech: 2010.
10. Peterson, E. J.; DeLaRiva, A. T.; Lin, S.; Johnson, R. S.; Guo, H.; Miller, J. T.; Hun Kwak, J.; Peden, C. H. F.; Kiefer, B.; Allard, L. F.; Ribeiro, F. H.; Datye, A. K., Low-temperature carbon monoxide oxidation catalysed by regenerable atomically dispersed palladium on alumina, *Nat Commun,* 2014, 5.
11. Liu, E. Synthesis of one-dimensional nanocomposites based on alumina nanofibres and their catalytic applications, Queensland University of Technology, 2011.

12. Shen, S. C.; Ng, W. K.; Chen, Q.; Zeng, X. T.; Chew, M. Z.; Tan, R. B. H., Solid-Phase Low Temperature Steam-Assisted Synthesis of Thermal Stable Alumina Nanowires, *Journal of Nanoscience and Nanotechnology,* 2007, 7 (8), 2726-2733.

13. Chowdhury, M. B. I.; Sui, R.; Lucky, R. A.; Charpentier, P. A., One-Pot Procedure to Synthesize High Surface Area Alumina Nanofibers Using Supercritical Carbon Dioxide, *Langmuir,* 2010, 26 (4), 2707-2713.

14. Saunders, Z.; Noack, C. W.; Dzombak, D. A.; Lowry, G. V., Characterization of engineered alumina nanofibers and their colloidal properties in water, *Journal of Nanoparticle Research,* 2015, 17 (3), 1-14.

15. Grodnensky, I., Alumina nanofiber reinforced cement-based materials and method for producing same. In Google Patents: 2015.

16. Voltsihhin, N.; Rodríguez, M.; Hussainova, I.; Aghayan, M., Low temperature, spark plasma sintering behavior of zirconia added by a novel type of alumina nanofibers, *Ceramics International,* 2014, 40 (5), 7235-7244.

17. Chevalier, J.; Gremillard, L., Ceramics for medical applications: A picture for the next 20 years, *Journal of the European Ceramic Society,* 2009, 29 (7), 1245-1255.

18. Zhang, L.; Zhao, Z.; Zheng, J.; Bai, H.; Wu, J., Microstructures and multi-toughening of ZrO_2 nano-micron fibers self-toughening Al_2O_3 ceramics from in-situ growth in the melts produced by combustion synthesis, *Key Engineering Materials,* 2007, 336-338, 2260-2263.

19. Dudkin, B. N.; Bugaeva, A. Y.; Zainullin, G. G.; Filippov, V. N., Corundum/lanthanum hexaaluminate/alumina nanofiber ceramic composite, *Inorganic Materials,* 2010, 46 (4), 445-448.

20. Santos-Beltrán, A.; Gallegos-Orozco, V.; Estrada-Guel, I.; Bejar-Gómez, L.; Espinosa-Magaña, F.; Miki-Yoshida, M.; Martínez-Sánchez, R., TEM characterization of $Al–C–Cu–Al_2O_3$ composites produced by mechanical milling, *Journal of Alloys and Compounds,* 2007, 434–435, 514-517.

21. Beguin, B.; Garbowski, E.; Primet, M., Stabilization of alumina toward thermal sintering by silicon addition, *Journal of Catalysis,* 1991, 127 (2), 595-604.

22. Chen, X.; Liu, Y.; Niu, G.; Yang, Z.; Bian, M.; He, A., High temperature thermal stabilization of alumina modified by lanthanum species, *Applied Catalysis A: General,* 2001, 205 (1–2), 159-172.

23. Iler, R. K., Effect of Silica on Transformations of Fibrillar Colloidal Boehmite and Gamma Alumina, *Journal of the American Ceramic Society,* 1964, 47 (7), 339-341.

24. Ivanov, R.; Hussainova, I.; Aghayan, M.; Drozdova, M.; Pérez-Coll, D.; Rodríguez, M. A.; Rubio-Marcos, F., Graphene-encapsulated aluminium oxide nanofibers as a novel type of nanofillers for electroconductive ceramics, *Journal of the European Ceramic Society,* 2015, 35 (14), 4017-4021.

25. Drozdova, M.; Hussainova, I.; Pérez-Coll, D.; Aghayan, M.; Ivanov, R.; Rodríguez, M. A., A novel approach to electroconductive ceramics filled by graphene covered nanofibers, *Materials & Design,* 2016, 90, 291-298.

26. Descorme, C.; Taha, R.; Mouaddib-Moral, N.; Duprez, D., Oxygen storage capacity measurements of three-way catalysts under transient conditions, *Applied Catalysis, A: General* 2002, 223 (1–2), 287-299.

27. Torncrona, A.; Sterte, J.; Otterstedt, J.-E., Preparation of a novel fibrous catalyst support, *Journal of Materials Chemistry,* 1995, 5 (1), 121-126.

28. Guo, J.; Lou, H.; Zhao, H.; Chai, D.; Zheng, X., Dry reforming of methane over nickel catalysts supported on magnesium aluminate spinels, *Applied Catalysis A: General,* 2004, 273 (1–2), 75-82.

29. Ribeiro, N. F. P.; Neto, R. C. R.; Moya, S. F.; Souza, M. M. V. M.; Schmal, M., Synthesis of NiAl2O4 with high surface area as precursor of Ni nanoparticles for hydrogen production, *International Journal of Hydrogen Energy,* 2010, 35 (21), 11725-11732.

30. Shih, K.; Leckie, J. O., Nickel aluminate spinel formation during sintering of simulated Ni-laden sludge and kaolinite, *Journal of the European Ceramic Society,* 2007, 27 (1), 91-99.

31. Johansson, M.; Mattisson, T.; Lyngfelt, A., Use of NiO/NiAl2O4 Particles in a 10 kW Chemical-Looping Combustor, *Industrial & Engineering Chemistry Research,* 2006, 45 (17), 5911-5919.

32. Ke, X. B.; Zhu, H. Y.; Gao, X. P.; Liu, J. W.; Zheng, Z. F., High-Performance Ceramic Membranes with a Separation Layer of Metal Oxide Nanofibers, *Advanced Materials,* 2007, 19 (6), 785-790.

33. Srivastava, V.; Weng, C. H.; Singh, V. K.; Sharma, Y. C., Adsorption of Nickel Ions from Aqueous Solutions by Nano Alumina: Kinetic, Mass Transfer, and Equilibrium Studies, *Journal of Chemical & Engineering Data,* 2011, 56 (4), 1414-1422.

34. Sharma, Y. C.; Srivastava, V.; Upadhyay, S. N.; Weng, C. H., *Ind. Eng. Chem. Res.,* 2008, 47, 8095.

35. Yu, H.; Guo, J.; Zhu, S.; Li, Y.; Zhang, Q.; Zhu, M., Preparation of continuous alumina nanofibers via electrospinning of PAN/DMF solution, *Materials Letters,* 2012, 74, 247-249.

36. Milanović, P.; Dimitrijević, M.; Jančić Heinemann, R.; Rogan, J.; Stojanović, D. B.; Kojović, A.; Aleksić, R., Preparation of low cost alumina nanofibers via electrospinning of aluminium chloride hydroxide/poly (vinyl alcohol) solution, *Ceramics International,* 2013, 39 (2), 2131-2134.

37. Tang, B.; Ge, J.; Zhuo, L.; Wang, G.; Niu, J.; Shi, Z.; Dong, Y., A Facile and Controllable Synthesis of γ-Al2O3 Nanostructures without a Surfactant, *European Journal of Inorganic Chemistry,* 2005 (21), 4366-4369.

38. Zhao, Y.; Frost, R. L.; Martens, W. N.; Zhu, H. Y., Growth and Surface Properties of Boehmite Nanofibers and Nanotubes at Low Temperatures Using a Hydrothermal Synthesis Route, *Langmuir,* 2007, 23 (19), 9850-9859.

39. Lu, C. L.; Lv, J. G.; Xu, L.; Guo, X. F.; Hou, W. H.; Hu, Y.; Huang, H., Crystalline nanotubes of γ-AlOOH and γ-Al 2 O 3 : hydrothermal synthesis, formation mechanism and catalytic performance, *Nanotechnology,* 2009, 20 (21), 215604.

40. Zhou, J.; Deng, S. Z.; Chen, J.; She, J. C.; Xu, N. S., Synthesis of crystalline alumina nanowires and nanotrees, *Chemical Physics Letters,* 2002, 365 (5–6), 505-508.

41. Guo, B.; Yim, H.; Luo, Z.-P., Formation of alumina nanofibers in carbon-containing coflow laminar diffusion flames, *Journal of Aerosol Science,* 2009, 40 (4), 379-384.

42. Chen, J.; Xu, L.; Li, W.; Gou, X., α-Fe2O3 Nanotubes in Gas Sensor and Lithium-Ion Battery Applications, *Advanced Materials,* 2005, 17 (5), 582-586.

43. Mou, X.; Wei, X.; Li, Y.; Shen, W., Tuning crystal-phase and shape of Fe_2O_3 nanoparticles for catalytic applications, *CrystEngComm,* 2012, 14 (16), 5107-5120.

44. Liotta, L. F.; Wu, H.; Pantaleo, G.; Venezia, A. M., Co_3O_4 nanocrystals and Co_3O_4-MO_x binary oxides for CO, CH_4 and VOC oxidation at low temperatures: a review, *Catalysis Science & Technology,* 2013, 3 (12), 3085-3102.

45. Liu, Y.; Sun, D., Effect of CeO_2 doping on catalytic activity of Fe_2O_3/γ-Al_2O_3 catalyst for catalytic wet peroxide oxidation of azo dyes, *Journal of Hazardous Materials,* 2007, 143 (1–2), 448-454.

46. Prakash, A. S.; Shivakumara, C.; Hegde, M. S., Single step preparation of CeO_2/$CeAlO_3$/γ-Al_2O_3 by solution combustion method: Phase evolution, thermal stability and surface modification, *Materials Science and Engineering: B,* 2007, 139 (1), 55-61.

47. Shutilov, A. A.; Zenkovets, G. A.; Tsybulya, S. V.; Gavrilov, V. Y., Effect of silica on the stability of the nanostructure and texture of fine-particle alumina, *Kinetics and Catalysis,* 2012, 53 (1), 125-136.

48. Timken, H. K. C., Homogeneous modified-alumina fischer-tropsch catalyst supports, In Google Patents: 2005.

49. Mo, L.; Kawi, S., An in situ self-assembled core-shell precursor route to prepare ultrasmall copper nanoparticles on silica catalysts, *Journal of Materials Chemistry A,* 2014, 2 (21), 7837-7844.

50. Yang, J.; Frost, R. L.; Yuan, Y., Synthesis and characterization of chromium doped boehmite nanofibres, *Thermochimica Acta,* 2009, 483 (1–2), 29-35.

51. Feng, Y.; Cho, I. S.; Cai, L.; Rao, P. M.; Zheng, X., Sol-flame synthesis of hybrid metal oxide nanowires, *Proceedings of the Combustion Institute,* 2013, 34 (2), 2179-2186.

52. Feng, Y.; Cho, I. S.; Rao, P. M.; Cai, L.; Zheng, X., Sol-Flame Synthesis: A General Strategy To Decorate Nanowires with Metal Oxide/Noble Metal Nanoparticles, *Nano Letters,* 2013, 13 (3), 855-860.

53. Zavyalova, U.; Girgsdies, F.; Korup, O.; Horn, R.; Schlögl, R., Microwave-Assisted Self-Propagating Combustion Synthesis for Uniform Deposition of Metal Nanoparticles on Ceramic Monoliths, *The Journal of Physical Chemistry C,* 2009, 113 (40), 17493-17501.

54. Biamino, S.; Fino, P.; Fino, D.; Russo, N.; Badini, C., Catalyzed traps for diesel soot abatement: In situ processing and deposition of perovskite catalyst, *Applied Catalysis B: Environmental,* 2005, 61 (3–4), 297-305.

55. Mukasyan, A. S.; Epstein, P.; Dinka, P., Solution combustion synthesis of nanomaterials, *Proceedings of the Combustion Institute,* 2007, 31 (2), 1789-1795.

56. Varma, A.; Rogachev, A. S.; Mukasyan, A. S.; Hwang, S., Combustion Synthesis of Advanced Materials: Principles and Applications, In *Advances in Chemical Engineering*, James, W., Ed. Academic Press: 1998; 24, 79-226.

57. Dinka, P.; Mukasyan, A. S., In Situ Preparation of Oxide-Based Supported Catalysts by Solution Combustion Synthesis, *The Journal of Physical Chemistry B,* 2005, 109 (46), 21627-21633.

58. Aruna, S. T.; Mukasyan, A. S., Combustion synthesis and nanomaterials, *Current Opinion in Solid State and Materials Science,* 2008, 12 (3–4), 44-50.

59. Colussi, S.; Gayen, A.; Llorca, J.; de Leitenburg, C.; Dolcetti, G.; Trovarelli, A., Catalytic Performance of Solution Combustion Synthesized Alumina- and Ceria-Supported Pt and Pd Nanoparticles for the Combustion of Propane and Dimethyl Ether (DME), *Industrial & Engineering Chemistry Research,* 2012, 51 (22), 7510-7517.

60. Zhuiykov, S, Structural and chemical modification of semiconductor nanocrystals, *Nanostructured Semiconductor Oxides for the Next Generation of Electronics and Functional Devices*, Woodhead Publishing: 2014, 50-94.

61. Lu, J. G.; Chang, P.; Fan, Z., Quasi-one-dimensional metal oxide materials—Synthesis, properties and applications, *Materials Science and Engineering: R: Reports,* 2006, 52 (1–3), 49-91.

62. Ogihara, H.; Sadakane, M.; Nodasaka, Y.; Ueda, W., Shape-Controlled Synthesis of ZrO_2, Al_2O_3, and SiO_2 Nanotubes Using Carbon Nanofibers as Templates, *Chemistry of Materials,* 2006, 18 (21), 4981-4983.

63. Niederberger, M., Nonaqueous Sol–Gel Routes to Metal Oxide Nanoparticles, *Accounts of Chemical Research,* 2007, 40 (9), 793-800.

64. Yamaguchi, T., Application of ZrO_2 as a catalyst and a catalyst support, *Catalysis Today,* 1994, 20 (2), 199-217.

65. Bhattacharyya, A.; Chang, V. W., CO_2 Reforming of Methane to Syngas: Deactivation Behavior of Nickel Aluminate Spinel Catalysts, *Studies in Surface Science and Catalysis*, Delmon, B.; Froment, G. F., Eds. Elsevier: 1994, 88, 207-213.

66. Deraz, N. M., Synthesis and Characterization of Nano-Sized Nickel Aluminate Spinel Crystals, *International Journal of Electrochemical Science,* 2013, 8, 5213-5222.

67. Kebin, Z.; Ruipu, W.; Boqing, X.; Yadong, L., Synthesis, characterization and catalytic properties of CuO nanocrystals with various shapes, *Nanotechnology,* 2006, 17 (15), 3939-3943.

68. Zhang, Q.; Zhang, K.; Xu, D.; Yang, G.; Huang, H.; Nie, F.; Liu, C.; Yang, S., CuO nanostructures: Synthesis, characterization, growth mechanisms, fundamental properties, and applications, *Progress in Materials Science,* 2014, 60, 208-337.

69. Feng, Y.; Zheng, X., Plasma-Enhanced Catalytic CuO Nanowires for CO Oxidation, *Nano Letters,* 2010, 10 (11), 4762-4766.

70. Wang, C.-H.; Lin, S.-S.; Chen, C.-L.; Weng, H.-S., Performance of the supported copper oxide catalysts for the catalytic incineration of aromatic hydrocarbons, *Chemosphere,* 2006, 64 (3), 503-509.

71. Acharyya, S. S.; Ghosh, S.; Tiwari, R.; Pendem, C.; Sasaki, T.; Bal, R., Synergistic Effect between Ultrasmall Cu(II) Oxide and $CuCr_2O_4$ Spinel Nanoparticles in Selective Hydroxylation of Benzene to Phenol with Air as Oxidant, *ACS Catalysis,* 2015, 5 (5), 2850-2858.

72. Kumar, A.; Wolf, E. E.; Mukasyan, A. S., Solution combustion synthesis of metal nanopowders: Nickel—Reaction pathways, *AIChE Journal,* 2011, 57 (8), 2207-2214.

73. Rao, G. R.; Mishra, B. G.; Sahu, H. R., Synthesis of CuO, Cu and CuNi alloy particles by solution combustion using carbohydrazide and N-tertiarybutoxy-carbonylpiperazine fuels, *Materials Letters,* 2004, 58 (27–28), 3523-3527.

74. Christy, A. J.; Nehru, L. C.; Umadevi, M., A novel combustion method to prepare CuO nanorods and its antimicrobial and photocatalytic activities, *Powder Technology,* 2013, 235, 783-786.

75. Schaber, P. M.; Colson, J.; Higgins, S.; Thielen, D.; Anspach, B.; Brauer, J., Thermal decomposition (pyrolysis) of urea in an open reaction vessel, *Thermochimica Acta,* 2004, 424 (1–2), 131-142.

ACKNOWLEDGEMENTS

I would like to thank my family, in particular my mother, for the huge support and encouragement she has given me throughout my work. I should mention my children and my husband for their understanding and my father for encouraging and giving me faith and strength to finish this work.

I would like to express my deepest appreciation to Prof. Irina Hussainova for discussions, guidance, making good environment to enjoy the work. Her support, patience and understanding makes the work a pleasure, and our group - more responsible for the work.

I am very grateful and appreciate Prof. Miguel A. Rodriguez for the immense support and valuable advice for the completion of this thesis.

I would like to thank our industrial collaborator Michael Kutuzov (Metallurg OÜ), for the guidance and nice materials offered to us.

Many thanks to Nikhil Kamboj, Marek Jõeleht, Roman Ivanov, Maria Drozdova for their friendship, support and help during the hardest time of this work. Many thanks to Olga Volobujeva, Fernando Rubio-Marcos, Rainer Traksmaa, Mart Viljus for analyzing the specimens. Moreover, I would like to express my appreciation to Dr. Hayk Khachatryan for contacting me with prof. Irina Hussainova, and my ex-supervisor Prof. Suren Kharatyan for teaching me to work.

ABSTRACT

One-dimensional (1D) nanostructures in a variety of arrangements have become an exciting, intellectually challenging, and rapidly expanding field of research. Due to their unique physical and chemical properties, anisotropic nanomaterials are expected to open new applications and, consequently, novel technological solutions. Over the past several years, considerable efforts have been devoted to the synthesis of different type of 1D nanostructures with tailored properties, such as nanowires, nanofibres, nanotubes, etc. owing to their unique performance in the fields of chemistry, physics and material science.

In many cases, nanocomposites display high complexity and wide range of properties. These properties are not only derived from the simple addition of functionality to the parent constituents, but also variety of morphology and interfacial characteristics. However, fabrication of anisotropic nanocomposite 1D structures requires comprehensive understanding of the processes of their development and intense efforts for their production.

Composite nanofibers of a large aspect ratio are important and versatile materials for generating building blocks in many applications, such as ceramic composites, catalysis, filters, sensors, batteries, solar cells and photo-electromagnetic devices. However, these applications are hindered by the lack of scalable and cost-effective methods for the production of the composite nanofibers. In this work, through utilizing the specific properties of alumina nanofibers with diameter of 7 ± 2 nm, a novel wet-combustion method was developed to fabricate several kinds of composite nanofibers. The designed approach is a simple, single-step wet-combustion method enabling synthesis of various composites nanofibers mesoporous network in a cost-effective way. Wet-combustion method includes coating the nanofibers with precursors of dopants mixed with fuels, following by dissociation/oxidation of the precursors in a combustion mode. Wet-combustion method uniquely combines the merits of a sol-gel method (e.g., homogeneous distribution of components, low temperature) and a solution combustion process (e.g., high temperature, fast heating rate and short duration). As a result, the composite 1D nanostructures maintaining the morphology of the original materials and desired composition can be produced.

Highly aligned alumina nanofibers were functionalized by zirconia, alumina, nickel oxide and copper oxide, by using a novel single-step wet-combustion synthesis and a template assisted sol-gel synthesis deposition methods. For the first time, the highly-aligned composite nanofibers with a core-shell structure were designed and produced for a wide variety of application.

KOKKUVÕTE

Hiljuti väljatöötatud ühedimensionaalsed γ-alumiiniumoksiidist (Al$_2$O$_3$) nanokiud, läbimõõduga 7±2 nm, on funktsionaliseeritud uudse märg-põlemise meetodiga. Funktsionaliseerimise eesmärgiks on laiendada nende kasutusvaldkonda erinevates funktsionaalsetes komposiitmaterjalides.

Märg-põlemise süntees on üheetapiline lähenemine võimaldades kuluefektiivselt sünteesida mesopoorseid komposiite, milledel on eesmärgipäraselt disainitud faasiline kompositsioon ja morfoloogia. Väljatöötatud meetodi raames kaetakse nanokiud lähtematerjalidest lisanditega, mis on segatud orgaaniliste kütustega. Sellele järgneb lähtematerjalide ja kütuse lagunemine/oksüdeerumine, mille tulemusel toimub nanokiudude pindamine uue faasiga või terve nanokiu faasi muutumine. Märg-põlemise meetod ühendab endas sool-geel meetodi (homogeenne komponentide jagunemine ja madal temperatuur), sisse-kastmis pindamise (lihtsus, mikrostruktuuri kontroll ja kuluefektiivsus) ja põlemise meetodi (kõrge temperatuur, kiire kuumutus ja lühike kestvus) eeliseid. Protsessis tulemusena saab valmistada 1D nanostruktuuridega komposiitmaterjale, millele jääb alles nende originaalne morfoloogia ning soovitud keemiline kompositsioon.

Alumiiniumoksiid nanokiude funktsionaliseeriti erinevate metallioksiididega (nt. ZrO$_2$, Al$_2$O$_3$, NiO ja CuO) rakendades uut väljatöötatud märg-põlemise sünteesi olles alternatiiv sool-geel süntees pindamisemeetoditele. Esmakordselt on valmistatud ühedimensionaalsed, kõrge parallelsusega, hierarhilised nanostruktuurid, mis omavad südamiku ja kooriku struktuure läbimõõduga alla 50 nm ilma, et oleks vaja järelkaltsineerimist. Lisaks on näidatud, et alternatiivina on võimalik sool-geel meetodiga funktsionaliseerida alumiiniumoksiid nanokiude.

Protsessi parameetrid on optimiseeritud kontrollimaks lõpliku materjali morfoloogiat. Muutes protsessi parameetreid, eelkõige reaktsiooni esile kutsuvate komponentide sisaldust lahuses, on võimalik mõjutada nanokiudude keemilist koostist.

APPENDICES

Curriculum vitae

1. Personal data

Name   Marina Aghayan
Date and place of birth   01.07.1987, Gyumri, Armenia
E-mail address   marina.aghayan@ttu.ee

2. Education

Period	Educational institution	Education (Programme/degree)
2010	Yerevan State University	Physical Chemistry / Master
2007	Yerevan State University	Physical Chemistry / Bachelor
2004	College "Photon"	Natural Science / High school

3. Language competence/skills (fluent, good, basic skills)

Language	Level
Armenian	Native
English	Fluent
Russian	Good
French	Good
Spanish	Basic
Estonian	Basic

4. Professional employment

Period	Organization	Position
2012-…	Tallinn University of Technology, Tallinn, Estonia	Early-stage researcher
2011	″Arpimed″ pharmaceutical company, Abovyan, Armenia	Chemist-analyst
2010-2011	Institute of Ceramics and Glasses, Madrid, Spain	Project researcher
2007-2010	Institute of Chemical Physics, Yerevan, Armenia	Junior scientist
2007-2008	"Britannia Coatings and Chemicals" CJSC, Yerevan, Armenia	Chemist

5. Activities

Period	Organisation	Position
2009-…	Young Biologist Association, NGO	Member
2008-2010	Institute of Chemical Physics, Yerevan, Armenia	Vice President of Trade Union
2005-2006	Chemical department of Yerevan State University	Councilor of Trade Union

6. Research visits

Period	Organisation
10.2013-11.2013	Aalto University Foundation; Espo, Finland
05.2012-06.2012	Institute of Ceramics and Glasses; Spanish Academy of Science, Madrid, Spain
06.2010-07.2010	Institute of Ceramics and Glasses; Spanish Academy of Science, Madrid, Spain

7. Fellowships and awards

Period	Organisation
2015	Award for the best student speakers, 21th International Conference BALTMATTRIB-2015
2003-2007	RA Governmental Fellowship for BSc. students

Elulookirjeldus

1. Isikuandmed

Ees- ja perekonnanimi   Marina Aghayan
Sünniaeg ja -koht   01.07.1987 Gyumri, Armeenia
E-posti aadress   marina.aghayan@ttu.ee

2. Hariduskäik

Lõpetamise aeg	Õppeasutus (nimetus lõpetamise ajal)	Haridus (kraad/eriala)
2010	Yerevan State University	Füüsikaline keemia / magister
2007	Yerevan State University	Füüsikaline keemia/ bakalaureus
2004	College "Photon"	Loodusteadused / gümnaasium

3. Keelteoskus

Keel	Tase
Armeenia	Emakeel
Inglise	Kõrg
Vene	Kõrg
Hispaania	Kesk
Prantsuse	Kesk
Eesti	Algtase

4. Töökogemus

Töötamise aeg	Tööandja nimetus	Ametikoht
2012-…	Tallinna Tehnikaülikool, Tallinn, Eesti	Nooremteadur
2011	″Arpimed″ farmaatsiafirma, Abovyan, Armeenia	Keemik-analüütik
2010-2011	Keraamika ja Klaasi instituut, Madriid, Hispaania	Projekti uurija
2007-2010	Füüsikalise Keemia Instituut, Yerevan, Armeenia	Nooremteadur
2007-2008	"Britannia Coatings and Chemicals", Yerevan, Armeenia	Keemik

5. Tegevus

Töötamise aeg	Asutus	Ametikoht
2009-…	Young Biologist Association, MTÜ	Liige
2008-2010	Füüsikalise Keemia Instituut, Yerevan, Armeenia	Ametiühingute asepresident
2005-2006	Chemical department of Yerevan State University	Ametiühingute nõustaja

6. Enesetäiendamine

Kestus	Asutus
10.2013-11.2013	Aalto University Foundation; Espoo, Finland
05.2012-06.2012	Institute of Ceramics and Glasses; Spanish Academy of Science, Madrid, Spain
06.2010-07.2010	Institute of Ceramics and Glasses; Spanish Academy of Science, Madrid, Spain

7. Stipendiumid ja auhinnad

Aasta	Asutus
2015	Award for the best student speakers, 21th International Conference BALTMATTRIB-2015
2003-2007	RA Governmental Fellowship for BSc. students

Publications that are not included in the thesis

1. Drozdova, M.; Hussainova, I.; Pérez-Coll, D.; <u>Aghayan, M.</u>; Ivanov, R.; Rodríguez, M.A. A novel approach to electroconductive ceramics filled by graphene covered nanofibers. *Materials & Design.* 2016, 90, 291−298. DOI: 10.1016/j.matdes.2015.10.148.

2. Drozdova, M.; Pérez-Coll, D.; <u>Aghayan, M.</u>; Ivanov, R.; Rodríguez M.A.; Hussainova, I., Hybrid graphene/alumina nanofibers for electrodonductive zirconia. *Key Engineering Materials*. 2016, 674, 15-20. DOI: 10.4028/www.scientific.net/KEM.674.15.

3. Ivanov, R.; Hussainova, I.; <u>Aghayan, M.</u>; Drozdova, M.; Pérez-Coll, D.; Rodríguez, M. A.; Rubio-Marcosc, F. Graphene-encapsulated aluminium oxide nanofibers as a novel type of nanofillers for electroconductive ceramics. *Journal of the European Ceramic Society*. 2015, 35 (14), 4017–4021.

4. Kharatyan, S.L.; <u>Aghayan, M.A.;</u> Chatilyan, H.A. Interaction Modes in Mo/Si diffusion couple at non-isothermal conditions. *International Journal of Self-Propagating High-Temperature Synthesis*. 2014, 23 (3), 138−140.

5. Voltsihhin, N.; Rodriguez, M.; Hussainova, I.; <u>Aghayan, M.</u> Low temperature spark plasma sintering behaviour of zirconia added by a novel type of alumina nanofibers. *Ceramics International*. 2014, 40, 7235−7244. DOI: 10.1016/j.ceramint.2013.12.063.

6. Hussainova, I.; Drozdova, M.; <u>Aghayan, M.;</u> Ivanov, R.; Pérez-Coll, D. Graphene covered alumina nanofibers as toughening agent in alumina ceramics. *Advances in Science and Technology*. 2014, 88, 49-53.

7. Kharatyan S.L.; Chatilyan H.A.; <u>Aghayan M.A.;</u> Rodríguez M.A. Non-iIsothermal phenomena in Mo/Si diffusion couple: reaction kinetics and structure formation. *International Journal of Self-Propagating High-Temperature Synthesis*. 2013, 22 (1), 18−26.

8. <u>Aghayan, M.;</u> Rodríguez, M. Influence of fuels and combustion aids on solution combustion synthesis of bi-phasic calcium phosphates (BCP). *Materials Science and Engineering C*. 2012, 32 (8), 2464−2468. DOI: 10.1016/j.msec.2012.07.027.

9. Rodríguez, M.; Aguilar, C.; <u>Aghayan, M.</u> Solution combustion synthesis and sintering behavior of $CaAl_2O_4$. *Ceramics International*. 2012, 38 (1), 395−399.

10. <u>Aghayan, M.;</u> Chatilyan, H.; Kharatyan, S., Distinctive features of nonisothermal interaction in micro-nanosize Mo/Si diffusion couple. *Chemical Journal of Armenia*. 2010, 63 (2), 172−192.

11. <u>Aghayan, M.;</u> Khachatryan, H.; Kharatyan, S., Synthesis of fine boron nitride powders by combining direct boron nitridation with carbothermic boron oxide reduction. *International Journal of Self-Propagating High-Temperature Synthesis*. 2009, 18 (1), 46−50.

Patent applications:

1. Authors: <u>Aghayan M.;</u> Hussainova I. Method for producing nanofibers composed of NiO and $NiAl_2O_4$ by combustion techniques and product comprising said nickel oxide doped nickel aluminate spinel nanofibers ($NiO/NiAl_2O_4$) thereof; Owner: Tallinn University of Technology. Applied in November 2014.

2. Authors: <u>Aghayan M.;</u> Kamboj N.; Hussainova I. Method for producing rhombohedral $FeAlO_3$ nanofibers and product comprising said nanofibers thereof; Owner: Tallinn University of Technology. Applied in February 2016.

PUBLICATIONS

Paper I.   Aghayan, M.; Hussainova, I.; Gasik, M.; Kutuzov, M.; Friman, M. Coupled thermal analysis of novel alumina nanofibers with ultrahigh aspect ratio. *Thermochimica Acta*. 2013, 574, 140−144. DOI: 10.1016/j.tca.2013.10.010.

Coupled thermal analysis of novel alumina nanofibers with ultrahigh aspect ratio

Marina Aghayan [a], Irina Hussainova [a], Michael Gasik [b,*],
Michael Kutuzov [c], Michael Friman [b]

[a] Tallinn University of Technology, Department of Materials Engineering, Ehitajate tee 5, 19180 Tallinn, Estonia
[b] Aalto University Foundation, School of Chemistry, Material Science and Engineering, P.O. Box 16200, FIN-00076 Aalto, Finland
[c] Metallurg Eng., Suur-Sojamae 35, Tallinn, Estonia

ARTICLE INFO

ABSTRACT

The phase conversions and morphological changes of commercial alumina nanofibers (ANF) with 7 and 40 nm in diameter during heat treatment were investigated. These super-high aspect ratio (length-to-diameter ratio is $\sim10^7$) fibers are mostly composed of partially hydrated (2–6 wt.%) gamma-alumina phase. The transformations of the ANF during heating up to 1480 °C were studied simultaneous coupled thermal analysis (TG-DSC-FTIR) supported by XRD and SEM examinations. It was found that for ANF gamma-phase starts to transform into stable α-alumina from ~1250 °C, but the water releases during most of the heating time at least in two stages. The behavior of the material and observed changes are discussed and compared with literature date for different alumina materials.

© 2013 Elsevier B.V. All rights reserved.

1. Introduction

Nowadays nanostructured materials have attracted great attention because of unusual and often promising mechanical, electrical and optical properties governed by confining dimensions. Being nano-sized in diameter, nanofibers possess high-surface-to-volume ratio leading to activation in interactions between the nanofibers and targeted substrates. Therefore exploitation of nanofibers could be a promising approach for a wide range of advanced applications. Alumina nano-powders and fibers are materials of interest in many application areas, such as catalysts and their supports, adsorbents, coatings, ceramics, and abrasives [1,2]. Aluminum oxide (Al_2O_3) exists in several polymorphs, such as metastable γ-, δ-, η-, θ-, χ- phases as well as thermodynamically stable α-Al_2O_3. The metastable (also known as transition) phases of alumina are intrinsically nanocrystalline in nature and can be synthesized by a variety of methods including hydrothermal and sol–gel processing as well as chemical vapor–liquid–solid deposition and electrospinning routines. Transition aluminas, especially γ-Al_2O_3, are widely produced for catalyst carrier in the automotive and petroleum industries, structural composites for spacecraft, abrasive and thermal wear coatings, and filters applications [3,4].

Gamma-alumina is reported to occur at wide interval of the temperatures between 350 and 1000 °C and is typically obtained from an amorphous or boehmite precursor. Properties of the final alumina products are highly dependent on the crystalline structure, morphology, and microstructure of the polymorph; therefore, many research efforts have been focused on study and characterization of the transition aluminas with respect to their transformation mechanisms, changes in porosity, specific surface area, surface structure and chemical reactivity, and the defect crystal structure [5,6]. The reports on the thermal treatment demonstrate that the thermal behavior depends essentially on phase composition and morphological parameters of the precursor material (usually boehmite AlOOH) such as degree of crystallinity, size of crystallites, porosity, etc. [1,5,7–11]. The morphology and size of the final Al_2O_3 strongly depend on the precursor used during the conversion process [12], synthesis method [9], defect content of the crystal [5], etc. This applies not only to different forms of boehmite, such as the gelatinous and highly crystalline types, but also to the conditions under which the boehmite was prepared. The transformations are also affected by the presence of chemically bounded water (in a form of gibbsite, diaspore or boehmite) and/or physically adsorbed water, especially for nano-sized materials with a high surface area. Gamma-alumina has also been shown to be thermodynamically stable relative to α-Al_2O_3 when a critical surface area is achieved [13]. According to molecular dynamic simulation [14] at 527 °C (in a typical temperature range of a hydroxide decomposition), γ-Al_2O_3

* Corresponding author. Tel.: +358 505609511.
E-mail address: michael.gasik@aalto.fi (M. Gasik).

might become thermodynamically stable at specific surface areas greater than only 75 m^2 g^{-1}. This outcome can open up endless possibilities for applications of γ-Al$_2$O$_3$. However, in the simulation [14], which strongly suggested that γ-Al$_2$O$_3$ is a surface-stabilized phase, it was not addressed the role of adsorbed species, and in particular H$_2$O, on the relative stability of the polymorphs, depending also on crystallinity [15].

Recently developed technology of controlled liquid phase oxidation of aluminum for manufacturing of the alumina nano-fibers (ANF) with extremely high aspect ratios of more than 10^7 and fiber diameter ranged from 5 to 50 nm gives a possibility to develop new types of alumina-based products with a very high and controlled anisotropy. Generally, the crystal growth from a melt of metal is an excellent technique for preparing nano-materials because of its low cost, high yield and the ability to achieve high purity of the oxide structures in the as-synthesized state. This study reports the results on thermal analysis of the γ-Al$_2$O$_3$ nano-fibers of extremely high aspect ratio and their possible phase transformation during heat treatment.

2. Materials and experimental procedure

The nano-fibers of gamma alumina with diameters of 7 and 40 nm, length of 5–6 cm and specific surface area 155 m^2 g^{-1} (BET method) represent tight bundles consisting of several thousands fibers, Fig. 1. These specimens are further designated as ANF-7 and ANF-40, respectively. Specimens were taken by cutting into the small samples to be fitted within the crucibles. The ANF were analyzed with simultaneous coupled thermal analysis (TG-DSC-FTIR) with STA449 C "Jupiter" (Netzsch Gerätebau GmbH) and Tensor 27 spectrometer (Bruker Optics). Experiments were performed in synthetic dry air (21% O$_2$, balance nitrogen; Linde AGA) flow of 20 ml/min with heating and cooling rates of 10 °C/min and maximal temperature of 1480 °C. Alumina crucibles were used without a lid and an empty crucible was used as a DSC reference. Evolved gas analysis by FTIR was performed with automatic CO$_2$ bands compensation in transmission mode on gas flow taken off the STA furnace via heated (300 °C) and shielded capillary. Data collection and analysis were made using Proteus 5 (Netzsch) and OPUS 5.5 (Bruker) software.

X-ray diffraction data were collected at room temperature using a D8 diffractometer (Bruker) in the CuK$_\alpha$ monochromatic radiation. The employed 2θ range was 10–80°, with a 0.05° step size.

The specimens heated up to the selected temperatures of 600, 1000, 1200, 1480 °C and quenched were studied to identify phases after heat treatment and associate possible phase transformations with observed thermal effects. The morphology of the nanofibers (Fig. 1) before and after treatment was examined by scanning electron microscopy (SEM Zeiss EVO MA 15, Germany) with a gold coating to improve specimens' conductivity. High-resolution transmission electron microscopy (HRTEM) was made with JEOL 2200-S (Jeol, Japan) with lattice resolution of 0.1 nm. Specimen ANF-7 was also examined with nuclear magnetic resonance (NMR Bruker Avance-400) in magnetic field of 9.4 T and 400 MHz (spectrum ^{1}H MAS) after heat treatment to ensure that absorbed water is removed to maximal possible extent.

3. Results and discussion

The results of thermal analysis are displayed in Figs. 2 (TG) and 3 (DSC). The total mass loss for both specimens during the whole scan was about 6 wt% for ANF-7 vs. 2.2 wt% for ANF-40. Additionally, ANF-7 has a clearly separated stage for mass loss over 1200 °C (which is about 1/10 of the total mass loss) that is not detected for ANF-40.
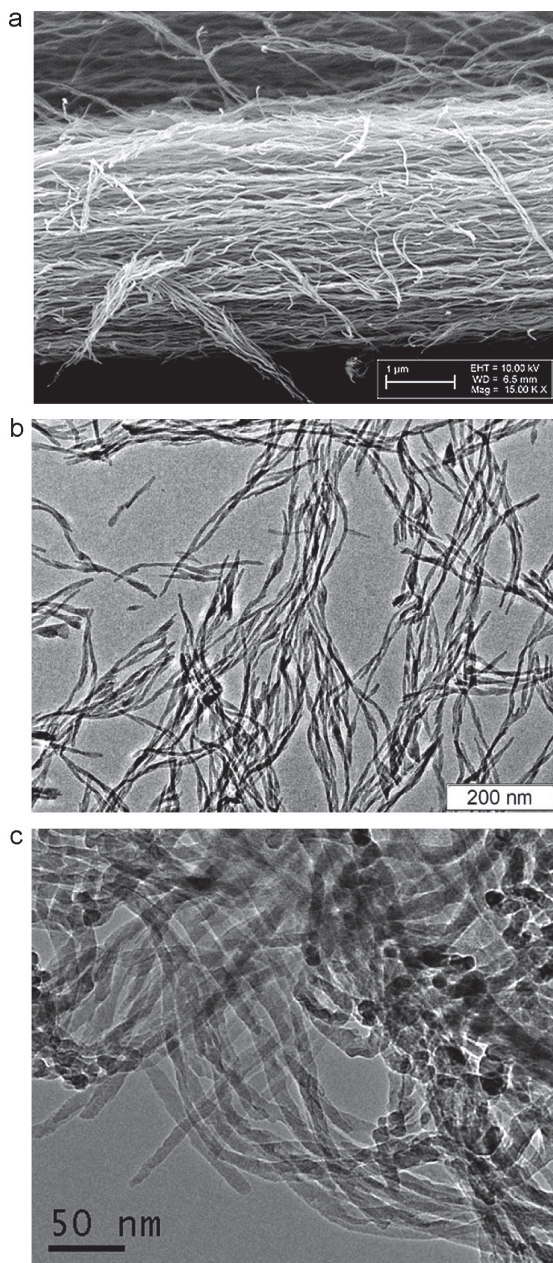

Fig. 1. A bundle of ANF with 7 nm average diameter: (a) SEM image, (b) and (c) HRTEM images, respectively.

Eventually all mass losses are corresponding to water release, as no other gases were observed by FTIR (Fig. 4), and no significant differences between evolved gases of these two specimens were found. The results are consistent with most of the water being lost during first 10–30 min of the heating segment. Some small water traces in the gas are still being observed at higher temperatures
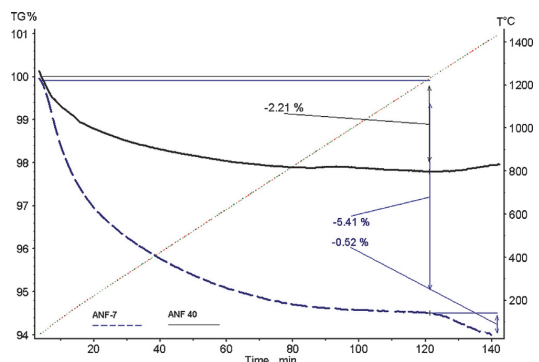
Fig. 2. Mass changes (TG) for the ANF-7 and ANF-40 specimens during heating.

but the origin of this water vapour cannot be determined in these experiments.

For differential scanning calorimetry (DSC) there are endothermic effects at the beginning of heating which could not be explained just by adsorbed or physisorbed water evaporation (Fig. 3). It might be assumed that unsaturated Al^{3+} linked to three oxygen atoms might lead to water dissociation. The cation Al^{3+} then binds to hydroxyl OH^-, and protons form hydrogen bonds localized on the neighboring Al–O–Al bridge. Formation of both terminal OH-groups and bridging groups as indicated by the IR spectra (absorption in 3790 and 3678 cm^{-1} respectively, Fig. 5) can be suggested. The spectrum ^1H NMR shown in Fig. 6 demonstrates that terminal OH-groups are preferentially linked to tetrahedral Al and bridging groups are linking tetrahedral and octahedral Al^{3+} positions. This might explain thermal effects as the brutto-composition could be written in a form typical for gamma-based aluminas $Al_2O_3 \cdot xH_2O$ ($x < 0.6$) [15]. Such hypothesis needs additional studies to be confirmed.

In the case of gibbsite $Al(OH)_3$ transformations, several reported temperature values could be found. Most data indicates temperature region of boehmite formation ~180 °C and for χ-alumina about 250–300 °C, finishing as high as 500–700 °C [15–18]. Bayerite $Al(OH)_3$ also transforms to boehmite at ~180 °C, but than preferably to γ- and η-alumina at 230–260 °C. γ-Al_2O_3 are known to transform into the δ-phase (~850 °C), and than to Θ-Al_2O_3 (>1050 °C). The η-alumina phase might also change into Θ-phase directly (>850 °C). All these phases in the long run give alpha-phase, but at different temperatures, which greatly depends on the precursor used, as observed by thermal analysis [15–19]. Brown et al.
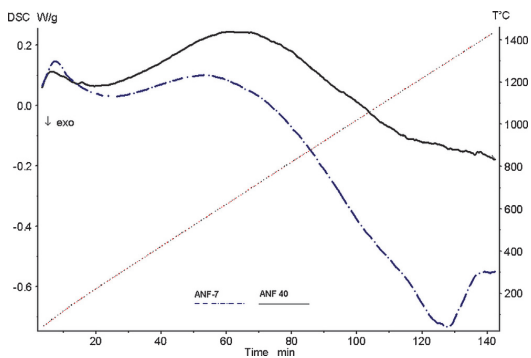

Fig. 3. DSC traces for the ANF-7 and ANF-40 specimens during heating.
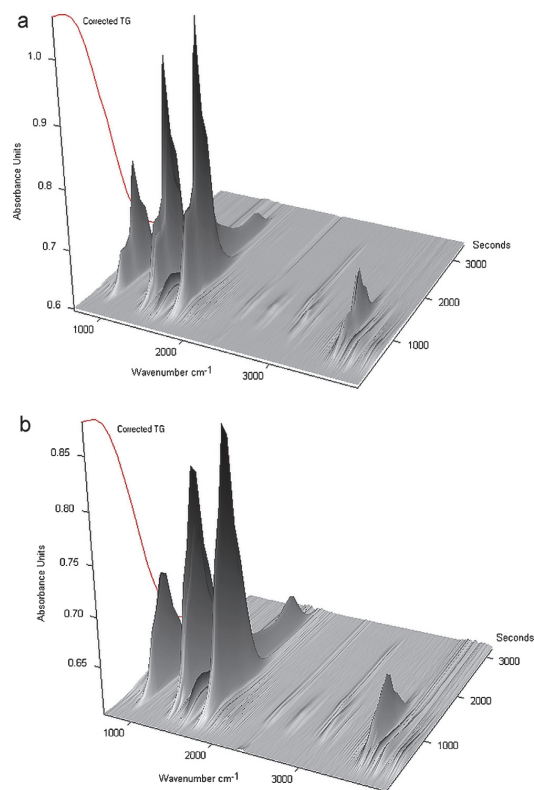

Fig. 4. 3D Chrom FTIR spectra of the gases evolution from the ANF-40 (a) and ANF-7 (b) specimens during coupled STA. Corrected TG trace (Fig. 2) is overlaid on the left side of the 3D plot. Absorbance peaks are essentially due to released water.

[20] have reported about problems which appear during STA studies of thermal decomposition of different alumina precursors. It appears due to formation of different products, and often due to 3-D diffusion limited reaction rate, which is strongly depended of local water partial pressure in particular. ANF-7 specimen has also a clear exothermal effect in the range 1200–1400 °C, which is slightly associated with release of additional water (~0.61%, Fig. 2). As most
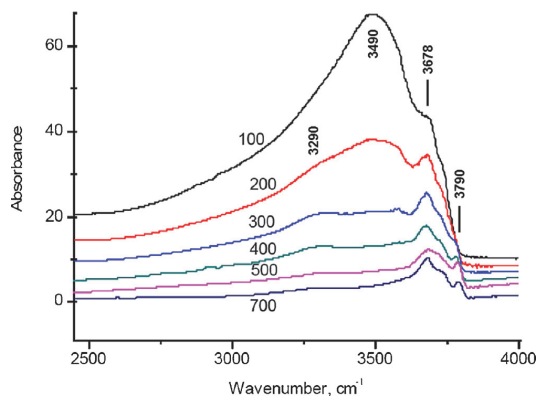

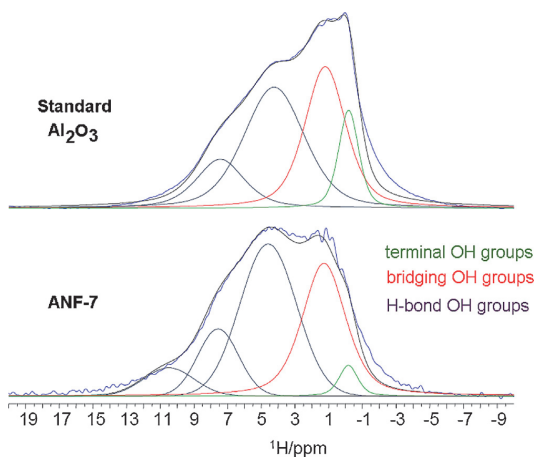**Fig. 5.** IR absorption spectra of ANF-7 fibers heat-treated at different temperatures.

Fig. 6. NMR ^{1}H spectrum of ANF-7 and standard reference alumina after heat treatment at 250 °C.

Fig. 8. The surface morphology of original ANF-7 fibers (a) and same fibers after thermal analysis (heating up to 1480 °C; b).

of the ANF material is gamma-alumina, it is expected to be transformed into more stable α-Al$_2$O$_3$ over 1150 °C. This transformation is exothermic for all alumina phases, which might be present, Fig. 4, and for $\gamma \rightarrow \alpha$ transformation at 1300 °C thermal effect is -25.636 kJ/mol Al$_2$O$_3$ (-251.43 J/g by HSC Chemistry 7.1 thermodynamic database [21]) or -26.25 kJ/mol (-257.54 J/g; according to [22]). Neglecting parallel water removal, this might give estimation that at least 60% of the virgin ANF-7 material is composed of the γ-alumina phase. The small release of water might be associated with this phase transformation, which release possible water traps inside the fibers and allows it to escape with gas.

Such $\gamma \rightarrow \alpha$ transformation was not observed clearly for ANF-40 (Fig. 3), neither respective water loss at these temperatures was recorded (Fig. 2). Since ANF-40 fibers are much more densely packed than ANF-7, it might be possible that water does not have easy route to escape. It could be indirectly justified that ANF-7 fibers are becoming "lossy" and more separated after heating, whereas ANF-40 stay more rigid and bundled together.

Mehta et al. [23] reported that alumina transformations could be approximated by a continuous sequence of structures from böhmite to α-Al$_2$O$_3$, described by formula Al$_2$QO$_{3-v/2}$(OH)$_v\varnothing_{1-v/2}$, where Q means cationic and $\varnothing$ – anionic vacancies respectively ($0 \leq v \leq 2$). They have found exact route depends much on the initial crystallinity of the specimen. With TG, DTA and following XRD analysis it was shown that highly amorphous phase proceeds
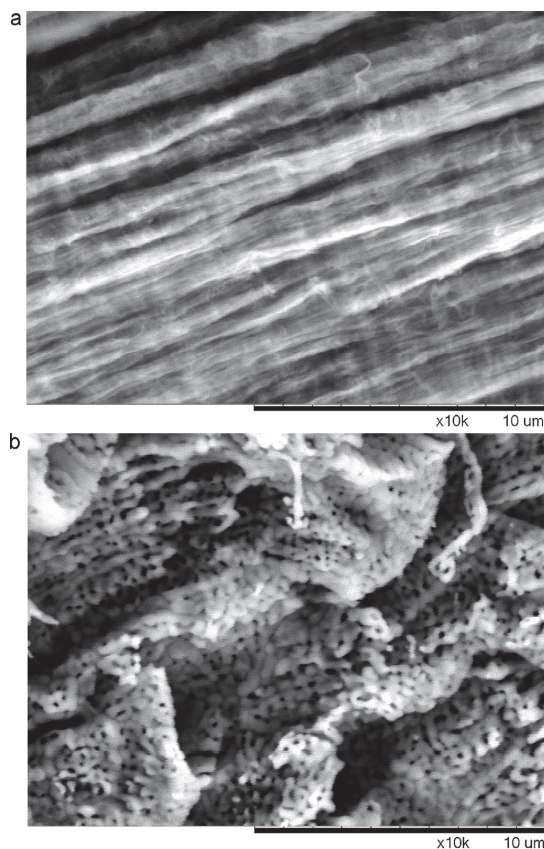
preferentially to χ-, κ- and α-alumina [23]. However, in the core of well-crystallized sample, the transformation sequence from γ- to θ- and to α-Al$_2$O$_3$ was dominating [23]. It was also observed that the temperature range and temperature of the DTA peaks are proportional to the degree of specimen crystallinity [23,24].

The XRD analysis made in this work of heat-treated ANF samples did not reveal differences in spectra below 1200 °C (Fig. 7),
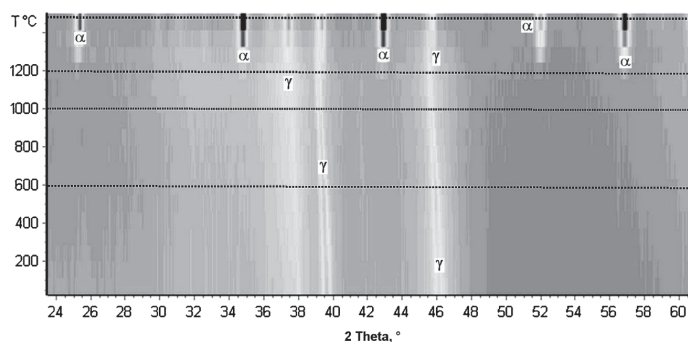

Fig. 7. XRD patterns made for different heat treatment temperatures. Dotted lines indicate the temperatures for quenching of the specimens.

expect some variations in intensities of γ-Al_2O_3. At the highest temperature, however, most of the phase is already converted into α-alumina which peaks sharpness also increases, indicating better crystalline degree. There was no clear indication of other possible alumina or hydrated alumina phases.

The example of the ANF morphology changes during heat treatment is shown in SEM micrograph for ANF-7 in Fig. 8. Whereas the general shape of the fibers is preserved, the morphology of the nanofibers has undergone significant changes. For instance, alumina fibers have taken more agglomerated/partially sintered cell shape with small pores ($\sim$50–200 nm) between them. Thermal analysis data indicate water playing a substantial role in the process and more water is removed from 7 nm fibers than from 40 nm. It is also evident from STA and XRD analyses that there is no single $\gamma \rightarrow \alpha$ transformation temperature or temperature range (Fig. 7), unlike for alumina powders reported in the literature previously. Nevertheless heat treatment of ANF over 1300 °C result in stable α-alumina phase, but to obtain higher crystallinity, 1400 °C or higher would be required at heating rates used in the present study. The ANF heat treatment regime might be optimized for obtaining stable alumina nanofibers based on α-alumina with a high surface area, suitable for a variety of applications.

4. Conclusions

The phase transformations and structural changes of alumina nanofibers (ANF) with 7 and 40 nm in diameter were studied in the 20–1480 °C temperature range using simultaneous coupled thermal analysis (TG-DSC-FTIR) and X-ray diffraction. Both studied fiber sizes behave similarly on heating, but 7 nm specimens have much higher mass loss than 40 nm ones. Besides release of water, no other phase transformation was found below 1200–1250 °C, although thermal effects and mass losses were significant. However the surface morphology of the fibers has changed substantially, which might be explained by the peculiarities of water release together with $\gamma \rightarrow \alpha$ transformation in a wide temperature range.

Acknowledgement

References

[1] X. Bokhimi, J.A. Toledo-Antonio, M.L. Guzmán-Castillo, B. Mar-Mar, F. Hernández-Beltrán, J. Navarrete, Dependence of boehmite thermal evolution on its atom bond lengths and crystallite size, J. Solid State Chem. 161 (2001) 319–326.

[2] H.A. Dabbagh, K. Taban, M. Zamani, Effects of vacuum and calcination temperature on the structure, texture, reactivity, and selectivity of alumina: experimental and DFT studies, J. Mol. Catal. A: Chem. 326 (2010) 55–68.

[3] H. Yang, M. Liu, J. Ouyang, Novel synthesis and characterization of nanosized γ-Al_2O_3 from kaolin, Appl. Clay Sci. 47 (2010) 438–443.

[4] Y. Men, H. Gnaser, Ch. Ziegler, Adsorption/desorption studies on nanocrystalline alumina surfaces, Anal. Bioanal. Chem. 375 (2003) 912–916.

[5] R.-S. Zhou, R.L. Snyde, Structures and transformation mechanisms of the η, γ, and θ transition aluminas, Acta Crystallogr. B 47 (1991) 617–630.

[6] K.J.D. MacKenzie, J. Temuujin, M.E. Smith, P. Angerer, Y. Kameshima, Effect of mechanochemical activation on the thermal reactions of boehmite (γ-AlOOH) and γ-Al_2O_3, Thermochim. Acta 359 (1) (2000) 87–94.

[7] Sh. Keysar, G.E. Shter, Y. de Hazan, Y. Cohen, G.S. Grader, Heat treatment of alumina aerogels, Chem. Mater. 9 (1997) 2464–2467.

[8] P.S. Santos, H.S. Santos, S.P. Toledo, Standard transition aluminas. Electron microscopy studies, Mater. Res. 3 (4) (2000) 104–114.

[9] A. Tonejc, A.M. Tonejc, D. Bagovid, C. Kosanovid, Comparison of the transformation sequence from γ-AlOOH (boehmite) to α-Al_2O_3 (corundum) induced by heating and by ball milling, Mater. Sci. Eng. (1994) 1227–1231, A181/A182.

[10] Y. Wang, J. Wang, M. Shen, W. Wang, Synthesis and properties of thermostable γ-alumina prepared by hydrolysis of phosphide aluminium, J. Alloys Compd. 467 (2009) 405–412.

[11] C.K. Kumara, W.J. Ng, A. Bandara, R. Weerasooriya, Nanogibbsite: synthesis and characterization, J. Colloid Interface Sci. 352 (2010) 252–258.

[12] T.S. Chang, J.H. Na, Ch.Y. Jung, S.M. Koo, An easy one-pot synthesis of structurally controlled aluminum hydroxide particles from an aqueous sodium aluminate solution, J. Ceram. Proc. Res. 10 (6) (2009) 832–839.

[13] J.M. McHale, A. Navrotsky, A.J. Perrotta, Effects of increased surface area and chemisorbed H_2O on the relative stability of nanocrystalline γ-Al_2O_3 and α-Al_2O_3, J. Phys. Chem. B 101 (4) (1997) 603–613.

[14] S. Blonski, S.H. Garofalini, Molecular dynamics simulations of α-alumina and γ-alumina surfaces, Surf. Sci. 295 (1–2) (1993) 263–274.

[15] M.M. Gasik, F.R.S. Sale, Decomposition of precipitated aluminium hydroxide studied by simultaneous thermal analysis, in: Proceedings of the 10th ICTA Congress, Hatfield, UK, 1992, p. 25.

[16] M. Mizuno, H. Saito, Preparation of highly pure fine mullite powder, J. Am. Ceram. Soc. 72 (3) (1989) 377–382.

[17] M.M. Gasik, P.N. Ostrik, E.B. Popov, Non-oxide ceramics with nanocrystalline layers made by chemical liquid deposition, Br. Ceram. Trans. 92 (5) (1993) 209–213.

[18] D.E. Clark, J.J. Lannutti, Phase transformations in sol–gel derived aluminas, in: L.L. Hench, D.R. Ulrich (Eds.), Ultrastructure Processing of Ceramics, Glass, and Composites, Wiley, New York, 1986, pp. 126–141.

[19] F.W. Dynys, M. Ljundberg, J.W. Halloran, Micro-structural transformations in alumina gels, in: C.J. Brinker, D.E. Clark, D.R. Ulrich (Eds.), Materials Research Society Symposium Proceedings, vol. 32, New York-Amsterdam-Oxford, North-Holland, 1984, pp. 321–326.

[20] M.E. Brown, D. Dollimore, A.K. Galwey, Reactions in the solid state, in: C.H. Bamford, C.F.H. Tipper (Eds.), Comprehensive Chemical Kinetics, vol. 22, Elsevier, Amsterdam, 1980, p. 340.

[21] HSC Chemistry 7.1 Software, Outotec, Corp., Finland, 2011, www.outotec.com/hsc

[22] , in: JANAF Thermochemical tables, 3rd ed., J. Phys. Chem. Ref. Data 14 (Supp. 1) (1985).

[23] S.K. Mehta, A. Kalsotra, M. Murat, A new approach to phase transformations in gibbsite: the role of the crystallinity, Thermochim. Acta 205 (1992) 191–203.

[24] H. Nagai, S. Hokazono, A. Kato, Synthesis of aluminium hydroxide by a homogeneous precipitation method. I – Effect of additives on the morphology of aluminium hydroxide, Br. Ceram. Trans. 90 (1991) 44–48.

Paper II.   Aghayan, M.; Voltsihhin, N.; Rodríguez, M.A.; Marcos, F.R.; Dong, M.; Hussainova, I. Functionalization of gamma-alumina nanofibers by alpha-alumina via solution combustion synthesis. *Ceramics International. 2014,* 40 (8), 12603−12607. DOI: 10.1016/j.ceramint.2014.04.087.

Short communication

Functionalization of gamma-alumina nanofibers by alpha-alumina via solution combustion synthesis

Marina Aghayan[a,*], Nikolai Voltsihhin[a], Miguel Angel Rodríguez[b], Fernando Rubio-Marcos[b], Minjie Dong[a], Irina Hussainova[a]

[a]Tallinn University of Technology, Department of Materials Engineering, Ehitajate tee 5, 19180 Tallinn, Estonia
[b]Instituto de Cerámica y Vídrio (CSIC), Campus Cantoblanco, 28049 Madrid, Spain

Abstract

In this study alpha-alumina thin films have been deposited continuously onto novel gamma-alumina nanofibers with 7 nm in diameter and 5 cm in length. This selective alpha phase deposition on gamma phase was carried out by a one-step solution combustion process using aluminum nitrite as the precursor of aluminum and urea as a fuel. Effect of the fuel amount on the combustion product was studied by adjusting Al/urea ratio in solution. Stoichiometric amount of urea was considered to be optimal for crystallization of alumina nanoparticles. The morphology of the resulting product was found to be insignificantly affected by aluminum–urea ratio. The possible catalytic behavior of urea in formation of alpha-alumina was discussed. Microstructural characterization by XRD, TEM, and FESEM has revealed a uniform deposition of ultra-fine grained alpha-alumina film on the surface of gamma-alumina nanofibers.
© 2014 Elsevier Ltd and Techna Group S.r.l. All rights reserved.

1. Introduction

Chemical and thermal stability, relatively high strength and corrosion resistance, good thermal and electrical insulation characteristics combined with high hardness and high melting point make the aluminum oxide based materials to be very attractive for many engineering applications [1,2]. Among many transition aluminas known, gamma-alumina (γ-Al_2O_3) is one of the most used catalyst and catalyst support in the automotive and petroleum industries. [3,4]. The high transmittance of alumina in the range from the ultraviolet to infrared band extends its application in optically transparent ceramic coatings, organic light emitting devices, solar selective coatings, optical lenses and windows, refractory coatings, antireflection coatings and optical wave-guides [5].

Aluminum oxide (Al_2O_3) exists in several polymorphs, such as metastable γ-, δ-, η-, θ-, and χ- phases as well as

thermodynamically stable high temperature α-Al_2O_3 phase. All these metastable phases can be irreversibly converted into α-Al_2O_3 by the appropriate heat treatments. Only α-Al_2O_3 polymorph is the stable phase above 1200 °C.

The properties of alumina ceramics are heavily affected by crystal size, morphology, and surface and phase homogeneity, which themselves are dependent on the processing method and parameters [5,6].

There are several physical and chemical approaches to prepare alumina films, such as pulse laser deposition [5], atomic layer deposition [7,8], laser-induced sol–gel deposition [9], chemical vapor deposition [10], combustion chemical vapor deposition [11], metal–organic chemical vapor deposition [12], reactive magnetron sputtering [13], and sol–gel processing [2,6,8,9,14,15]. Formation of a proper coating or thin film is a critical issue for using fibers as reinforcing constituents in composite materials. For example, Bao and Nicholson [16] deposited a uniform alumina film on alumina fibers by means of modified electrophoretic infiltration

*Corresponding author.

deposition (EPID) from ethanol suspension of submicron sized alumina particles under constant current. Holmquist and Lange [17] developed a process to manufacture fiber-reinforced alumina–alumina ceramic matrix composites (CMC) using a pre-consolidated slurry with a very high volume fraction of powder for infiltration of the fiber cloths. A sol–gel method is a well-studied routine allowing deposition of uniform thin films on substrates of different types of alumina coatings on ceramic powders of wide variety in particle shapes and sizes. As a first step of the process, a layer of amorphous alumina is developed and then followed by transformation into gamma-polymorph after calcination at intermediate temperatures and alpha-polymorph at higher temperatures [2,15,18].

Ruhi et al. used Al-iso-propoxide as aluminum-carrying precursor in order to deposit alumina by the sol–gel method [14]. Adraider et al. used a laser of high energy density to precipitate alumina coating from sol–gel solution onto substrates [9].

To synthesize α-alumina films, Kelekanjeri et al. applied combustion chemical vapor deposition techniques using aluminum acetylacetonate as a source of aluminum and isopropyl alcohol as a fuel for combustion flame; therefore, the alpha-alumina layer was produced in a one-step process [11].

The aim of the present study is deposition of a homogeneous alpha-alumina thin film onto the surface of novel commercial gamma-alumina nanofibers of extremely high aspect ratio without influencing the morphology of the fibers. For this purpose the solution combustion method has been used. Typically, solution combustion synthesis involves a self-sustained reaction in solutions of metal nitrates and different fuels [19]. High reaction temperatures, which ensure high product purity and crystallinity, allow skipping some additional steps (for example, high temperature product calcination) to achieve the desired phase composition and formation of fine particles due to short process' duration as well as elimination of gases as outputs.

This paper describes the functionalization of γ-alumina nanofibers (γ-ANF) by α-alumina via a solution combustion

5 nm

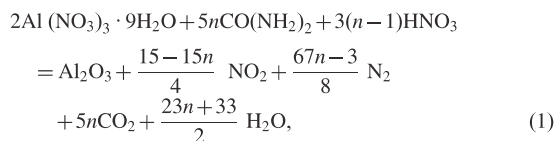Fig. 1. TEM micrograph of original ANF.

deposition process that is conducted in an open atmosphere. To our knowledge, this is the first report on depositing selectively alpha-alumina on gamma-alumina nanofibers (ANF) by the solution combustion method. Fig. 1 shows the TEM micrograph of original ANF, which has extremely high aspect ratios of more than 10^7 and high specific surface area. The average diameter of the fibers is ${\sim}7$ nm. Precursors for a material to be deposited and a fuel to provide combustion were dissolved in water, which was soaked by a bundle of fibers, that when combusted, deposits the desired (alpha-alumina) coating on a surface of fibers by a single-step. In this study, aluminum nitrite was used as a source of alumina and urea was used as a fuel. The role of urea in the process of deposition, influence of the urea amount on the deposited material properties and product morphology were thoroughly studied in the present work.

2. Experimental

2.1. Solution combustion synthesis

Solutions were prepared by dissolving aluminum nitrite and urea in water, which served as the fuel for the combustion. Aluminum metal-ion concentrations were held constant at a molarity of 0.0015 M.

Different amounts of fuel were used to find the optimum concentration for formation of alpha-alumina layer by the solution combustion method. The appropriate amounts of Al $(NO_3)_3 \cdot 9H_2O$ (95%, Merck) as an aluminum precursor and oxidizer, and urea (99%, Merck) as a fuel were dissolved in the deionized water (0.15 mol Al$(NO_3)_3 \cdot 9H_2O$ into 100 ml H_2O) (see N1–3 in Table 1). A concentrated HNO₃ (70%) was added into the solution N3 according to the stoichiometry

$$2Al\,(NO_3)_3 \cdot 9H_2O + 5nCO(NH_2)_2 + 3(n-1)HNO_3$$
$$= Al_2O_3 + \frac{15-15n}{4}\,NO_2 + \frac{67n-3}{8}\,N_2$$
$$+ 5nCO_2 + \frac{23n+33}{2}\,H_2O, \tag{1}$$

where n is the ratio of the amount of the used urea to the amount of the urea needed for providing stoichiometric ratio of fuel to oxidizer ($n=1$).

The optimal proportion of the components was found in the solution N4 (Table 1). An appropriate amount of bundled alumina nanofibers (ANF) with 7 nm in diameter and 50 mm in length [20] was kept in the solution N4 for 15 min allowing the fibers to soak as much solution as possible. A ceramic beaker with the solution-
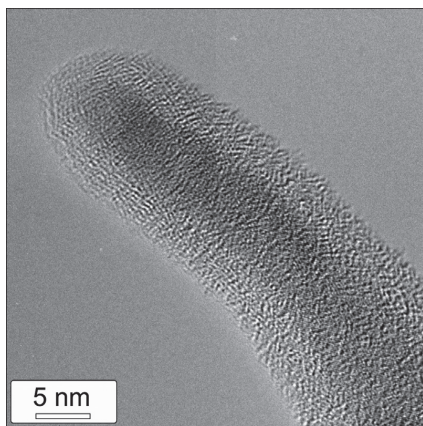
Table 1
Composition of the initial solutions.

N	n	n (Al(NO₃)₃·9H₂O) (mol)	n (urea) (mol)	n (HNO₃) (mol)	n (ANF) (mol)
1	0.5	0.1	0.125	–	–
2	1	0.1	0.25	–	–
3	2	0.1	0.5	0.3	–
4	1	0.1	0.25	–	0.033
5	1	–	0.25	0.3	0.033

soaked fibers was treated at 400 °C for 30 min in a furnace (LM312, Linn High Therm, Germany) that was heated at the rate of 25°/min for ignition. Produced brittle foam can easily be crumbled into a powder.

To study the influence of combustion on the structure and morphology of ANF, a solution was prepared (N5, Table 1), which contains certain amount of urea. Appropriate amount of HNO_3 was used as an oxidizer instead of aluminum nitrate.

2.2. Structural characterization

The phase identification of the combustion synthesized powder was carried out by X-ray diffraction using a Bruker diffractometer (D8) with CuKα radiation at 40 kV in a scanning range θ from 20° to 60° with a step of 0.02°.

Field emission scanning electron microscopy (FESEM S-4700, Hitachi, Japan) and a transmission electron microscope (TEM/STEM JEOL 2100F) operating at 200 kV equipped with a field emission electron gun providing a point resolution of 0.19 nm were used to characterize the microstructure of the combustion product.

3. Results and discussion

3.1. Synthesis of alpha-Al₂O₃ via solution combustion

In order to find an optimal quantity of urea in deposition of alpha-alumina on ANF, possibility of alpha-alumina synthesis was studied. Using urea as a fuel, a white compressed mass was obtained as a combustion product (Fig. 2).

The XRD analysis of the combustion products obtained from the systems containing different amounts of urea shows evident influence of urea quantity on the composition of the final product (Fig. 3). An amorphous mass of material was developed when an inferior amount of urea ($n=0.5$) was added into the solution. This is in good agreement with the results of Sherikar and Umarji [21], according to which amorphous mass forms when the fuel to oxidizer ratio (F/O) is 0.4, and alpha-alumina with the trace of theta-phase forms when F/O=0.6, which is a result of a low enthalpy.

Increasing the amount of urea up to the stoichiometric one ($n=1$) results in formation of alpha-alumina polymorph characterized by sharp and well-developed XRD peaks (Fig. 3b). The formation of alpha-alumina from the solution of this ratio of urea as a fuel is due to generation of enough energy and catalytical capability of urea during the combustion process.

Further increase in fuel amount (up to $n=2$) results in more pronounced and stronger XRD peaks indicating high crystallinity of the final product (Fig. 3c). The addition of an excess of fuel and simultaneously keeping fuel to oxidizer ratio stoichiometric results in higher energy of a system, higher temperature during combustion and, therefore, larger particle size of the final product.

Thus, the stoichiometric amount of fuel (when fuel to aluminum nitrite ratio is 2.5) is sufficient to boost and sustain the reactions up to the formation of alpha-alumina. On the contrary, the employment of a fuel amount inferior to the
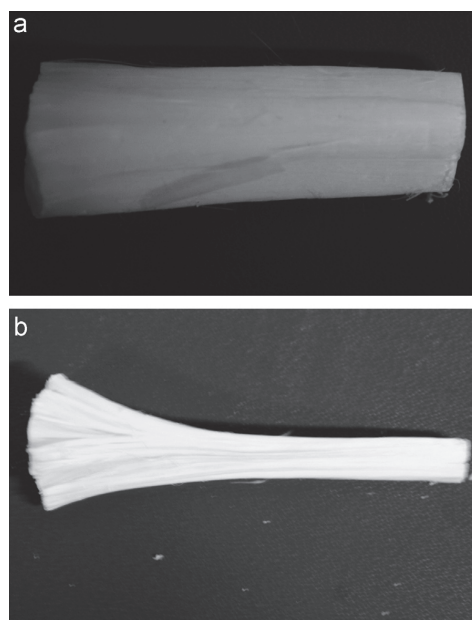

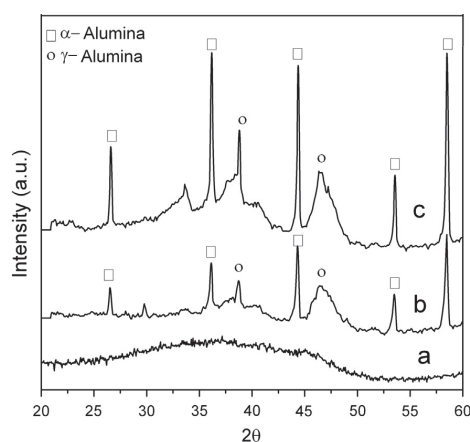Fig. 2. The bundle of (a) original ANF and (b) ANF covered by alumina ($n=1$) after combustion treatment.

Fig. 3. X-ray diffraction pattern of the synthesized powders using different amounts of urea: (a) $n=0.5$; (b) 1; (c) 2.

stoichiometric one is not sufficient to sustain the crystallization of the product keeping it in an amorphous state.

3.2. Deposition of alpha-alumina on gamma-alumina nanofibers

To deposit alpha-alumina on ANFs the stoichiometric amount of fuel ($n=1$) was used to sustain the combustion process (solution N4 in Table 1). By this method, it is possible

to deposit over 60% of Al_2O_3 onto the surface of ANFs in a single step.

XRD diffraction pattern of as deposited alpha-alumina/ANF specimen is depicted in Fig. 4. Two polymorphs of alumina, including α-Al_2O_3 and γ-Al_2O_3, are clearly recognized.

It is believed that the revealed gamma phase is related to γ-alumina fibers assuming that ANF could withstand the condition of combustion (high temperature, presence of the aggressive chemical compounds in the system, etc.). To prove this hypothesis the untreated fibers were tested under the similar combustion condition. The comparison of virgin and treated ANFs has indicated a higher degree of crystallinity while there was no phase transformation of the gamma-ANFs (Fig. 5) during heat treatment. Therefore, no phase transformation of gamma-Al_2O_3 takes place caused by solution combustion synthesis.

In the authors' previous study [20] it was shown that the morphology of γ-alumina nanofibers remains unchanged up to about 1200 °C and transformation $\gamma \rightarrow \alpha$ occurs at temperatures above 1200 °C. Heat treatment of ANF over 1300 °C results in

a stable α-alumina polymorph. Based on this data, it can be established that the combustion temperature does not exceed 1200 °C in the system during the combustion process.

Therefore, the peaks related to alpha-alumina (Fig. 4) belong to the synthesized alumina. It is supposed that the formation of alpha-alumina from aluminum nitrate via the combustion process occurs at lower temperature.

Sherikar and Umarji [21] studied the synthesis of alpha-alumina by the solution combustion method. The highest temperature they detected during combustion was approximately 900 °C, which was recorded at the moment of explosion. However, as it was mentioned above, the alpha-polymorph forms at higher temperature. The formation of alpha-phase at lower temperature can be caused by the high heating rate of system, which is a characteristic feature of the combustion process. Moreover, urea is one of the fuels that decompose very vigorously with flame formation. Notwithstanding, in this work, only alumina obtained from aluminum nitrate was alpha, while gamma-ANF stands gamma withstanding combustion condition. Thus, it is supposed that urea was not only a source of energy but also had an important role in formation of alpha-phase.
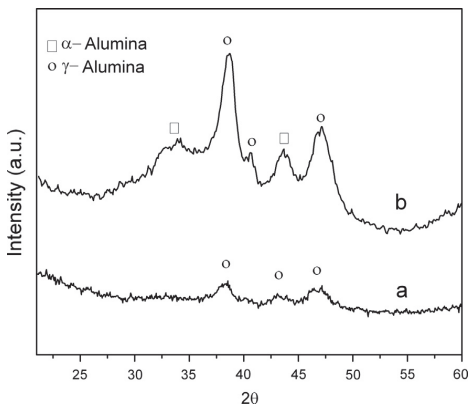

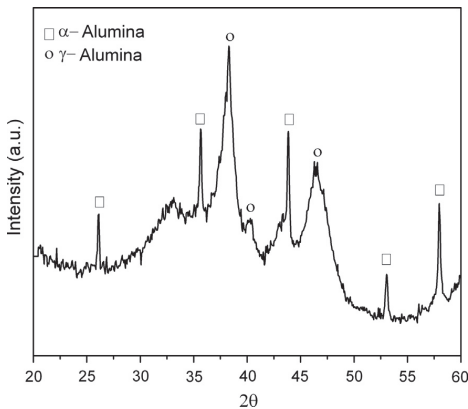Fig. 4. The XRD pattern of ANF (a) before and (b) after combustion treatment.

Fig. 5. X-ray diffraction pattern of as synthesized alumina/ANF sample.
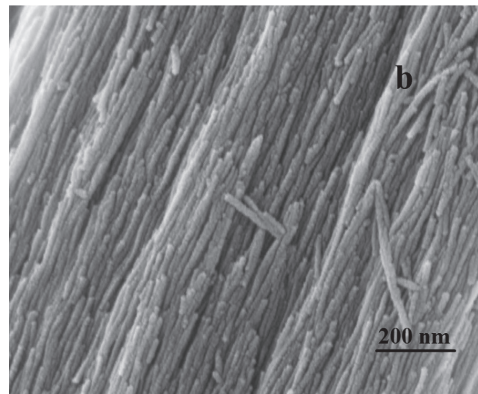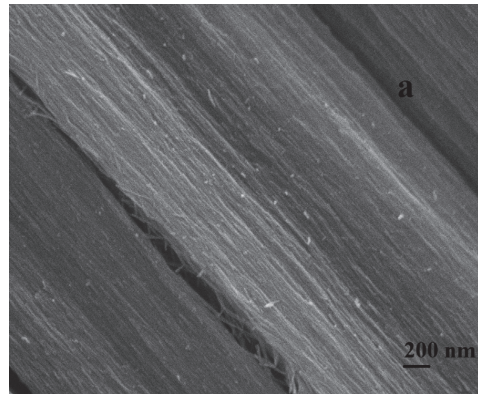

Fig. 6. FESEM micrograph of (a) original ANF and (b) alumina/ANF sample obtained after combustion.

Zhuravlev et al. [22] demonstrated that the combustion of a stable aluminum nitrate and urea complex results in formation of alpha-alumina at even lower temperature. They explained it by the specific behavior of urea with the metal salts represented by formation of stable urea complex compounds with aluminum nitrite, which decompose into α-AlO(OH) (diaspore) with further transformation into alpha-alumina. Therefore, urea can be considered not only as an energy supplier to the system but also as a kind of "catalyst" for α-Al$_2$O$_3$ formation.

3.3. Microstructural characterization

Fig. 6 shows the FESEM micrographs of original ANFs and α-Al$_2$O$_3$/ANF sample obtained by the combustion deposition. As it can be seen in Fig. 6b, alpha-alumina was deposited onto ANF very homogeneously and continuously. It is remarkable that the common microshape of ANF bundle was not changed after depositing alpha-alumina via solution combustion.

4. Conclusions

The solution combustion technique was used to selectively deposit alpha-alumina thin films onto the gamma-alumina nanofibers of extremely high aspect ratio by a single step process. Aluminum nitrate was used as a precursor of aluminum and urea as a fuel.

It was concluded that urea served not only as a fuel for the process running but also as a "catalyst" for the formation of alpha alumina from alumina nitrate.

The XRD analyses confirmed that alumina nanofibers of gamma phase can withstand the combustion conditions without significant morphological changes during processing. The microstructural analysis showed that the deposited alpha-alumina particles were of ultra-fine or/and nanosized. Moreover, alpha-alumina was deposited on ANF very homogeneously.

Acknowledgment

References

[1] M.I.F. Macedo, C.C. Osawa, C.A. Bertran, Sol–gel synthesis of transparent alumina gel and pure gamma alumina by urea hydrolysis of aluminum nitrate, J. Sol–Gel Sci. Technol. 30 (2004) 135–140.

[2] B. Hu, M. Yao, P. Yanga, W. Shana, X. Yao, Preparation and dielectric properties of dense and amorphous alumina film by sol–gel technology, Ceram. Int. 39 (2013) 7613–7618.

[3] N. Yao, G. Xiong, Y. Zhang, M. He, W. Yang, Preparation of novel uniform mesoporous alumina catalysts by the sol–gel method, Catal. Today 68 (2001) 97–109.

[4] M. Trueba, S.P. Trasatti, γ-alumina as a support for catalysts: a review of fundamental aspects, Eur. J. Inorg. Chem. 17 (2005) 3393–3403.

[5] G. Balakrishnan, P. Kuppusami, S. Tripura Sundari, R. Thirumurugesan, V. Ganesan, E. Mohandas, D. Sastikumar, Structural and optical properties of γ-alumina thin films prepared by pulsed laser deposition, Thin Solid Films 518 (2010) 3898–3902.

[6] M.R. Karim, M.A. Rahman, M.A.J. Miah, H. Ahmad, M. Yanagisawa, M. Ito, Synthesis of γ-alumina particles and surface characterization, Open Colloid Sci. J. 4 (2011) 32–36.

[7] A. Bulusu, H. Kim, D. Samet, S. Graham, Improving the stability of atomic layer deposited alumina films in aqueous environments with metal oxide capping layers, J. Phys. D: Appl. Phys. 46 (8) (2013) 084014.

[8] T. Jõgiaas, T. Arroval, L. Kollo, J. Kozlova, T. Käämbre, H. Mändar, A. Tamm, I. Hussainova, K. Kukli, Atomic layer deposition of alumina on γ-Al$_2$O$_3$ nanofibers, Phys. Status Solidi A 211 (2) (2013) 403–408.

[9] Y. Adraider, Y.X Pang, F Nabhani, S.N Hodgson, M.C Sharp, A Al-Waidh, Deposition of alumina coatings on stainless steel by a combined laser/sol–gel technique, Mater. Lett. 91 (2013) 88–91.

[10] S. Blittersdorf, N. Bahlawane, K. Kohse-Höinghaus, B. Atakan, J. Müller, CVD of Al$_2$O$_3$ thin films using aluminum tri-isopropoxide, Chem. Vapor Depos. 9 (4) (2003) 194–198.

[11] V.S.K.G. Kelekanjeri, W.B. Carter, J.M. Hampikian, Deposition of α-alumina via combustion chemical vapor deposition, Thin Solid Films 515 (2006) 1905–1911.

[12] S.K. Pradhana, P.J. Reucrofta, Y. Ko, Crystallinity of Al$_2$O$_3$ films deposited by metalorganic chemical vapor deposition, Surf. Coat. Technol. 176 (2004) 382–384.

[13] T. Kohara, H. Tamagaki, Y. Ikari, H. Fujii, Deposition of α-Al$_2$O$_3$ hard coatings by reactive magnetron sputtering, Surf. Coat. Technol. 185 (2004) 166–171.

[14] G. Ruhi, O.P. Modi, A.S.K. Sinha, I.B. Singh, Effect of sintering temperatures on corrosion and wear properties of sol–gel alumina coatings on surface pre-treated mild steel, Corros. Sci. 50 (2008) 639–649.

[15] P. Vitanov, A. Harizanova, T. Ivanova, T. Dimitrova, Chemical deposition of Al$_2$O$_3$ thin films on Si substrates, Thin Solid Films 517 (2009) 6327–6330.

[16] Y. Bao, P.S. Nicholson, Constant current electrophoretic infiltration deposition of fiber-reinforced ceramic composites, J. Am. Ceram. Soc. 90 (4) (2007) 1063–1070.

[17] M.G. Holmquist, F.F. Lange, Processing and properties of a porous oxide matrix composite reinforced with continuous oxide fibers, J. Am. Ceram. Soc. 86 (10) (2003) 1733–1740.

[18] K.R. Murali, P. Thirumoorthy, Characteristics of sol–gel deposited alumina films, J. Alloys Compd. 500 (2010) 93–95.

[19] A.S. Mukasyan, P. Dinka, Novel approaches to solution-combustion synthesis of nanomaterials, Int. J. Self-Propagating High-Temp. Synth. 16 (1) (2007) 23–35.

[20] M. Aghayan, I. Hussainova, M. Gasik, M. Kutuzov, M. Friman, Coupled thermal analysis of novel alumina nanofibers with ultrahigh aspect ratio, Thermochim. Acta 574 (2013) 140–144.

[21] B.N. Sherikar, A.M. Umarji, Effect of adiabatic flame temperature on nanoalumina powders during solution combustion process, Trans. Indian Ceram. Soc. 70 (3) (2011) 167–172.

[22] V.D. Zhuravlev, V.G. Bamburov, A.R. Beketov, L.A. Perelyaeva, I. V. Baklanova, O.V. Sivtsova, V.G. Vasilev, E.V. Vladimirova, V. G. Shevchenko, I.G. Grigorov, Solution combustion synthesis of α-Al$_2$O$_3$ using urea, Ceram. Int. 39 (2013) 1379–1384.

Paper III.   Aghayan, M.; Gasik, M.; Hussainova, I.; Rubio-Marcos, F.; Kollo, L.; Kubarsepp, J. Thermal and microstructural analysis of doped alumina nanofibers. *Thermochimica Acta.* 2015, 602, 43−48. DOI: 10.1016/j.tca.2015.01.009.

CrossMark
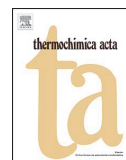
Thermal and microstructural analysis of doped alumina nanofibers

Marina Aghayan [a], Michael Gasik [b,*], Irina Hussainova [a,c], Fernando Rubio-Marcos [d], Lauri Kollo [a], Jakob Kübarsepp [a]

[a] Tallinn University of Technology, Ehitajate tee 5, 19086 Tallinn, Estonia
[b] Aalto University Foundation, School of Chemistry, P.O. Box 16200, FIN-00076 Aalto, Finland
[c] ITMO University, Kronverskiy av. 49, St. Petersburg 197101, Russia
[d] Instituto de Cerámica y Vídrio, CSIC, Kelsen 5, ES-28049 Madrid, Spain

ABSTRACT

Gamma-alumina nanofibers of 7 nm in diameter and aspect ratio $\sim 10^6$ were doped with 10% of zirconia or alpha-alumina by in situ chemical liquid deposition (CLD) technique. Thermal behavior and decomposition kinetics of dopant nano-layers were conducted using simultaneous coupled thermal analysis (TG-DSC-FTIR) to optimize the processing conditions and suggest possible reaction mechanisms. SEM and TEM analysis of fine structure of functionalized nanofibers revealed changes in dopants localization at the base nanofibers. The effect of dopants on thermally-treated materials properties treatment was evaluated after consolidation of the samples by HIP at 1200 °C and 150 MPa. These sintered specimens have shown an increase in microhardness (HV) by 30% and 55% for alumina- and zirconia-doped materials, respectively. The mechanism and kinetics of the dopants precursor reactions are discussed on the basis of the simultaneous thermal analysis.

© 2015 Elsevier B.V. All rights reserved.

1. Introduction

Various nanofibers are known to possess high-surface-to-volume ratio and extreme degree of anisotropy. In the simplest structure, such nanofibers are aligned in one dimension, leading to the possibility of their applications as filters or reinforcing phases. Among variety of ceramic fibers available on market, alumina fibers have received a particular attention due to unique high-temperature properties and chemical stability [1–3]. The key challenge to successful fabrication of fiber reinforced nano-composites that combine outstanding mechanical and tribological properties is understanding of their processing behavior during high-temperature consolidation. In advanced composite materials, a proper interphase developed between matrix and reinforcement during processing determines the performance of the final product.

In authors' previous study [3], the comprehensive thermal analysis of alumina nanofibers (ANF) with 7 and 40 nm nominal diameter was carried out. These ultrahigh aspect ratio fibers (length-to-diameter ratio $\sim 10^7$) are mostly composed of partially hydrated (2–6% wt) gamma-alumina phase. It was found that, besides water release, phase transformation from gamma to alpha

polymorph ($\gamma \rightarrow \alpha\text{-Al}_2\text{O}_3$) was occurring at temperature over 1200–1250 °C [1,3]. In this work, we report further studies on these ultra-high aspect ratio ANF, which were doped with alumina (homophase) and zirconia (xenophase) from the solutions of respective nitrate precursors by method known as a chemical liquid deposition (CLD) [3,4]. The concept of CLD is to deposit nitrates on the surface of the matrix material in controlled conditions and to apply a subsequent thermal treatment to decompose them [4]. This leaves (meta)-stable oxide phases of a higher chemical activity compared with similar phases obtained from, e.g., mechanical addition of nanopowders [4]. The dopants chosen here were to study possible effects of homophase and xenophase on thermal behavior of ANF and perspectives to use the functionalized nanofibers for ceramic matrices reinforcements. Alumina as a homophase has no direct chemical reactivity with alumina nanofibers, and zirconia as a xenophase should not chemically react with alumina either, but it is known to restrict alumina grains growth in $\text{Al}_2\text{O}_3\text{-ZrO}_2$ nanocomposites [5,6], so one should be able to detect whether similar effect might be also in this case.

The effect of dopants and/or nanolayer coatings on the properties of nanostructured aluminas was studied in several cases. For example, Zhao et al. [7] have prepared iron-doped boehmite nanofibers synthesized using soft chemical hydrother-mal methodology and found that Fe-doped boehmite thermally decomposes at higher temperatures compared to undoped

* Corresponding author.
E-mail address: michael.gasik@aalto.fi (M. Gasik).

boehmite. Yang et al. [8] have synthesized chromium-doped boehmite nanofibers by low temperature co-precipitation of aluminium nitrate and chromium nitrate. The dehydroxylation temperature of boehmite was also visibly increased [8]. Additions of zirconia and titania were exploited to process ZrO_2-Al_2O_3 and TiO_2-Al_2O_3 nanocomposites using boemite nanofibers as a starting material [9]. Extensive studies of transformation and thermal behavior of γ-alumina, boehmite and their intermediate phases have been carried out in [10–13]. However, the thermal behavior of highly aligned fibers of diameter less than 50 nm coated by nanolayers of zirconia or alumina has not been studied yet.

Whereas the CLD was reported to be a convenient, solvent-free way to fabricate ceramic nanocomposites [4], to achieve a complete control of the procedure and, therefore, to perform a suitable tailoring of the final microstructure requires thorough study of the composite material evolution during decomposition process. In the present study, thermal analysis was conducted on doped nanofibers for better understanding synthesis procedure and thereof optimizing the applied conditions.

2. Experimental

The nanofibers of γ-alumina with diameters of 7 and 40 nm [3] are well-aligned fibers bundles, Fig. 1. The specific surface area measured for 7 nm nanofibers was $155 \, m^2 g^{-1}$ (BET method). Alumina and zirconia were selected as demonstration coatings of these bundles. Chemical liquid deposition (CLD) technique [4] was used to cover ANF by 10% vol. of ZrO_2 and 10% vol. α-Al_2O_3. Zirconium(IV) oxynitrate (zirconyl nitrate) hydrate $ZrO(NO_3)_2 \cdot xH_2O$ (99%, Sigma–Aldrich) and aluminium nitrate non-ahydrate $Al(NO_3)_3 \cdot 9H_2O$ (95%, Merck) were used as zirconia and alumina precursors. The first precursor is usually produced by water hydrolysis of the zirconium(IV) nitrate and thus the amount of molecular water (x) in the crystallohydrate is generally

Fig. 1. Aligned alumina nanofibers structure (7 nm average diameter) shown with low (a) and high (b) magnifications.

manufacturing process-dependent. To determine the water content and check temperature ranges of precursors decomposition, thermal analysis was conducted.

The decomposition kinetics of dopants was studied with simultaneous coupled thermal analysis (TG-DSC-FTIR) with STA449C "Jupiter" (Netzsch Gerätebau GmbH) and "Tensor-27" FTIR spectrometer (Bruker Optics). Experiments were performed in synthetic dry air (21% O_2, balance nitrogen; Linde AGA) flow of 20 ml/min with heating and cooling rates of 10 K/min and maximal temperature of 1480 °C. Alumina crucibles were used without a lid and an empty crucible was used as a DSC reference. Evolved gas analysis by FTIR was performed with automatic CO_2 bands compensation in transmission mode on gas flow taken off the STA furnace via heated (300 °C) and shielded capillary. Data collection and analysis were made using Proteus 6.1 (Netzsch Gerätebau GmbH) and OPUS 5.5 (Bruker Optics) software with a proprietary spectral database. Thermal analysis results for the undoped ANF were recently reported in [3] by the authors.

Three batches of suspensions were prepared dispersing 1 g of ANF bundles in 40 g of distilled water by stick ultrasound (Hielscher Ultrasonic Homogenizer UP200Ht) for 5 min at 100 W (pulse mode 3 s work and 1 s pause). A mass of 0.39 g of zirconium (IV) oxynitrate hydrate and 0.74 g of aluminium nitrate non-ahydrate was added into the obtained suspensions. The blank (control) specimen was also made containing only nanofibers suspension (marked further as ANF-0). The mixtures were stirred (800 rpm) for 15 min to completely dissolve the precursors and homogenize mixtures. Upon mixing, the resulting pH of nanofibers suspension (ANF-0) was 6.6, for aluminum nitrate-added suspension (ANF-A10) ~3.8 and for zirconyl nitrate-added suspension (ANF-Z10) was ~2.2. These numbers were found to be similar to intrinsic pH caused by partial hydrolysis of the respective nitrates. The obtained slurry was dried slowly at 90 °C for 20 h and at 95 °C for 10 h to remove unbound water. Decomposition of deposited dopants was carried out at 600 °C for 2 h. These treatment temperature and time were determined by thermal analysis as shown below, selected yet to keeping ANF substrate still in the gamma-phase form.

The morphology of the ANF-0, zirconia-covered ANF (ANF-Z10) and alumina-covered ANF (ANF-A10) after heat-treatment (before pressing) was examined by JEOL 2100F transmission electron microscope (HRTEM) operating at 200 KV and equipped with a field emission electron gun providing a point resolution of 0.19 nm. The EDXS (energy dispersive X-ray spectrometer) INCA x-sight (Oxford Instruments) was used for chemical elemental analysis.

Sets of three specimens of each composition were prepared for sintering and HIP. The cylindrical specimens 12 mm of diameter and 3 mm in height were compacted by uniaxial pressing at 100 MPa. The specimens were then encapsulated in steel capsule, outgassed and hot isostatically pressed (HIP) at 1200 °C and 150 MPa for microstructure and properties evaluation. Microstructural analysis of composites before and after sintering was performed by scanning electron microscopy (SEM Zeiss EVO MA 15, Germany). The samples were cut and polished with 1 μm diamond paste. Microhardness measurements were conducted according to ISO 14,577 on a Buehler Micromet 2001 (Buehler GmbH) applying an indentation load of 0.5 N. The Vickers microhardness value for each composition was taken as the average of at least 12 measurements made on each specimen.

3. Results and discussion

The results of thermal analysis of decomposition of the dopants precursors are shown in Fig. 2 (aluminum nitrate) and Fig. 3 (zirconyl nitrate). As seen from the data, the decomposition of precursors is very complex and contains many different stages.
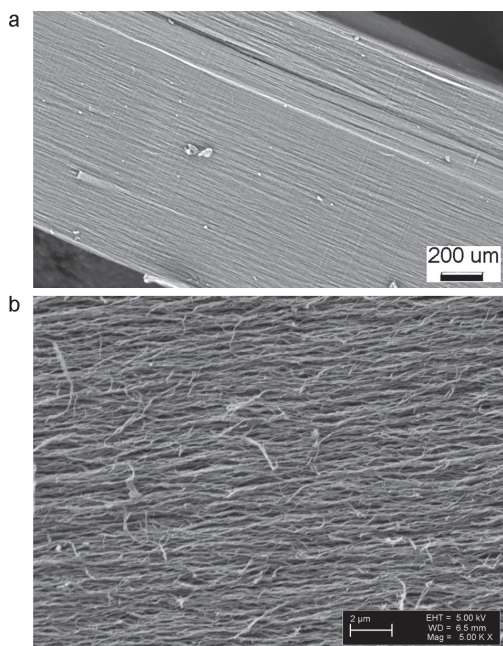
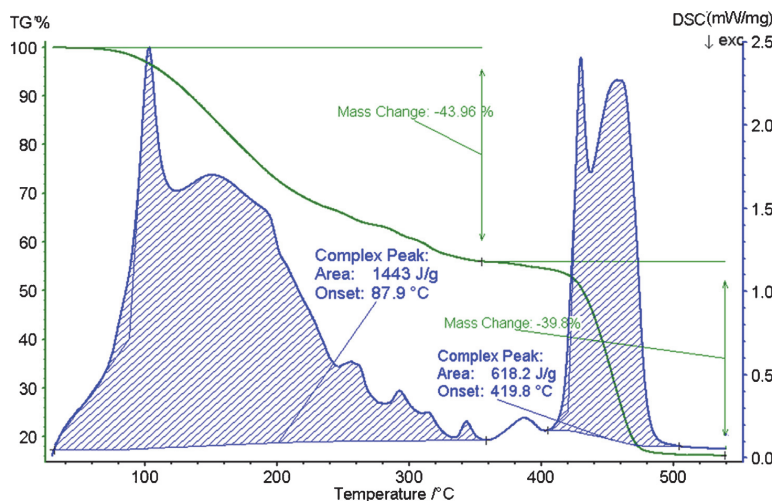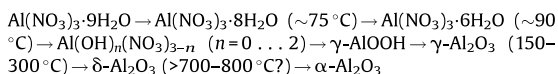**Fig. 2.** Thermal analysis (TG-DSC) of $Al(NO_3)_3 \cdot 9H_2O$ precursor at heating rate 10 K/min.

In the case of aluminum nitrate, the release of first and two subsequent molecules of water from the hydrate proceeds at low temperatures ($<100\,°C$). This causes dehydrated salt being partially dissolved in its own water, which also evaporate simultaneously upon continuous heating. At higher temperatures, aluminum nitrate forms hydroxonitrates, which process eventually terminates upon formation of boehmite and gamma-alumina. Release of nitrogen oxides and water completes below $500\,°C$ and the following signals changes are associated eventually with alumina phase transformations. Thus all these process stages may be expressed by the scheme [1,3,14]:

$Al(NO_3)_3 \cdot 9H_2O \rightarrow Al(NO_3)_3 \cdot 8H_2O$ ($\sim 75\,°C$) $\rightarrow Al(NO_3)_3 \cdot 6H_2O$ ($\sim 90\,°C$) $\rightarrow Al(OH)_n(NO_3)_{3-n}$ ($n = 0\ldots2$) $\rightarrow \gamma$-AlOOH $\rightarrow \gamma$-Al_2O_3 (150–300\,°C) $\rightarrow \delta$-Al_2O_3 (>700–$800\,°C$?) $\rightarrow \alpha$-Al_2O_3

The brutto-reaction of the aluminum nitrate decomposition was elaborated by matching the experimental enthalpy changes (area under DSC curve) to the theoretical enthalpy changes as follows:

$2Al(NO_3)_3 \cdot 9H_2O \rightarrow Al_2O_3 + 6NO_2 + 9H_2O + 1.5O_2$,
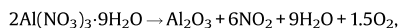
i.e., it is a redox reaction where nitrogen reduces and oxygen oxidizes. The formation of different alumina phases (including those with amorphous structures) should be considered beneficial to phase transformations of ANF, as it might be more active during sintering.

Zirconyl nitrate $ZrO(NO_3)_2 \cdot xH_2O$ is the result of a hydrolysis reaction of zirconium(IV) nitrate $Zr(NO_3)_4$ in water and acid solutions. It was suggested [15] that the crystalline structure of $ZrO(NO_3)_2 \cdot xH_2O$ is better stated as $Zr(OH)_2(NO_3)_2 \cdot (4+y)H_2O$, where $y \leq 6$. For each zirconium atom there are 2–3 water molecules and an additional nitrate group located in between the chains. Half of the nitrate groups present in the formula are directly coordinated to the zirconium atoms and the other half are ionically bound between the chains in the crystal lattice [15,16]. The first two peaks in the DSC signal and mass loss stages in TG (Fig. 3) can be attributed to endothermic reactions correlated with the loss of water (85–180\,°C and the conversion of nitrate groups to gaseous NOx (180–350\,°C). The exothermic crystallization peak of

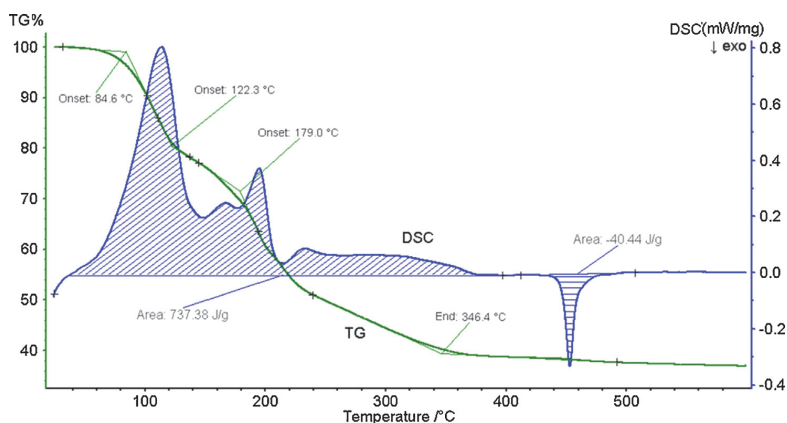**Fig. 3.** Thermal analysis (TG-DSC) of $ZrO(NO_3)_2 \cdot xH_2O$ precursor at heating rate 10 K/min.
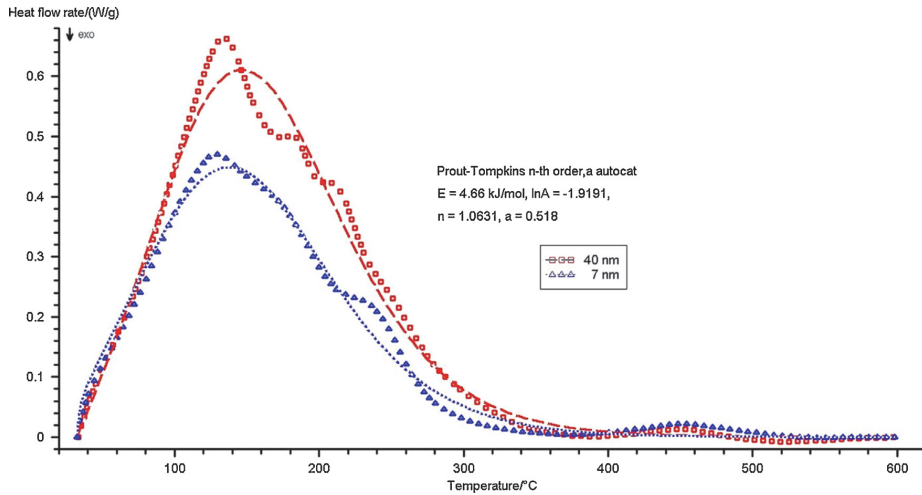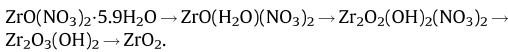
Fig. 4. A formal non-linear regression fit of the DSC signal for alumina-doped ANF with 7 and 40 nm diameter.

amorphous in situ formed ZrO_2 can be seen at ~460 °C, which temperature corresponds well to the value of 469 °C found in the independent DTA study [16]. The total decomposition process is endothermic, requiring about 740 J/g mostly for removal of water and nitrate, whereas zirconia crystallization is slightly exothermic (40 J/g for initial specimen mass, i.e., ~100 J/g of zirconia mass after nitrate decomposition), and is not associated with the mass changes. The mass loss analysis shows that used zirconyl nitrate has x = 5.908 mol of water per 1 mol of salt. This value was used in calculation of the solution composition required for doping. Thus the following scheme might be suggested for zirconyl nitrate decomposition [15,16]:

$ZrO(NO_3)_2 \cdot 5.9H_2O \rightarrow ZrO(H_2O)(NO_3)_2 \rightarrow Zr_2O_2(OH)_2(NO_3)_2 \rightarrow Zr_2O_3(OH)_2 \rightarrow ZrO_2$.

For designing the proper heat treatment regime of doped ANF, the kinetic model has been set up, shown here in the case of ANF-A10 material. Using ANF with two different fiber diameters, 7 and 40 nm respectively [3], but with the same added alumina volume fraction (10%), the kinetic analysis has shown DSC traces to be reasonably fit with a Prout–Tompkins autocatalytic model [17], Fig. 4. This formal non-linear regression fit is not the confirmation of the nitrate decomposition mechanism, but rather a formal equation aimed to be used for the process optimization. The objective for the heating procedure in the muffle furnace was to ensure close-to-linear decomposition kinetics of the nitrates deposited on the ANF with 7 nm diameter in the range 50–500 °C. This predictive calculation based on the model parameters (Fig. 4) is shown in Fig. 5. The first temperature plateau was added because of substantial amount of water to be vaporized before
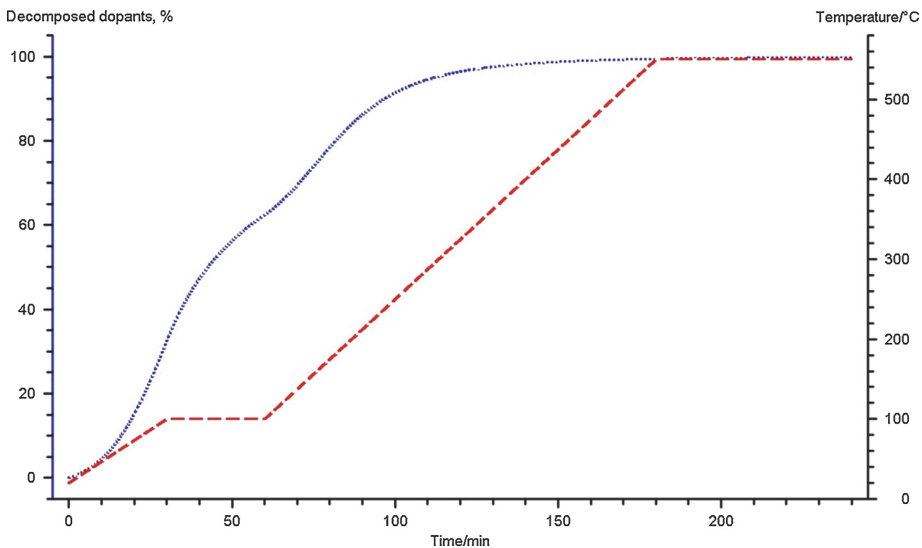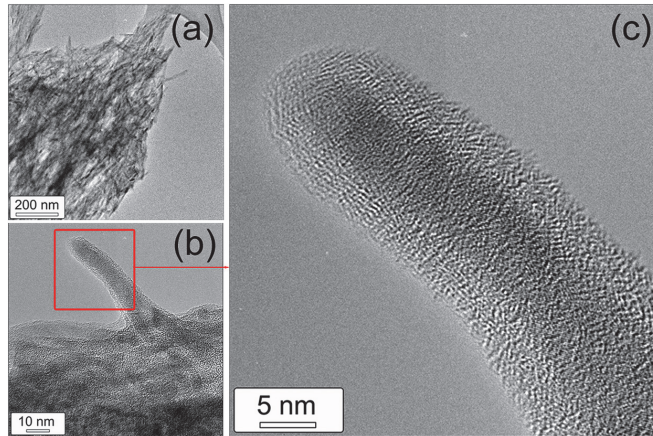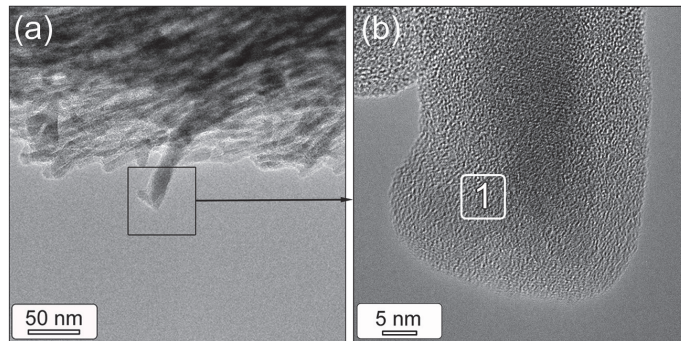

Fig. 5. Calculated heating regime for thermal treatment of alumna-doped ANF of 7 nm diameter.

Fig. 6. HRTEM images of ANF-0 (undoped), with increased magnifications from (a) to (c).
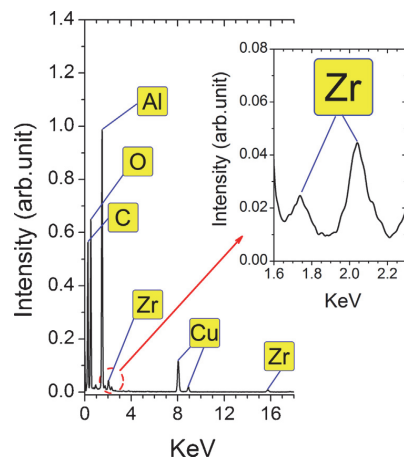

Fig. 7. HRTEM images of ANF-10Z nanocomposite, with increased magnifications from (a) to (b).

main stage of nitrate decomposition. Similar calculation was made for zirconia-doped ANF. Thus, both dopants undergo complete nitrates decomposition to oxides below 600 °C. Therefore, this temperature was chosen for a heat treatment of the doped ANF and all specimens, including the non-doped ANF.

Fig. 6 shows the high-resolution transmission electron microscopy (HRTEM) images of undoped γ-ANF. It is noticeable that the original fibers exist in core–shell structure type: two distinct materials zones corresponding to aluminium hydroxide-rich layer and amorphous γ-alumina nano-fibers core could be seen due to variation of contrast.

Fig. 7 shows similar HRTEM images of ANF covered with 10 vol. % of zirconia (ANF-10Z). XRD analysis indicates that ANF substrate has a thin ZrO_2 coating with low crystallinity. Notably, no free exposed surface of ANF appears in the TEM visualization, suggesting that there exists a strong interaction between the ZrO_2 coating and the ANF. EDX analysis was used for the semi-quantitative determination of zirconium content in resultant ANF-ZrO_2 nanocomposite (Fig. 8). In the spectra marked as point 1 (Fig. 7b), zirconium peaks were detected at the Al_2O_3 nanofiber (Cu signals originate from the supporting TEM grid). This reveals that the CLD process produces a good homogenous ZrO_2 coating on the ANF support.

Fig. 8. EDX spectra of the zirconia coating, corresponding to the point 1 in Fig. 7, (b).
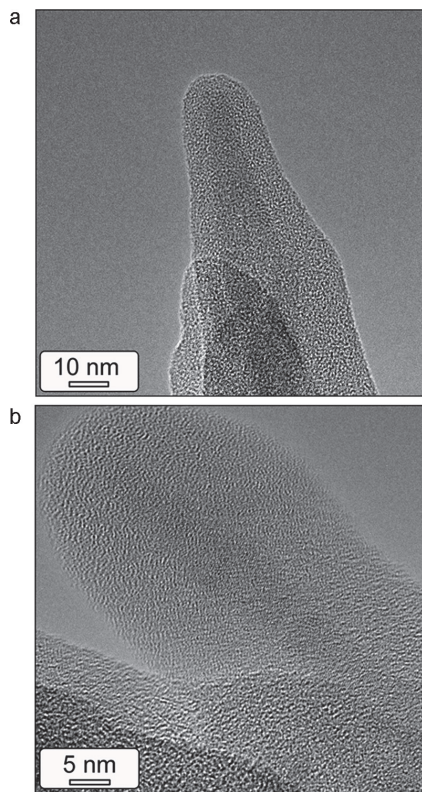
Fig. 9. TEM images of ANF-A10 nanocomposite, with increased magnifications from (a) to (b).

Fig. 9 shows the TEM picture of ANF-10A (ANF was covered 10 vol.% of alumina) composite nanofiber. According to TEM examination, ANF covered with Al_2O_3 consist two zones, where the relative core diameter is smaller (compare with Fig. 6 for ANF-0). During these studies, it was not possible to see a clear difference between the extra homophase layer of deposited alumina and original extra alumina shell (Fig. 6), as both seem to constitute a continuous structure of the shell of ANF-A10.

The effect of zirconia and alumina nanolayers addition on the mechanical properties of ANF was estimated by measuring microhardness in the consolidated state. Undoped ANF after hot isostatic pressing was found to have hardness of $\sim$830 ± 43 HVμ (500 g load) that is lower than commonly described nanostructured α-alumina. It is expected because the ANF material mainly has retained the γ-phase state. The hardness of sintered ANF-10A was found to be of 30% higher (1090 ± 70 HVμ) and for ANF-10Z is 55% higher (1283 ± 68 HVμ) compared to undoped ANF.

4. Conclusions

The alumina composite nanofibers (ANF) (undoped and doped with 10% of alumina and zirconia) were prepared by chemical liquid deposition (CLD) method. Thermal analysis of decomposition kinetics of nitrate dopants shown them to be completely decomposed over 600 °C, although the reaction paths are rather complex and cannot be clearly verified by thermal analysis alone.

Nevertheless, the DSC and TG have given enough data to perform a formal kinetic analysis and to make optimized thermal treatment of the doped ANF with nearly linear decomposition rate.

The microstructure of ANF after thermal treatment represents a clear core–shell type, where dopants are uniformly distributed along the fiber longest axis. In the case of zirconia, deposited layer fine structure can be observed, but for alumina dopant, there is no clear separation between original ANF alumina and that brought in by CLD process.

The hardness of the sintered doped ANF nanocomposites was 30% (with alumina) and 55% (with zirconia) higher than undoped ANF at the identical sintering conditions.

References

[1] M. Aghayan, N. Voltsihhin, M.A. Rodríguez, F. Rubio-Marcos, M. Dong, I. Hussainova, Functionalization of gamma-alumina nanofibers by alpha-alumina via solution combustion synthesis, Ceram. Int. 40 (8A) (2014) 12603–12607.
[2] A.M. Azad, M. Noibi, M. Ramachandran, Fabrication and characterization of 1-D alumina (Al_2O_3) nanofibers in an electric field, Bull. Polish Acad. Sci. Tech. Sci. 55 (2007) 195–201.
[3] M. Aghayan, I. Hussainova, M. Gasik, M. Kutuzov, M. Friman, Coupled thermal analysis of novel alumina nanofibers with ultrahigh aspect ratio, Thermochim. Acta 574 (2013) 140–144.
[4] M. Gasik, P. Ostrik, E. Popov, Non-oxide ceramics with nano-layers made by chemical liquid deposition process, Brit. Ceram. Trans. 92 (5) (1993) 209–213.
[5] P. Lukas, M. Vrana, J. Saroun, V. Ryukhtin, J. Vleugels, G. Anne, O. van der Biest, M. Gasik, Neutron diffraction studies of functionally graded alumina/zirconia ceramics, Mater. Sci. Forum 492–493 (2005) 201–206.
[6] M. Gasik, B. Zhang, Optimization of sintering of zirconia/alumina functionally graded material, Functionally Graded Materials, VII, TransTech Publ, Switzerland, 2003, pp. 183–186.
[7] Y. Zhao, R.L. Frost, W.N. Martens, H.Y. Zhu, XRD, TEM and thermal analysis of Fe-doped boehmite nanofibres and nanosheets, J. Thermal Anal. Calorim. 90 (3) (2007) 755–760.
[8] J. Yang, R.L. Frost, Y. Yuan, Synthesis and characterization of chromium-doped boehmite nanofibres, Thermochim. Acta 483 (2009) 29–35.
[9] E. Liu, Synthesis of one-dimensional nanocomposites based on alumina nanofibers and their catalytic applications, PhD Thesis, Queensland University of Technology, 2011.
[10] D.E. Clark, J.J. Lannutti, Phase transformations in sol–gel derived aluminas, in: L.L. Hench, D.R. Ulrich (Eds.), Ultrastructure Processing of Ceramics, Glass, and Composites, John Wiley and Sons, NY, 1986, pp. 126–141.
[11] J.M. McHale, A. Navrotsky, A.J. Perrotta, Effects of increased surface area and chemisorbed H_2O on the relative stability of nanocrystalline γ-Al_2O_3 and α-Al_2O_3, J. Phys. Chem. B 101 (4) (1997) 603–613.
[12] Y. Wang, J. Wang, M. Shen, W. Wang, Synthesis and properties of thermostable γ-alumina prepared by hydrolysis of phosphide aluminium, J. Alloys Compd. 467 (2009) 405–412.
[13] R.-S. Zhou, R.L. Snyde, Structures and transformation mechanisms of the η, γ, and θ transition aluminas, Acta Cryst. B 47 (1991) 617–630.
[14] M. Gasik, F.R.S. Sale, Decomposition of precipitated aluminium hydroxide studied by simultaneous thermal analysis, Proc. 10th ICTA Congress, Hatfield, UK, 1992, pp. 25.
[15] P. Southon, Structural evolution during the preparation and heating of nanophase zirconia gels, PhD Thesis, University of Technology, Sydney, 2000.
[16] K. De Buysser, P.F. Smet, B. Schoofs, E. Bruneel, D. Poelman, S. Hoste, I. Van Driessche, Aqueous sol–gel processing of precursor oxides for ZrW_2O_8 synthesis, J. Sol-Gel Sci. Technol. 43 (2007) 347–353.
[17] M.E. Brown, D. Dollimore, A.K. Galwey, Reactions in the solid state, in: C.H. Bamford, C.F.H. Tipper (Eds.), Comprehensive Chemical Kinetics, 22, Elsevier, Amsterdam, 1980, pp. 340.

Paper IV.   Aghayan, M.; Hussainova, I., Fabrication of NiO/NiAl$_2$O$_4$ nanofibers by combustion method. *Key Engineering Materials*. 2016, 674, 31-34.
DOI:10.4028/www.scientific.net/KEM.674.31.

Fabrication of NiO/NiAl2O4 nanofibers by combustion method

Marina Aghayan[1, a *], Irina Hussainova[1,2,b]

[1]Tallinn University of Technology, Department of Materials Engineering, Ehitajate 5, 19180 Tallinn, Estonia

[2]ITMO University, Kronverksky 49, St. Petersburg, 197101, Russian Federation

[a]marina.aghayan@ttu.ee, [b] Irina.Hussainova@ttu.ee

Keywords: nickel aluminate, nanofibers, combustion synthesis, glycine.

Abstract

Nickel aluminate spinel (NiAl2O4) has received attention as a catalyst solid support due to its stability, strong resistance to acids and alkalis and high melting point. The properties and quality of the catalysts are heavily affected by crystal size, morphology, phase homogeneity and surface characteristics of the materials, which themselves are dependent on method and parameters of processing rout. In this work, we report on the fabrication of novel NiAl2O4 nanofibers covered by NiO nanolayer by combustion method.

The XRD patterns show that the combustion technique was excellent to prepare NiO/NiAl2O4 nanofibers. The crystallite sizes of NiAl2O4 and NiO were found to be around 27 and 19 nm correspondingly. Scanning electron micrographs (SEM) and Energy dispersive X-ray (EDX) analysis showed that the NiO/NiAl2O4 nanofibers with more than 20 nm in diameter were consist of NiAl2O4 core and NiO outer layer.

Introduction

Nickel aluminate (NiAl2O4) is a transition metal ion spinel material with common spinel structure, in which Al occupies the octahedral and Ni the tetrahedral sites. Nickel aluminate exhibits good chemical stability in acidic and alkaline conditions. It has a high melting point and a stable structure at high temperatures [1]. Moreover, nickel aluminate and/or nickel oxide doped nickel aluminate is considered as a very effective catalyst material in many chemical processes [1-6]. Therefore, NiAl2O4 and/or NiO/NiAl2O4 composition is extremely important material for many industrial applications, including catalysis.

Usually, the nickel aluminate spinel powder is synthesised by the high-temperature solid-state reactions between the constituent oxides. The produced particles are large in size ($\geq$ 1 µm) and of wide size distribution. Several preparation methods have been applied to obtain the crystalline nickel aluminate spinels of ultra-fine grains, among others there are: sol-gel synthesis, sono-chemical method, microwave heating, mechano-chemical [7] and polymer solution. Solution combustion is one of the advantageous methods for synthesis of the nickel aluminate powder using the well adjusted proportions of nickel and aluminium nitrates.

The essential requirements for the preparation of the materials with well controlled uniformity and high-purity encourages the development of wet chemical methods described in [8]. The method comprises steps of adding nickel nitrate into a suspension liquid of nano-grade aluminium oxide, adding dispersant, stirring to obtain a mixed solution, dropping ammonia to obtain nickel-ammonia complex ($[Ni(NH_3)_6]^{2+}$)-alumina mixed solution and water under stirring to obtain green precipitate, washing, drying and inducing a carbon thermo-reduction calcination to obtain the final product. The nano-powder of NiAl2O4 consists of the particles with average particle size $\leq$ 100 nm. One of the important methods to prepare aluminates is a combustion route described elsewhere [9]. A process includes proportionally mixing the nickel nitrate, aluminium nitrate and urea to obtain the solution, which was put into a preheated furnace to produce NiAl2O4 material. The advantage of the solution combustion technique is the quasi-atomic dispersion of the component cations in the liquid precursors, which facilitates synthesis of the crystallized powder with a small particle size and a high purity at low temperatures [10, 11].

One-dimensional (1D) structures have received great attention due to their specific properties and potential applications. Furthermore, the development of methods for synthesizing a wide variety of 1D structures of novel materials has become increasingly important. Their configurations with a large specific surface area indicate their potentially useful physical and chemical properties. Accordingly, a variety of applications including electrodes, sensors, and insulators is expected.

Kim et al. [12] have succeeded in growing cubic submicron-sized NiAl2O4 rods on sapphire substrates by means of heating mixture of NiO and graphite powders. According to the SEM images given in the paper, the diameter of the rods is > 100 nm and the length is less than 3 μm.

In the present paper, we report on the fabrication of 1D nickel aluminate spinel nanofibers at the submicron scale. This has been performed by combustion synthesis using bundle of the alumina nanofibers, described elsewhere [13], and nickel aluminate as precursors and glycine as a fuel.

Experimental

5.7 g of nickel (II) nitrate hexahydrate [Ni(NO3)2*6H2O] (≥98.5%, Sigma-Aldrich) as a source of nickel and 1.6 g of glycine [C2H5NO2] (≥99%, Sigma) as a fuel were dissolved in 15 ml of deionized. The obtained solution was dropped onto 2 g of bundled alumina nanofibers (ANF) with 7 nm in diameter and 50 mm in length and left 30 minutes at room temperature for homogenization. The wetted bundles of ANF were placed on a netting, which was placed in a preheated muffle furnace at 400 $^{\circ}$C and left there for 30 min.

The phase identification of the combustion product was carried out by X-ray diffraction using a Bruker diffractometer (D8) with CuKα radiation at 40 kV in a scanning range Θ from 20o to 70o with a step of 0.02o. The morphology of the obtained product was examined by Scanning electron microscopy (SEM Zeiss EVO MA 15, Germany) and JEOL 2100F transmission electron microscope (HRTEM) operating at 200KV and equipped with a field emission electron gun providing a point resolution of 0.19 nm. The EDXS (energy dispersive X-ray spectrometer) INCA x-sight (Oxford Instruments) was used for chemical elemental analysis.

Results and discussion

Combustion synthesis is an attractive method to synthesis different materials with different shapes and scale due to its rapidness, simplicity and flexibility. This process not only allows to produce nanosized oxide materials but also allows uniform, nanoscale deposition of different materials in nanoscale matrix in a single step. The method requires addition of fuel to the metal nitrate solution and ignition of this fuel at an appropriate temperature. The self-sustaining process of fuel burning, decomposition of nitrate and oxidation of the metal ion takes place simultaneously and results in the formation of the appropriate product. As the process is accompanied by large quantities of gases (COx, NOy, N2 and H2O) the as obtained products are in fine particles with a high surface area. For preparation of 1D NiO/NiAl2O4, the wetted alumina nanofibers were combusted at 400 $^{\circ}$C as it was described above. The X-ray diffraction pattern of the synthesised combustion product is shown in Fig.1. Although the appropriate amount of Nickel nitrate and alumina is used in order to obtain single NiAl2O4 phase, NiO cubic phase is obtained in detriment to NiAl2O4 cubic spinel. The presence of NiO phase in the synthesis of NiAl2O4 has also been reported by other researchers [14-15].

The peaks of both NiAl2O4 and NiO phases are quite broad and indicate the fine particle nature of the product. The crystallite sizes, D were calculated using Scherrer's formula—$D = 0.9\lambda/\beta\cos\theta$, where λ is the radiation wavelength of the X-rays (0.15406 nm, Cu Kα radiation) and θ is the diffraction peak angle, β is the corrected half width of the diffraction peak. The obtained cubic NiAl2O4 with normal spinel structure with lattice constants α=8.048Å has crystal size of about 19 nm, while cubic NiO with lattice constants α=4.177Å has crystal size of 27 nm.
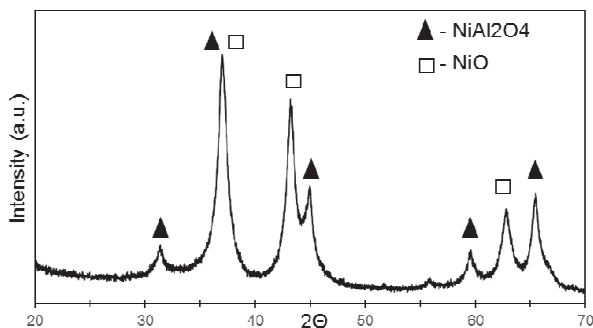
Figure 1. X-ray diffractogram of the combustion product.

The morphology of combustion products is shown on the SEM and TEM images (Figure 2). 1D NiAl2O4 nanostructures produced with the help of the present route typically have diameters ranging from ~ 20 to several tens of nanometres and with lengths up to several tens of microns. However, the shape of the initial alumina nanofibers were kept to by fibrous, while the diameter of the fibres slightly increases after combustion process due to phase change. As well as, NiO phase serves like a glue for NiAl2O4 fibres bonding them together. The threadlike microstructures corresponded to diameters in a relatively wide range with the aspect ratio well above 10^4. It should be noted, that the combustion process could produce a huge amount of heat, and results in high temperatures [16]. Meanwhile, a big amount of gases eliminates during this process, which provides high cooling rate, consequently rapidness for the process. Due to this features of combustion method, it was possible to obtain fibres at nanoscale. The chemical composition analysis by EDX spectroscopy shows that the atomic ratio of Ni atoms to Al atoms is 0.9. However, the further insight into the structure of the nanofibers shows (EDX) that the core nanofiber is wrapped in a uniform thin outer layer of NiO.
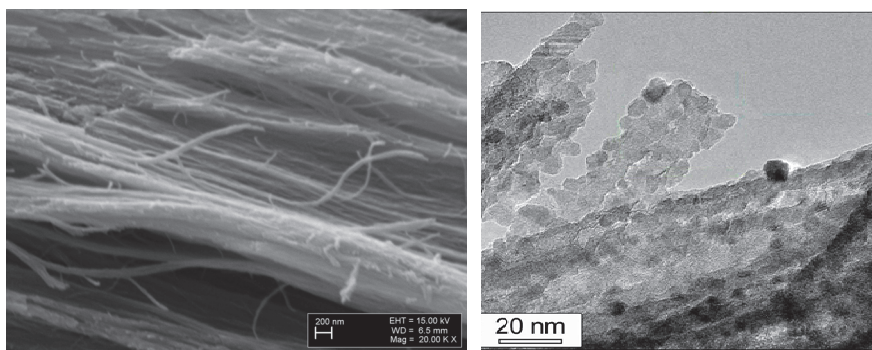
Figure 2. (a) SEM image of the combustion product; (b) TEM image of the combustion product

Conclusions

In conclusion, we succeeded in synthesizing NiAl2O4 nanofibers covered with homogeneous layer of NiO by combustion method without any additional step. The obtained fibers has diameter ranging from ~ 20 to several tens of nanometres and with lengths up to several tens of microns.

References

[1] A. Fritz, V. Pitchon, The current state of research on automotive lean NOx catalysis, Applied Catalysis B: Environmental, 13 (1) (1997), 1-25.

[2] H. Fang, L. Haibin, Z. Zengli, Advancements in Development of Chemical-Looping Combustion: A Review, Intern. J. Chem. Eng., 2009 (2009), Article ID 710515, 16 pages.

[3] T. Mattisson, E. Jerndal, C. Linderholm, A. Lyngfelt, Reactivity of a spray-dried NiO/NiAl2O4 oxygen carrier for chemical-looping combustion, Chem. Eng. Sci., 66 (2011) 4636-4644.

[4] N. Salhi, A. Boulahouache, C. Petit, A. Kiennemann, C. Rabia, Steam reforming of methane to syngas over NiAl2O4 spinel catalysts, Int. J. Hydrogen Energy, 36 (2011) 1433-1439.

[5] J. Mary Fisher, T. Ian Hyde, D. Thompsett, Manganese containing oxygen storage component comprising three-way catalyst composition, U.S. Patent 7,396,516 B2, 2001.

[6] J.C. González, J.M. Benito López, M.A. Rodríguez Barbero, I. Rodríguez Ramos, A. Guerrero Ruiz, Development of Nanostructured Catalytic Membranes (NCMs) for Partial Benzene Hydrogenation to Cyclohexene, J. Nanosci. & Nanotech., 7 (2007) 1-11.

[7] M.K. Nazemi, S. Sheibani, F. Rashchi, V.M. Gonzalez-DelaCruz, A. Caballero, Preparation of nanostructured nickel aluminate spinel powder from spent NiO/Al2O3 catalyst by mechano-chemical synthesis, Advanced Powder Technology 23 (2012) 833–838.

[8] Ch. Zhao, Y. Guo, X. Cang, Preparation method of NiAl2O4 nano-powder, CN Patent 101580279B, 2011

[9] N. Xiaoshan, S. Tao, Ch. Kexin, Burning synthesis method of NiAl2O4 spinelle powder, CN Patent 1556031A, 2004

[10] S.T. Aruna, A.S. Mukasyan, Combustion synthesis and nanomaterials, Current Opinion in Solid State and Materials Science, 12 (2008) 44-50.

[11] M. Aghayan, N. Voltsihhin, M.A. Rodriguez, F.R. Marcos, M. Dong, I. Hussainova, Functionalization of gamma-alumina nanofibers by alpha-alumina via solution combustion synthesis. Ceramics International, 40, 8A (2014) 12603–12607.

[12] S.S. Kim, G.-J. Sun, H.W. Kim, Y.J. Kwon, P. Wu, Thermochemical analysis on the growth of NiAl2O4 rods, RSC Adv., 4 (2014) 1159–1162.

[13] M. Aghayan, I. Hussainova, M. Gasik, M. Kutuzov, M. Friman, Coupled thermal analysis of novel alumina nanofibers with ultrahigh aspect ratio, Thermochimica Acta, 574 (2013) 140–144.

[14] Y.S. Han, J.B. Li, X.S. Ning, X.Z. Yang, B. Chi, Study on NiO excess in preparing NiAl2O4 Mater.Sci.Eng., A369 (2004) 241–244.

[15] N.A.S. Nogueira, E.B. Silva, P.M. Jardim, J.M. Sasaki, Synthesis and characterization of NiAl2O4 nanoparticles obtained through gelatin, Mater.Lett., 61 (2007) 4743–4746.

[16] A. Huczko, M. Bystrzejewski, H. Lange, A. Fabianowska, S. Cudziło, A. Panas, M. Szala, Combustion synthesis as a novel method for production of 1-D SiC nanostructures, J. Phys. Chem. B 109 (2005) 16244-16251.

Fabrication of NiO/NiAl$_2$O$_4$ Nanofibers by Combustion Method

DOI References

[1] A. Fritz, V. Pitchon, The current state of research on automotive lean NOx catalysis, Applied Catalysis B: Environmental, 13 (1) (1997), 1-25.

10.1016/s0926-3373(96)00102-6

[2] H. Fang, L. Haibin, Z. Zengli, Advancements in Development of Chemical-Looping Combustion: A Review, Intern. J. Chem. Eng., 2009 (2009), Article ID 710515, 16 pages.

10.1155/2009/710515

[3] T. Mattisson, E. Jerndal, C. Linderholm, A. Lyngfelt, Reactivity of a spray-dried NiO/NiAl2O4 oxygen carrier for chemical-looping combustion, Chem. Eng. Sci., 66 (2011) 4636-4644.

10.1016/j.ces.2011.06.025

[4] N. Salhi, A. Boulahouache, C. Petit, A. Kiennemann, C. Rabia, Steam reforming of methane to syngas over NiAl2O4 spinel catalysts, Int. J. Hydrogen Energy, 36 (2011) 1433-1439.

10.1016/j.ijhydene.2010.11.071

[5] J. Mary Fisher, T. Ian Hyde, D. Thompsett, Manganese containing oxygen storage component comprising three-way catalyst composition, U.S. Patent 7, 396, 516 B2, (2001).

10.1016/s0925-4005(00)00683-3

[6] J.C. González, J.M. Benito López, M.A. Rodríguez Barbero, I. Rodríguez Ramos, A. Guerrero Ruiz, Development of Nanostructured Catalytic Membranes (NCMs) for Partial Benzene Hydrogenation to Cyclohexene, J. Nanosci. & Nanotech., 7 (2007) 1-11.

10.1166/jnn.2007.903

[7] M.K. Nazemi, S. Sheibani, F. Rashchi, V.M. Gonzalez-DelaCruz, A. Caballero, Preparation of nanostructured nickel aluminate spinel powder from spent NiO/Al2O3 catalyst by mechanochemical synthesis, Advanced Powder Technology 23 (2012) 833-838.

10.1016/j.apt.2011.11.004

[8] Ch. Zhao, Y. Guo, X. Cang, Preparation method of NiAl2O4 nano-powder, CN Patent 101580279B, (2011).

10.1016/j.powtec.2009.11.014

[16] A. Huczko, M. Bystrzejewski, H. Lange, A. Fabianowska, S. Cudziło, A. Panas, M. Szala, Combustion synthesis as a novel method for production of 1-D SiC nanostructures, J. Phys. Chem. B 109 (2005) 16244-16251.

10.1021/jp050837m

[15] N.A.S. Nogueira, E.B. Silva, P.M. Jardim, J.M. Sasaki, Synthesis and characterization of NiAl2O4 nanoparticles obtained through gelatin, Mater. Lett., 61 (2007) 4743-4746.

10.1016/j.matlet.2007.03.042

[14] Y.S. Han, J.B. Li, X.S. Ning, X.Z. Yang, B. Chi, Study on NiO excess in preparing NiAl2O4 Mater. Sci. Eng., A369 (2004) 241-244.

10.1016/j.msea.2003.11.026

[13] M. Aghayan, I. Hussainova, M. Gasik, M. Kutuzov, M. Friman, Coupled thermal analysis of novel alumina nanofibers with ultrahigh aspect ratio, Thermochimica Acta, 574 (2013) 140- 144.

10.1016/j.tca.2013.10.010

[12] S.S. Kim, G. -J. Sun, H.W. Kim, Y.J. Kwon, P. Wu, Thermochemical analysis on the growth of NiAl2O4 rods, RSC Adv., 4 (2014) 1159-1162.

10.1039/c3ra43196g

[11] M. Aghayan, N. Voltsihhin, M.A. Rodriguez, F.R. Marcos, M. Dong, I. Hussainova, Functionalization of gamma-alumina nanofibers by alpha-alumina via solution combustion synthesis. Ceramics International, 40, 8A (2014) 12603-12607.

10.1016/j.ceramint.2014.04.087

[10] S.T. Aruna, A.S. Mukasyan, Combustion synthesis and nanomaterials, Current Opinion in Solid State and Materials Science, 12 (2008) 44-50.

10.1016/j.cossms.2008.12.002

[9] N. Xiaoshan, S. Tao, Ch. Kexin, Burning synthesis method of NiAl2O4 spinelle powder, CN Patent 1556031A, (2004).

10.1016/j.ceramint.2005.03.017

Paper V.   Kirakosyan, K.; <u>Aghayan, M.</u>; Taleb, M.; Hussainova, I.; Rodríguez, M. A., Homogeneous deposition of copper oxide on mesoporous 1D alumina nanofibers by combustion approach. *Proceedings of the Estonian Academy of Sciences*. 2016, 65 (2) 1−4. DOI: 10.3176/proc.2016.2.06

Homogeneous deposition of copper oxide on mesoporous 1D alumina nanofibres by combustion approach

Khachatur Kirakosyan[a,b], Marina Aghayan[a], Miguel A. Rodríguez[c], Masoud Taleb[a*], and Irina Hussainova[a,d]

[a] Tallinn University of Technology, Ehitajate tee 5, 19180 Tallinn, Estonia
[b] Institute of Chemical Physics, P. Sevak Str. 5/2, 0014 Yerevan, Armenia
[c] Instituto de Ceramica y Vidrio (ICV-CSIC), C/Kelsen 5, 28049 Madrid, Spain
[d] ITMO University, Kronverksky 49, St. Petersburg, 197101 Russian Federation

Abstract. Copper oxide-doped alumina nanofibres were fabricated by the solution combustion method. The bundled alumina nanofibres were impregnated with a copper nitrate–glycine (oxidizer–fuel) solution and heat-treated in an open-air environment at 400 °C for 30 min. The microstructure and phase composition of the final product were characterized by XRD, SEM, and EDS analyses. A uniform distribution of a fine-grained CuO film on the surface of gamma-alumina nanofibres was revealed. The obtained results showed a dramatical effect of the amount of fuel, the ratios of fuel to oxidizer and fibres to Cu(II) ions in the reaction mixture on the particle size of the combustion product, its phase composition, and microstructure morphology.

Key words: copper oxide, alumina, nanofibres, solution combustion synthesis.

INTRODUCTION

The synthesis and application of CuO nanostructures are of practical and fundamental importance for gas and bio-sensors [1,2], photodetectors [3], electrode material in lithium ion batteries [4], etc. due to their high theoretical capacity, hazard-safety, and environmental friendliness. Other major applications of CuO nanostructures include solar energy conversion [5], supercapacitors [6], removal of inorganic pollutants [7], heterogeneous catalysts [8–10], etc.

The CuO nanoparticles are characterized by a high surface area combined with high reactivity. Furthermore, heterogeneous catalysts can be easily separated and recycled, which is beneficial for their industrial use. Due to the versatile properties of the nanostructured CuO, it has been synthesized through

solid-phase reaction method [11], sol–gel method [12], thermal decomposition process of precursor [13], electro-chemical methods [14], vapour-phase deposition [15], and many other techniques. Among these techniques the solution combustion synthesis (SCS) is a unique widely used method for the production of different types of nanomaterials [16–19] due to its versatility and simplicity as well as cost-effectiveness.

However, one-step synthesis of nano-CuO particles on a specific carrier is of special interest. For this purpose, a solution combustion synthesis method accompanied by an impregnation method was used to deposit a copper oxide nano-layer on commercially available gamma-alumina nanofibres [20]. The aim of the present work was to study the effect of glycine as a fuel, the ratios of fuel to oxidizer and alumina nanofibres (ANF) to Cu(II) ions, as well as the chemical composition and morphology of as-formed powders on the combustion behaviour.

* Corresponding author, masoud.taleb@ttu.ee

EXPERIMENTAL

Copper nitrate trihydrate [$Cu(NO_3)_2 \cdot 3H_2O$] (≥98%, Sigma-Aldrich) as the source of copper oxide and glycine [$C_2H_5NO_2$] (≥99%, Sigma) as the fuel were dissolved by a deionized water and mixed during 10 min by a magnetic mixer for homogenization. The obtained solution was dropped onto bundled ANF 7 nm in diameter and 50 μm in length and kept for an hour at room temperature. The wetted bundles were heat-treated at 400 °C for 30 min in a preheated muffle furnace where the combustion process takes place.

The combustion product phase identification was performed by an X-ray diffraction using a Bruker diffractometer (D8) with CuKα radiation at 40 kV and scan rate of 0.02 °/s. The morphology of the obtained product was examined by Zeiss EVO MA-15 scanning electron microscope (SEM) (Germany). An energy dispersive X-ray spectrometer (EDS) (INCA x-sight, Oxford Instruments) was used for chemical elemental analysis.

RESULTS AND DISCUSSION

The proportions of the prepared three kinds of samples are presented in Table 1. In samples S1 and S2 the copper nitrate to glycine ratio is stoichiometric, while the ANF to copper nitrate-glycine ratio is changed. In sample S3 the amount of copper is twice larger than stoichiometric.

The X-ray diffraction patterns of the synthesized combustion product (S1 and S3) containing different amounts of glycine are shown in Fig. 1. As it can be seen, mainly CuO is obtained as a result of the combustion of the stoichiometric mixture ($f = 1$) (Fig. 1, curve (a)). However, at fuel-rich composition ($f = 2$) (Fig. 1, curve (b)) the X-ray diffraction (XRD) pattern mostly contains CuO diffraction lines. Low intensity of $CuAlO_2$ and Cu_2O diffraction lines can also be registered. The formation of reduced copper oxide along with CuO points to a decreasing oxygen concentration. In this case the oxygen is supplied to the system in two ways: from the decomposition of copper nitrate and from air. It is supposed that when the supply of oxygen
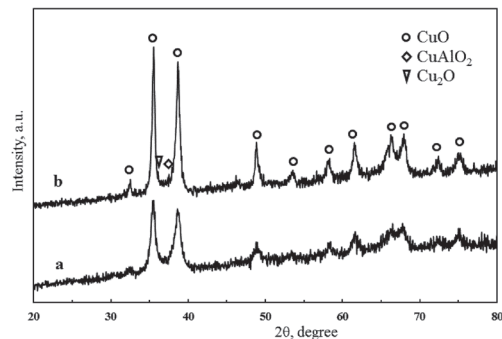
Fig. 1. XRD pattern of the combustion product using (curve **a**) the stoichiometric amount of fuel ($f = 1$) and (curve **b**) a fuel-rich mixture ($f = 2$).

is not sufficient in the combustion system, metals or their reduced oxides or fuel contaminations may form. When the amount of fuel was increased, only CuO phase was determined. This is caused by the smaller size of the particles, which can oxidize very fast in air after the combustion process. Pure Al_2O_3 is not found on the XRD pattern because of the large difference in the atomic scattering factors of copper and aluminium and low content of alumina in the combustion product.
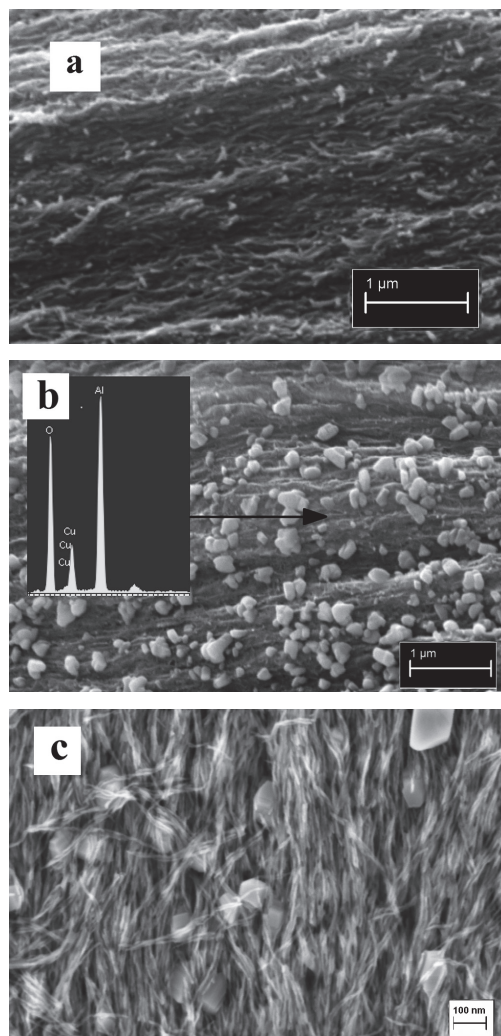
The SEM images of the combustion product with a low and a high content of CuO are presented in Fig. 2. It is obvious that the CuO particles are developed as separate fine-sized particles in the mixtures with the low concentration of CuO (Fig. 2a and b). The CuO particle sizes can be further decreased by increasing the amount of glycine in the starting mixture at a constant content of CuO (Fig. 2b and c).

It should be noted that a high concentration of glycine results in an increase in the temperature of the combustion process. The adiabatic combustion temperature can increase up to 1890 °C as calculated by ISMAN-THERMO software [21]. A high combustion temperature could create suitable conditions for further CuO particle growth and agglomeration. On the other hand, the extra amount of glycine also results in an increase in the amount of the emitted gas due to a reaction with oxygen from the environment. As a result, the gas outflow decreases the system's energy more rapidly and hampers further particle growth and agglomeration (Fig. 2b). During the combustion process, the developed CuO nanoparticles remain separated from one another on the surface of ANFs.

As presented in Fig. 2a, CuO is present in a wide range of particle sizes starting from some nanometres up to 200 nm. The EDS analysis proved that nanoparticles located in between nanofibres were copper oxide (Fig. 2b).

Table 1. Composition of the initial compounds

Number of sample	Content of copper	Amount of ANF, mg	Amount of $Cu(NO_3)_2 \cdot 3H_2O$, mg	Amount of glycine, mg
S1	High	1.8	7.3	2.5
S2	Low	1.8	0.73	0.25
S3	High	1.8	7.3	5

Fig. 2. SEM and EDS analyses of combustion products with (a) a low content of copper (f = 1), (b) a high content of copper (f = 1), and (c) a high content of copper (f = 2).

CONCLUSIONS

It was the first time that in situ preparation of alumina nanofibres doped with CuO by the SCS method was realized and studied. The obtained results show that the composition of CuO/ANF can be developed due to the high exothermic interaction of copper nitrate and the glycine system. The particle size of CuO can be controlled by the concentration of copper nitrate and the copper nitrate to glycine ratio.

REFERENCES

1. Li, D., Hu, J., Wu, R., and Lu, J. G. Conductometric chemical sensor based on individual CuO nanowires. *Nanotechnology*, 2010, **21**(48), 485502–485508.
2. Rahman, M. M., Ahammad, A., Jin, J.-H., Ahn, S. J., and Lee, J.-J. A comprehensive review of glucose biosensors based on nanostructured metal-oxides. *Sensors*, 2010, **10**(5), 4855–4886.
3. Wang, S., Hsiao, C., Chang, S., Lam, K., Wen, K., Hung, S., et al. A CuO nanowire infrared photodetector. *Sensor. Actuat. A-Phys.*, 2011, **171**(2), 207–211.
4. Venkatachalam, S., Zhu, H., Masarapu, C., Hung, K., Liu, Z., Suenaga, K., and Wei, B. In-situ formation of sandwiched structures of nanotube/Cu_xO_y/Cu composites for lithium battery applications. *ACS Nano*, 2009, **3**(8), 2177–2184.
5. Xu, Y., Chen, D., and Jiao, X. Fabrication of CuO pricky microspheres with tunable size by a simple solution route. *J. Phys. Chem. B*, 2005, **109**(28), 13561–13566.
6. Zhang, X., Shi, W., Zhu, J., Kharistal, D. J., Zhao, W., Lalia, B. S., et al. High-power and high-energy-density flexible pseudocapacitor electrodes made from porous CuO nanobelts and single-walled carbon nanotubes. *ACS Nano*, 2011, **5**(3), 2013–2019.
7. Yu, X.-Y., Xu, R.-X., Gao, C., Luo, T., Jia, Y., Liu, J.-H., and Huang, X.-J. Novel 3D hierarchical cotton-candy-like CuO: surfactant-free solvothermal synthesis and application in As(III) removal. *ACS Appl. Mater. Interfaces*, 2012, **4**(4), 1954–1962.
8. Zhou, K., Wang, R., Xu, B., and Li, Y. Synthesis, characterization and catalytic properties of CuO nanocrystals with various shapes. *Nanotechnology*, 2006, **17**(15), 3939.
9. Xu, L., Sithambaram, S., Zhang, Y., Chen, C.-H., Jin, L., Joesten, R., and Suib, S. L. Novel urchin-like CuO synthesized by a facile reflux method with efficient olefin epoxidation catalytic performance. *Chem. Mater.*, 2009, **21**(7), 1253–1259.
10. Zhou, K. and Li, Y. Catalysis based on nanocrystals with well-defined facets. *Angew. Chem. Int. Ed.*, 2012, **51**(3), 602–613.
11. Xu, J., Ji, W., Shen, Z., Tang, S., Ye, X., Jia, D., and Xin, X. Preparation and characterization of CuO nanocrystals. *J. Solid State Chem.*, 1999, **147**(2), 516–519.
12. Zhang, Q., Li, Y., Xu, D., and Gu, Z. Preparation of silver nanowire arrays in anodic aluminum oxide templates. *J. Mater. Sci. Lett.*, 2001, **20**(10), 925–927.
13. Xu, C., Liu, Y., Xu, G., and Wang, G. Preparation and characterization of CuO nanorods by thermal decomposition of CuC_2O_4 precursor. *Mater. Res. Bull.*, 2002, **37**(14), 2365–2372.

14. Yin, A., Li, J., Jian, W., Bennett, A., and Xu, J. Fabrication of highly ordered metallic nanowire arrays by electro-deposition. *Appl. Phys. Lett.*, 2001, **79**(7), 1039–1041.

15. Okuyama, K., Lenggoro, W., and Iwaki, T. Nanoparticle preparation and its application − a nanotechnology particle project in Japan. In *International Conference on MEMS, NANO and Smart Systems, 2004*. IEEE, 2004, 369–372.

16. Mukasyan, A. S., Epstein, P., and Dinka, P. Solution combustion synthesis of nanomaterials. *P. Combust. Inst.*, 2007, **31**(2), 1789–1795.

17. Aruna, S. T. and Mukasyan, A. S. Combustion synthesis and nanomaterials. *Curr. Opin. Solid St. M.*, 2008, **12**(3), 44–50.

18. Patil, K. C., Hegde, M., Rattan, T., and Aruna, S. *Chemistry of Nanocrystalline Oxide Materials-Combustion Synthesis, Properties and Applications.* World Scientific, New Jersey, 2008.

19. Aghayan, M., Voltsihhin, N., Rodríguez, M. A., Rubio-Marcos, F., Dong, M., and Hussainova, I. Functionalization of gamma-alumina nanofibers by alpha-alumina via solution combustion synthesis. *Ceram. Int.*, 2014, **40**(8), 12603–12607.

20. Aghayan, M., Hussainova, I., Gasik, M., Kutuzov, M., and Friman, M. Coupled thermal analysis of novel alumina nanofibers with ultrahigh aspect ratio. *Thermochim. Acta*, 2013, **574**, 140–144.

21. Zeldovich, Ya. B., Barenblatt, G. I., Librovich, V. B., and Makhviladze, G. M. *The Mathematical Theory of Combustion and Explosions*. Consultants Bureau, New York, 1985, 22–26.

Vaskoksiidi homogeenne sadestamine mesopoorsetele 1D alumiiniumnanokiududele

Khachatur Kirakosyan, Marina Aghayan, Miguel A. Rodríguez, Masoud Taleb ja Irina Hussainova

On vaadeldud alumiiniumnanokiududele (ANF) vaskoksiidi sadestamist lahustipõletusmeetodil. Alumiiniumnano-kiudude kimp immutati vasenitraat-glütsiinlahusega (oksüdeerija-kütus) ja termotöödeldi õhu käes temperatuuril 400 °C 30 min. Lõpp-produkti mikrostruktuuri ja koostise iseloomustamiseks kasutati XRD-, SEM- ning EDS-analüüsi, mille tulemusena selgitati välja peeneteralise CuO kile ühtlane jagunemine gamma-alumiiniumoksiidist nanokiududel. Saadud tulemused näitasid, et põletusprodukti osakeste suurus, faasiline koostis ja mikrostruktuuri morfoloogia on dramaatiliselt mõjutatud kütuse hulgast, kütuse ja oksüdeerija kui ka alumiiniumnanokiudude ning Cu(II) ioonide vahekorrast reageerivas segus.

DISSERTATIONS DEFENDED AT
TALLINN UNIVERSITY OF TECHNOLOGY ON
MECHANICAL ENGINEERING

1. **Jakob Kübarsepp**. Steel-Bonded Hardmetals. 1992.

2. **Jakub Kõo**. Determination of Residual Stresses in Coatings &Coated Parts. 1994.

3. **Mart Tamre**. Tribocharacteristics of Journal Bearings Unlocated Axis. 1995.

4. **Paul Kallas**. Abrasive Erosion of Powder Materials. 1996.

5. **Jüri Pirso**. Titanium and Chromium Carbide Based Cermets. 1996.

6. **Heinrich Reshetnyak**. Hard Metals Serviceability in Sheet Metal Forming Operations. 1996.

7. **Arvi Kruusing**. Magnetic Microdevices and Their Fabrication methods. 1997.

8. **Roberto Carmona Davila**. Some Contributions to the Quality Control in Motor Car Industry. 1999.

9. **Harri Annuka**. Characterization and Application of TiC-Based Iron Alloys Bonded Cermets. 1999.

10. **Irina Hussainova**. Investigation of Particle-Wall Collision and Erosion Prediction. 1999.

11. **Edi Kulderknup**. Reliability and Uncertainty of Quality Measurement. 2000.

12. **Vitali Podgurski**. Laser Ablation and Thermal Evaporation of Thin Films and Structures. 2001.

13. **Igor Penkov**. Strength Investigation of Threaded Joints Under Static and Dynamic Loading. 2001.

14. **Martin Eerme**. Structural Modelling of Engineering Products and Realisation of Computer-Based Environment for Product Development. 2001.

15. **Toivo Tähemaa**. Assurance of Synergy and Competitive Dependability at Non-Safety-Critical Mechatronics Systems design. 2002.

16. **Jüri Resev**. Virtual Differential as Torque Distribution Control Unit in Automotive Propulsion Systems. 2002.

17. **Toomas Pihl**. Powder Coatings for Abrasive Wear. 2002.

18. **Sergei Letunovitš**. Tribology of Fine-Grained Cermets. 2003.

19. **Tatyana Karaulova**. Development of the Modelling Tool for the Analysis of the Production Process and its Entities for the SME. 2004.

20. **Grigori Nekrassov**. Development of an Intelligent Integrated Environment for Computer. 2004.

21. **Sergei Zimakov**. Novel Wear Resistant WC-Based Thermal Sprayed Coatings. 2004.

22. **Irina Preis**. Fatigue Performance and Mechanical Reliability of Cemented Carbides. 2004.

23. **Medhat Hussainov**. Effect of Solid Particles on Turbulence of Gas in Two-Phase Flows. 2005.

24. **Frid Kaljas**. Synergy-Based Approach to Design of the Interdisciplinary Systems. 2005.

25. **Dmitri Neshumayev**. Experimental and Numerical Investigation of Combined Heat Transfer Enhancement Technique in Gas-Heated Channels. 2005.

26. **Renno Veinthal**. Characterization and Modelling of Erosion Wear of Powder Composite Materials and Coatings. 2005.

27. **Sergei Tisler**. Deposition of Solid Particles from Aerosol Flow in Laminar Flat-Plate Boundary Layer. 2006.

28. **Tauno Otto**. Models for Monitoring of Technological Processes and Production Systems. 2006.

29. **Maksim Antonov**. Assessment of Cermets Performance in Aggressive Media. 2006.

30. **Tatjana Barashkova**. Research of the Effect of Correlation at the Measurement of Alternating Voltage. 2006.

31. **Jaan Kers**. Recycling of Composite Plastics. 2006.

32. **Raivo Sell**. Model Based Mechatronic Systems Modeling Methodology in Conceptual Design Stage. 2007.

33. **Hans Rämmal**. Experimental Methods for Sound Propagation Studies in Automotive Duct Systems. 2007.

34. **Meelis Pohlak**. Rapid Prototyping of Sheet Metal Components with Incremental Sheet Forming Technology. 2007.

35. **Priidu Peetsalu**. Microstructural Aspects of Thermal Sprayed WC-Co Coatings and Ni-Cr Coated Steels. 2007.

36. **Lauri Kollo**. Sinter/HIP Technology of TiC-Based Cermets. 2007.

37. **Andrei Dedov**. Assessment of Metal Condition and Remaining Life of In-service Power Plant Components Operating at High Temperature. 2007.

38. **Fjodor Sergejev**. Investigation of the Fatigue Mechanics Aspects of PM Hardmetals and Cermets. 2007.

39. **Eduard Ševtšenko**. Intelligent Decision Support System for the Network of Collaborative SME-s. 2007.

40. **Rünno Lumiste**. Networks and Innovation in Machinery and Electronics Industry and Enterprises (Estonian Case Studies). 2008.

41. **Kristo Karjust**. Integrated Product Development and Production Technology of Large Composite Plastic Products. 2008.

42. **Mart Saarna**. Fatigue Characteristics of PM Steels. 2008.

43. **Eduard Kimmari**. Exothermically Synthesized B_4C-Al Composites for Dry Sliding. 2008.

44. **Indrek Abiline**. Calibration Methods of Coating Thickness Gauges. 2008.

45. **Tiit Hindreus**. Synergy-Based Approach to Quality Assurance. 2009.

46. **Karl Raba**. Uncertainty Focused Product Improvement Models. 2009.

47. **Riho Tarbe**. Abrasive Impact Wear: Tester, Wear and Grindability Studies. 2009.

48. **Kristjan Juhani**. Reactive Sintered Chromium and Titanium Carbide-Based Cermets. 2009.

49. **Nadežda Dementjeva**. Energy Planning Model Analysis and Their Adaptability for Estonian Energy Sector. 2009.

50. **Igor Krupenski**. Numerical Simulation of Two-Phase Turbulent Flows in Ash Circulating Fluidized Bed. 2010.

51. **Aleksandr Hlebnikov**. The Analysis of Efficiency and Optimization of District Heating Networks in Estonia. 2010.

52. **Andres Petritšenko**. Vibration of Ladder Frames. 2010.

53. **Renee Joost**. Novel Methods for Hardmetal Production and Recycling. 2010.

54. **Andre Gregor**. Hard PVD Coatings for Tooling. 2010.

55. **Tõnu Roosaar**. Wear Performance of WC- and TiC-Based Ceramic-Metallic Composites. 2010.

56. **Alina Sivitski**. Sliding Wear of PVD Hard Coatings: Fatigue and Measurement Aspects. 2010.

57. **Sergei Kramanenko**. Fractal Approach for Multiple Project Management in Manufacturing Enterprises. 2010.

58. **Eduard Latõsov**. Model for the Analysis of Combined Heat and Power Production. 2011.

59. **Jürgen Riim**. Calibration Methods of Coating Thickness Standards. 2011.

60. **Andrei Surzhenkov**. Duplex Treatment of Steel Surface. 2011.

61. **Steffen Dahms**. Diffusion Welding of Different Materials. 2011.

62. **Birthe Matsi**. Research of Innovation Capasity Monitoring Methodology for Engineering Industry. 2011.

63. **Peeter Ross**. Data Sharing and Shared Workflow in Medical Imaging. 2011.

64. **Siim Link**. Reactivity of Woody and Herbaceous Biomass Chars. 2011.

65. **Kristjan Plamus**. The Impact of Oil Shale Calorific Value on CFB Boiler Thermal Efficiency and Environment. 2012.

66. **Aleksei Tšinjan**. Performance of Tool Materials in Blanking. 2012.

67. **Martinš Sarkans**. Synergy Deployment at Early Evaluation of Modularity of the Multi-Agent Production Systems. 2012.

68. **Sven Seiler**. Laboratory as a Service – A Holistic Framework for Remote and Virtual Labs. 2012.

69. **Tarmo Velsker**. Design Optimization of Steel and Glass Structures. 2012.

70. **Madis Tiik**. Access Rights and Organizational Management in Implementation of Estonian Electronic Health Record System. 2012.

71. **Marina Kostina**. Reliability Management of Manufacturing Processes in Machinery Enterprises. 2012.

72. **Robert Hudjakov**. Long-Range Navigation for Unmanned Off-Road Ground Vehicle. 2012.

73. **Arkadi Zikin**. Advanced Multiphase Tribo-Functional PTA Hardfacings. 2013.

74. **Alar Konist**. Environmental Aspects of Oil Shale Power Production. 2013.

75. **Inge Roos**. Methodology for Calculating CO_2 Emissions from Estonian Shale Oil Industry. 2013.

76. **Dmitri Shvarts**. Global 3D Map Merging Methods for Robot Navigation. 2013.

77. **Kaia Lõun**. Company's Strategy Based Formation of e-Workplace Performance in the Engineering Industry. 2013.

78. **Maido Hiiemaa**. Motion Planner for Skid-Steer Unmanned Ground Vehicle. 2013.

79. **Dmitri Goljandin**. Disintegrator Milling System Development and Milling Technologies of Different Materials. 2013.

80. **Dmitri Aleksandrov**. Light-Weight Multicopter Structural Design for Energy Saving. 2013.

81. **Henrik Herranen**. Design Optimization of Smart Composite Structures with Embedded Devices. 2014.

82. **Heiki Tiikoja**. Experimental Acoustic Characterization of Automotive Inlet and Exhaust System. 2014.

83. **Jelena Priss**. High Temperature Corrosion and Abrasive Wear of Boiler Steels. 2014.

84. **Aare Aruniit**. Thermoreactive Polymer Composite with High Particulate Filler Content. 2014.

85. **Dmitri Gornostajev**. Development of the Calculation Method for Barge Hull. 2014.

86. **Liina Lind**. Wear of PVD Coatings on Fineblanking Punches. 2014.

87. **Nikolai Voltšihhin**. Design and Technology of Oxides-Containing Ceramic-Based Composites. 2014.

88. **Aleksander Šablinski**. RANS Numerical Modelling of Turbulent Polydispersed Flows in CFB Freeboard. 2015.

89. **Tanel Aruväli**. Wireless Real-time Monitoring of Machining Processes. 2015.

90. **Andrei Bogatov**. Morphological Changes on Diamond and DLC Films During Sliding Wear. 2015.

91. **Raimo Kabral**. Aero-Acoustic Studies and Innovative Noise Control with Application to Modern Automotive Gas Exchange System. 2015.

92. **Jevgeni Sahno**. Dynamic Management Framework for Continuous Improvement of Production Processes. 2015.

93. **Ott Pabut**. Optimal Design of Slotless Permanent Magnet Generators. 2015.

94. **Merili Kukuškin**. Value Centric Business Development for Estonian Manufacturing Small and Medium Sized Enterprises. 2015.

95. **Kaimo Sonk**. Development of Additive Manufacturing Based on Functional Requirements. 2015.